Cranfield University

Aleksandra Kosmala

Development of high loading Ag nanoparticle inks for inkjet printing and Ag nanowire dispersions for conducting and transparent coatings

School of Applied Sciences

PhD Thesis

CRANFIELD UNIVERSITY
SCHOOL OF APPLIED SCIENCES
DEPARTMENT OF MATERIALS
MICROSYSTEMS AND NANOTCHNOLOGY CENTRE

PhD Thesis

Aleksandra Kosmala

Development of high loading Ag nanoparticle inks for inkjet printing and Ag nanowire dispersions for conducting and transparent coatings

Supervisors: Dr. Qi Zhang and Dr. Paul Kirby
March 2012

This thesis is submitted in partial fulfilment of the requirements for the Degree of PhD

Abstract

The work presented in this thesis focuses on the synthesis of nanomaterials, formulation and printing of Ag nanoparticle and nanowire inks for two distinct applications: a) inkjet printing of Ag nanoparticle films on ceramic substrates with the aim of providing a smaller size of printed feature at lower cost than that can be obtained with the conventionally used screen printing, and b) Ag nanowires films prompted by the wide quest of electronics industry for materials with increased flexibility, lower cost and higher transmittance to replace indium tin oxide.

Ag nanoparticles with a size of 50 nm were successfully synthesized and dispersed in aqueous medium. Two preparation routes were compared in order to distinguish the effects of solvents treatment of particles and their influence on the suspension characteristics including Ag loading, rheology, surface tension and later the electrical film properties. The co-polymer Pluronic F127 was found to be an effective as a stabiliser leading to the formulation of high silver loading in inks.

The processing and characterization of silver films was performed. The aim was to reduce the number of layers in the silver nanoparticles film by increasing the thickness of a single layer with the goal of obtaining a dense and conductive film. An increase in the Ag loading, from 5 wt % to 45 wt % favoured the achievement of denser and thicker film with one layer printing. Addition of SiO_2 to the ink formula resulted in denser structure and better adhesion of the printed track then the one without SiO_2.

A new method for improving the morphology of inkjet printed tracks has been proposed by printing the ink into the structured channels with predefined topography.

Silver nanowires were synthesised and dispersed in methanol with help of copolymer F127. They were subsequently deposited on plastic and glass substrates forming conductive and transparent films.

Acknowledgments

I would like to thank my two supervisors Dr. Qi Zhang and Dr. Paul Kirby for their help and advice throughout the past three years and for giving me the opportunity to conduct this research at Cranfield University.

I wish to thank all my colleagues, Zsuzanna, Daniel, Nathan, Ewa, Alice, Alessandro, Vlad, and other members of the Nanotechnology Centre for creating a great place to work.

I would like to express my gratitude to the support and technical staff of the Material Department including, Enza Giaracuni, Andy Stallard and Matthew Taunt for all of their assistance and patience.

I would like to thank Rob Wright for valuable discussions and sharing his knowledge. Very special thanks to Dominika for her continuous trust and support.

Finally I would like to thank my mum, sister, brother, Sylwia and Jakob for love and for encouraging me to begin this journey in Cranfield. Thanks for helping me to find a path I am keen to travel further upon.

Table of Contents

List of Figures

List of Tables

Nomenclature

θ	Contact angle
γ	Surface tension
τ	Relaxation time
δ	Density
η	Viscosity
σ	Shear stress
$\dot{\gamma}$	Shear rate
ρ	Resistivity
CTAB	Cetyltrimethylammonium bromide
De	Deborah number
DoD	Drop on demand ink jet printer
E	Energy
EG	Ethylene glycol
F127	copolymer Pluronic F127
GAS	Gas Anti Solvent
H	Hardness
HIFU	High intensity focused ultrasounds
I	Current
IJP	Ink jet printing
l	Length
M	Mass
PVP	Poly(*N*-vinyl-2-pyrrolidone
PZT	Lead zirconatetitanate
R	Resistance
r	Radius
Re	Reynolds number
RESS	The rapid expansion of supercritical solution
RESS-SC	Rapid Expansion of a Supercritical Solution-Solid Co-solvent
SAS	Supercritical Anti Solvent operated in semi-continuous mode
SDS	Sodium dodecyl sulphate
SEM	Scanning Electron Microscopy
T	Temperature

t	Layer thickness
TEM	Transmision Electron Microscopy
V	Voltage
We	Weber number
Z	Jettability of fluid
XRD	X-ray diffraction

List of Equations

(2.1) $E = P\,t$

(2.2) $De = \tau / t_{0\ldots\ldots}$

(2.3) $\eta = \sigma/\dot{\gamma}$

(2.4) $\gamma = dy / dt$

(2.5) $\sigma = F / A$

(2.6) $(\eta/\eta_s) = 1+2.5\,\varphi$

(2.7) $\eta=[1-(\varphi/\varphi_m)]^{-[\eta]}$

(2.8) $\gamma=F/d$

(2.9) $\Gamma = \gamma_1 * m_2/m_1$

(2.10) $F_{drag}= 6\pi r V\eta = 4\pi r^3 g(\rho_p - \rho_L)/3 = F_{gravity}$

(2.11) $x^2= 2Dt$

(2.12) $D = \frac{kT}{3\pi\eta r}$

(2.13) $V_T = V_R + V_A$

(2.14) $Re = \frac{\rho d v}{\eta}$

(2.15) $We = \frac{\rho d v^2}{\gamma}$

(2.16) $Z = Oh^{-1} = \frac{Re}{\sqrt{We}} = \frac{\sqrt{\rho d v}}{\eta}$

(2.17) $H=P_{max}/A_r$

(2.18) $\rho = RA/l$

(2.19) $R_{AB,CD} = \frac{VoltageA-B}{CurrentC-D}$

(2.20) $R_{AB,CD} = R_{BC,\,DA}$

(2.21) $\rho = \frac{\pi d}{ln\,2}\,(R_{AB,CD} + R_{BC,DA}/2)\,f\,(R_{AB,CD}/R_{BC,DA})$.

(2.22) $\Delta G = -nF\Delta E + RTlnK$

(4.1) $2AgNO_3 + 4N_2H_4OH \longrightarrow 2Ag + 5N_2 + 10H_2O$

(4.2) $t = k\,\lambda / \beta\,cos\,\theta$

(4.3) $\Delta G = \Delta H - T\Delta S > 0$

(4.4) $\Delta H = U_{sys} + PV$

(4.5) $HO\text{-}CH_2\text{-}CH_2\text{-}OH \longrightarrow 2\,CH_3CHO + 2\,H_2O$

(4.6) $2\,CH_3CHO + 2\,Ag^+ \longrightarrow CH_3CO\text{-}OCCH_3 + 2\,Ag + 2H^+$

(4.7) $\Delta G^* = 16\pi\gamma^3 / 3\Delta G_v^2$

(4.8) $(\frac{\partial \Delta G^*}{\partial P})_T = (\frac{3\Delta G^*}{\gamma})(\frac{\partial \gamma}{\partial P})_T - (\frac{2\,\Delta G^*}{\Delta G\, v})(\frac{\partial \Delta Gv}{\partial P})_T$

(5.1) $\tau = \tau 0 + \eta$

(5.2) $\sqrt{\tau} = \sqrt{\tau_0} + \sqrt{\eta + \gamma}$

(5.3) $\rho = R \cdot A / l$

(5.4) $C_{20}H_{37}NaO_7S\,(s) \longrightarrow 74CO(s) + 34CO_2\,(g) + 2SO_3 + Na_2O_2 + 37H_2$

(5.5b) $V = \frac{\pi R^3\left(2-3\,sin(90-\theta)+sin^3(90-\theta)\right)}{3}$

(5.6) $V = M_{Ag}/\rho_{Ag} + M_{H2O}/\rho_{H2O}$

(5.7) $L = \frac{M_{Ag}}{M_{Ag} + M_{H2O}}$

(5.8) $M_{Ag} = \frac{V}{1/\rho_{Ag} + (1-L)/L\rho_{H2O}} = \pi r^2 t$

(6.1) $H = P_m/A$

(7.1) $\gamma = \gamma^p + \gamma^d$

(7.2) $y = ax + b$

(7.3) $x = \frac{\sqrt{\gamma_L^p}}{\sqrt{\gamma_L^p}}$

(7.4) $y = \frac{1+cos\theta}{2} * \frac{\gamma_L}{\sqrt{\gamma_L^d}}$

(7.5) $a = \sqrt{\gamma^p}$

(7.6) $b = \sqrt{\gamma^d}$

(7.7) $R = \frac{n\,(\sum(xy)) - (\sum(x))(\sum(y))}{\sqrt{[n\sum x^2 - (\sum x)^2]\,[n\sum y^2 - (\sum y)^2]}}$

(8.1) $2HOCH_2 - CH_2OH \longrightarrow 2CH_3CHO + 2H_2O$

(8.2) $CH_3CHO + PtCl_2 \longrightarrow CH_3CO - COCH_3 + Pt + 2HCl$

(8.3) $HO\text{-}CH_2\text{-}CH_2\text{-}OH \longrightarrow 2\,CH_3CHO + 2\,H_2O$

(8.4) $2\,CH_3CHO + 2\,Ag^+ \longrightarrow CH_3CO\text{-}OCCH_3 + 2\,Ag + 2H^+$

(8.5) $\%\ extractability = C_1/C * 100$

Publications

- A.Kosmala, R.Wright, Q. Zhang, and P. Kirby, 'Synthesis of silver nano particles and fabrication of aqueous Ag inks for inkjet printing' *Material Chemistry and Physics, January,* 129, (2011), 1075-1080
- A.Kosmala, R.Wright, Q. Zhang, and P. Kirby, 'Development of high concentrated aqueous silver nanofluid and inkjet printing on ceramic substrates', Material Chemistry and Physics, 132, (2012), 788-795

Oral presentations

- A. Kosmala, 'Silver inks for printed electronics', University of Cambridge, Printing and Graphics Science Group conference, December 2011
- A. Kosmala, ' Silver inks for inkjet printing', KTH Production Engineering, 24M Meeting for the project MULTILAYER, Sweden, March 2011
- A. Kosmala, 'Functional printing', 18M Meeting for the project MULTILAYER**,** Italy, September 2010
- A.Kosmala, 'Synthesis of nanomaterials', Karlsruhe Institute of Technology (KIT), 12M Meeting for the project MULTILAYER Germany, March, 2010

Poster presentation

- A.Kosmala, Q. Zhang, R.Wright, and P. Kirby, 'Nano-silver inks for inkjet printing applications' Science of Inkjet and Printed Drops, IOP, London, 10th September 2010
- A.Kosmala, Q. Zhang, R.Wright, and P. Kirby, Nano-silver inks for inkjet printing applications',CN Roadshow, Cranfield University, July 2012

Patent

‘A method for preparing silver nanoparticles and high loading, aqueous silver dispersions’**,** Patent application number GB 1117825 via Cranfield University

Chapter 1

Introduction

1.1 Context of the research

Printed electronics is a term that describes the printing of circuits which include various components, e.g. antennas, diodes, transistors, etc., with liquid source materials on the surface of paper, plastics or ceramics. Printed electronics is consisted of various fields, including semiconductor device physics, ink chemistry and formulation, and printing technology. There has been growing interest in the development of printed electronics as a potential application of inkjet technology. The idea is to replace the conventional photolithography-based semiconductor manufacturing with printing technology. Printed electronic can potentially reduce the process complexity as the pattern deposition is used to deposit the film directly. It opens a new world of low-cost printed circuits based on conductive, semiconductive and dielectric printed materials aiming at high-volume market segments. Among the broad printed electronic technologies, there are various techniques for producing conductive components, one of them, very promising, is inkjet printing technique.

The inkjet printing is a technique where inks are printed only at the locations where they are desired. It is a non-contact process where the thin or thick structures are created under computer control. While the printing processes are applied, the main cost consumption in printing electronics, are inks used to produce the electronic components. The innovations in materials to enable printing depend mainly on advances of material science that can produce functional inks. Inkjet printing must be considered as a complete system, bringing together a number of disciplines, such as material science, engineering, software, and electronics. The main challenges apply to feature size, resolution, productivity, and drop placement accuracy.

Since there is no such a thing like an universal ink, many factors have to be taken into account, namely, functionality, print quality, drying time, adhesion, and jetting characteristic including viscosity, surface tension, particle size, and stability of the ink. The smaller size of the printed feature enables the use of inkjet printing in functional printed electronics.

Increasing the print resolution by decreasing the size of the drops and improving their accurate place is still a challenge. Joining the effect of surface treatment of the substrate and the unique rheology behaviour of the ink might lead to reduced feature size.

Another huge attention in electronic industry is paid to the materials that show high electrical conductivity and optical transparency. The most extensively used material for transparent electrodes is indium tin oxide (ITO). However there has been a quest to look for materials with improved bending, lower cost and higher transmittance that can replace ITO. Towards this objective, various types of new materials have been developed among which carbon nanotube (CNT) films, graphene films and Ag nanowires.

1.2 Thesis Objectives

The aims of this thesis are: 1) to develop high loading aqueous Ag nanoparticles ink for inkjet printing and 2) to develop a new method to deposit highly conductive transparent Ag coating. Towards these, the objectives are:

1. To develop new chemical methods for the syntheses of silver nanoparticles and nanowires.
2. To formulate and optimise silver inks suitable for ink jet printing application.
3. To understand how the fluid ingredients influence the silver suspension, the film density and morphology.
4. To assess the behaviour of inks and develop processes (jetting parameters).
5. To investigate the influence of substrate surface condition on the morphology of the subsequent printing features.
6. To evaluate the performances obtained on the ink formula including functional properties.
7. To investigate inkjet printing of a silver nanoparticle ink onto a predefined topography pattern in a surface (embossed structures).
8. To synthesize and formulate a silver nanowire fluid and deposit it onto transparent plastic substrate.
9. To compare the transparency and conductivity of Ag nanowire coating with ITO coating.

1.3 Thesis structure

The thesis is presented in nine chapters. Chapter 1 is an introduction to the topic of the research.

Chapter 2 focuses on the Literature review. In the first section of the literature survey, the conceptual basis for printed electronic and the motivation for the technology is discussed. Section 2 covers the fundamental aspect of inkjet printing including the technology trends and challenges. Section 3 focuses on ink chemistry; it discusses the principal issues that control the overall performance of the ink. In section 4, synthesis of silver nanoparticles and nanowires as well as their application is revived.

Chapter 3 summarises all the experimental procedures that were employed within this project.

The results and discussion regarding synthesis of silver nanoparticles and influence of various factors on size and morphology of the final product are presented in Chapter 4.

Chapter 5 focuses on the results obtained from experiments on high loading Ag ink development, where ink formulation and characterisation is discussed.

In Chapter 6 the results of experiment in improving physical properties of the silver film, and the effect of SiO_2 on hardness, adhesion and resistivity are analysed.

Chapter 7 focuses on improving the resolution of printed features and describes the experimental details of inkjet printing of a silver nanoparticle ink onto a predefined topography pattern in ceramic substrates.

The following Chapter 8 presents and discusses the results obtained from experiments of Ag nanowires synthesis and their deposition on glass and plastic substrates.

Chapter 9 summarizes the major conclusions of this work and suggests further work in this area of the research.

Chapter 2

Literature Review

The aim of this chapter is to cover the development of technologies, nanomaterials and nanofluids research that have led to the present project. In this chapter an overview is presented of what has been done within the printed electronics area. An introduction to the synthesis of nanoparticles and ink chemistry is given followed by a background to an inkjet printing technology including the trends and challenges. Silver nanowires synthesis and processing will be also discussed.

2.1 Printed electronics

2.1.1 Motivation

The first printing revolution started with Johannes Gutenberg in the 1440's. The information stored in books stabilized scientific discussion and made it possible to refer to books [1]. The second printing revolution came with the Internet and private printing making paper and books old fashioned and reformed our society and science all the time. The third printing revolution is still approaching. Around five hundred years after the first, this revolution integrates the achievements of the printing industry and those of the electronics and digitalization world. Printed electronics opens the door to a future of electronic innovations that are lightweight, flexible, and could be produced on cheap materials such as paper or flexible film. Printed electronics is a term that describes the printing of circuits which include various components, e.g. antennas, diodes, transistors, etc., with conductive ink on the surface of paper, plastics or ceramics.

There has been growing interest in the development of printed electronics as a potential application of inkjet technology. The idea is to replace the conventional

photolithography-based semiconductor manufacturing with printing technology. This is motivated by the fact of low-cost means of depositing ink at the location where it is desired. That led to high-throughput production of electronic devices that are lightweight, small, flexible, inexpensive, and disposable [2]. For fabrication conventional electronic systems, photolithographic process is used. In order to create a pattern the process steps can be summarised as follows [3]. The first step is the electronic material deposition on the substrate, usually using chemical vapour deposition or physical vapour deposition. Then the substrate is coated with photoresist and the excess of solvent is removed by heating the substrate at a temperature that depends on the photoresist utilised. The photoresist is subjected to ultraviolet (UV) light through a mask containing the desired pattern. The photoresist is then developed revealing the pattern. A chemical agent (typically acid, e.g. hydrofluoric (HF) or hydrochloric (HCl)) is then used to etch the deposited film and the material in the areas not protected by photoresist is removed. The remaining photoresist is then removed to expose the patterned film. In this technique, the numerous steps that are required to create a single patterned film increase the complexity of the process. Although this process is suitable for the fabrication of large volumes of devices, there is a limit of printed patterns and the disadvantage of a big amount of wasted material [4]. Moreover, the energy consumption is high [5] and dangerous materials are used in the etching step.

Printed electronic can potentially reduce the process complexity as the pattern deposition is used to deposit the film directly, which means the overall process has reduced from seven steps per pattern layer to ideally a single step. This leads to reduced capital expenditure where the cost per unit area of printed electronic is expected to be one to three orders of magnitude less than the cost per unit area of photolithography process. However printing electronics are attractive as a means of fabricating electronic system with low functional density, where the high performance of conventional electronics is not required. It

opens a new world of low-cost printed circuits based on conductive, semiconductive and dielectric printed materials aiming at high-volume market segments.

While traditional printing processes are applied, the main cost consumptions in printing electronics are inks used to produce the electronic components. The innovations in materials to enable printing depend mainly on the advance of material science that can produce functional inks. Among the broad printed electronic technologies; there are various techniques for producing conductive components as shown in table 2.1. The inkjet is one of them and will be discussed in more details in Section 2.2.

Table 2.1 Comparison of technologies of printed electronics for conductive features [6]

Printing technology	Advantages	Disadvantages
Screen Printing	• Set up technology and inks for printed electronic • Low-cost equipment and inks	• Expensive due to amount of needed material
Inkjet	• Printing thin films and fine features • Manageable to prototyping • Digital customization • Individual design of equipment for electronics • Non-contact method	• Low throughput • Complex system
Gravure	• High speed • High definition of printed features • Possibility of printing on various substrates	• High set-up costs
Flexography	• Lower technology costs than gravure printing • Relatively good resolution	• Instead of printing a dot it prints a ‘donut’ • Exposed to ‘halos’ effect • Possible inconsistent release of ink.
Offset Lithography	• High throughput • High resolution	• Thickness limited to less than 1 μm • Additives used in graphics printing might negatively affect electronic painting
Pad Printing	• Possible printing of irregular • Configurations	• Low throughput • Not a large scale process
Spin Coating	• Easy experiments set up for testing basic properties • Non- contact method	• Poor resolution • Not a commercial scale process for printed electronics.

2.1.2 Application of printed electronics

Printed electronics utilise liquid source of electrically active materials that can be used as a conductors, semiconductors, and other functional materials. Flexible displays are one of the promising applications of printed electronics. They are light weight and have high mechanical reliability. Electronic printing can be utilized for obtaining display elements, such as:

- Liquid crystals displays (LCDS)

By using small organic molecules liquid crystal displays make use of a light switch implemented [7].

- Organic light emitting diodes (LEDs)

Polymer LEDs (PLEDs) are diodes with light-emitting polymer sandwiches [8]. When current flows through the diode, electrons and holes recombine in order to emit a light [9]. The advantage of PLEDs is that it possesses much simpler structure than LCDs.

- Electrophoretic displays

Sometimes called e-paper [10]. Applied external voltage to the cell causes the up and down movement (depending on the voltage polarity) of particles resulting in light and dark appearance of the cell. They are potentially very compatible with printed transistors, since only low current driving is required, as the cells do not emit the light.

- Printed radio-frequency identification (RFID) tags

Silicon based RFID are used in many applications, including management, inventory, security and transit [11].

- Printed sensors [11]
- Printed transistors [12]
- Printed semiconductors [13]
- Printed dielectrics [14]

2.2 Inkjet printing technology

Inkjet printing is a technique where inks are printed only at the locations where they are desired. It is a non-contact process where the thin or thick structures under computer control are created [15-17]. Since it is a non-contact method, the material contamination possibly produced in contact deposition is reduced. It is easy to change the pattern design without the use of expensive masks used in the case of screen printing. This results in a fast and cost effective prototyping process. In addition, since the material is deposited only when and where it is needed the wastage of material is very low. In the continuing demand for finer feature sizes the inkjet printing has emerged as an attractive option for bridging the gap between high resolution (1 μm and below) which is likely to remain the province of conventional lithography, and the ~100 μm resolution achievable with for example screen printing.

Recently inkjet printing technology has been used to fabricate polymeric electroluminescence devices, controlled-release drug delivery devices, and refractive micro lenses made of hybrid organic- inorganic materials [18-20].

Developing material is the main challenge of printing electronics since various conditions of the printing process have to be met, like low temperature deposition, high throughput, interplay with other layers including compatibility of printed layers in terms of wetting, adhesion and dissolving as well as drying procedures after deposition of liquid layers, all having a large influence on the device performance. The main requirement of printed materials, besides actual electronic functionality, is their processability in liquid form, i.e. solution, dispersion or suspension. Typically inorganic materials used for printing are dispersion of metallic micro and nano particles, e.g. silver, gold or copper particles in a retaining matrix.

2.2.1 Process

Two different categories of ink jet printer exist and they can be distinguished depending on the ink delivery mode: continuous and drop-on-demand (DoD) [15, 16, 21] and this is further divided into subgroups (figure 2.1).

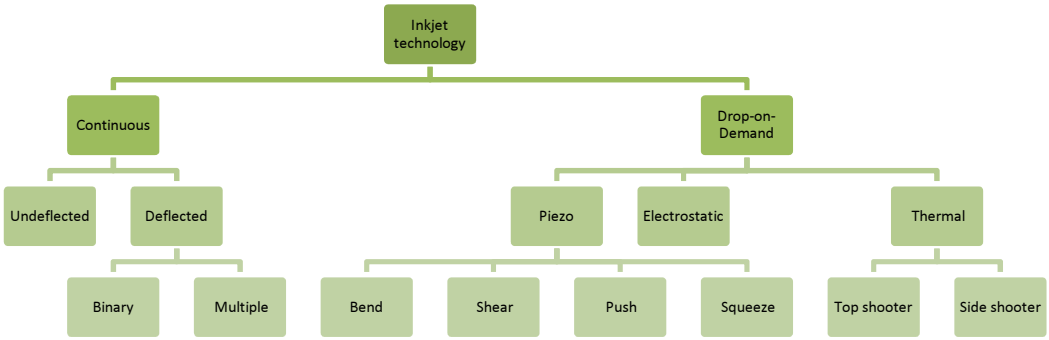

Figure 2.1 Classifications of inkjet printing techniques, adapted from [22]

Continuous mode

In order to force ink to pass through an orifice forming a jet at the outlet high pressure is applied. The ink flow breaks up into single droplets that are initially charged by electrodes and then deflected by deflecting plates to be settled at desired positions [22]. The ink must be conductive as the droplet deposition on the substrate is controlled by the charge of the functional material in the ink and plate charge [23]. The formed drops are uniform and with a size approximately double that of the orifice diameter in a range of 20-150 µm [24, 25].

Compared to DoD technology, this technique offers a higher speed process and allows large areas to be patterned in shorter periods of time [26]. Figure 2.2 schematically represents a continuous mode printer in inkjet printing process.

.

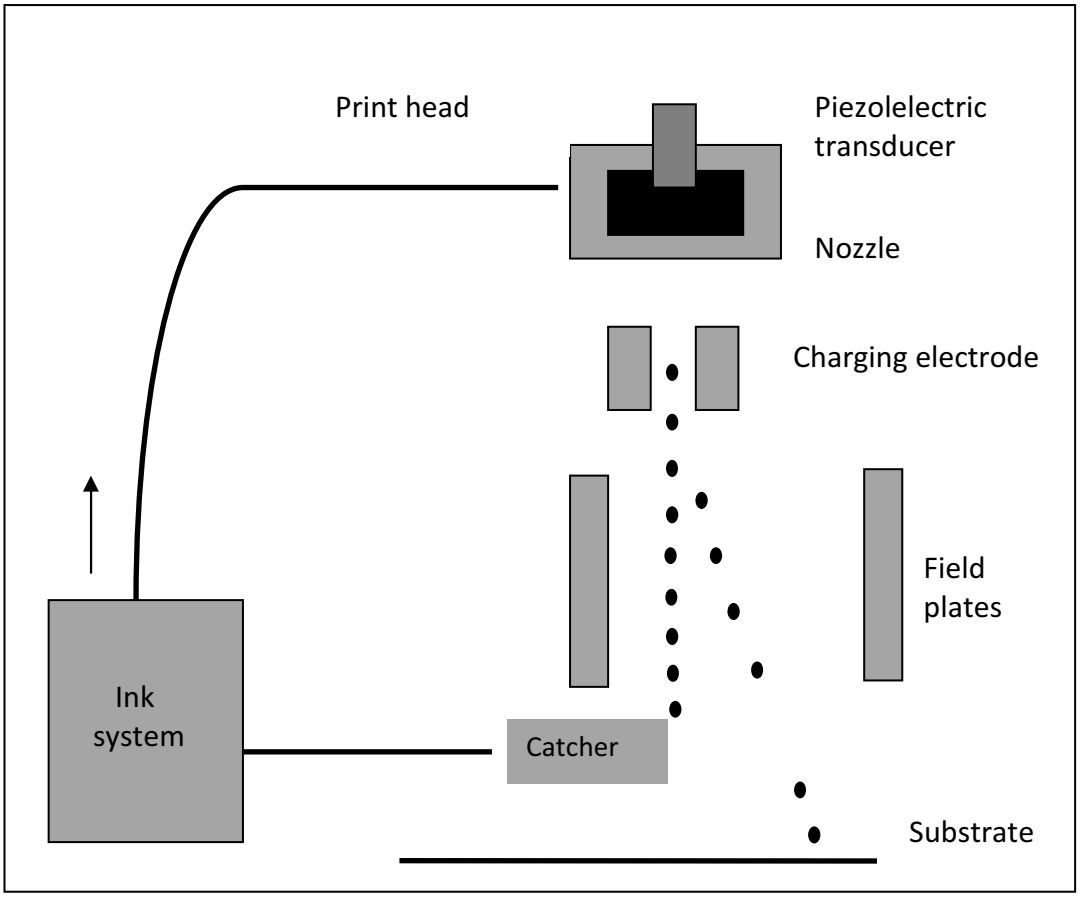

Figure 2.2 Schematic diagram of continuous inkjet printer

Drop- on-demand mode

In DoD mode the droplets are ejected only when required. As with the continuous method, DoD is a non contact method. The droplet deposition on the substrate is controlled by the movement of the printhead across it [21]. When a voltage is applied, the piezoelectric material changes shape, which generates a pressure wave in the fluid forcing a droplet of ink to be ejected from the nozzle [15, 26]. A schematic representation of a DoD printer is shown in figure 2.3.

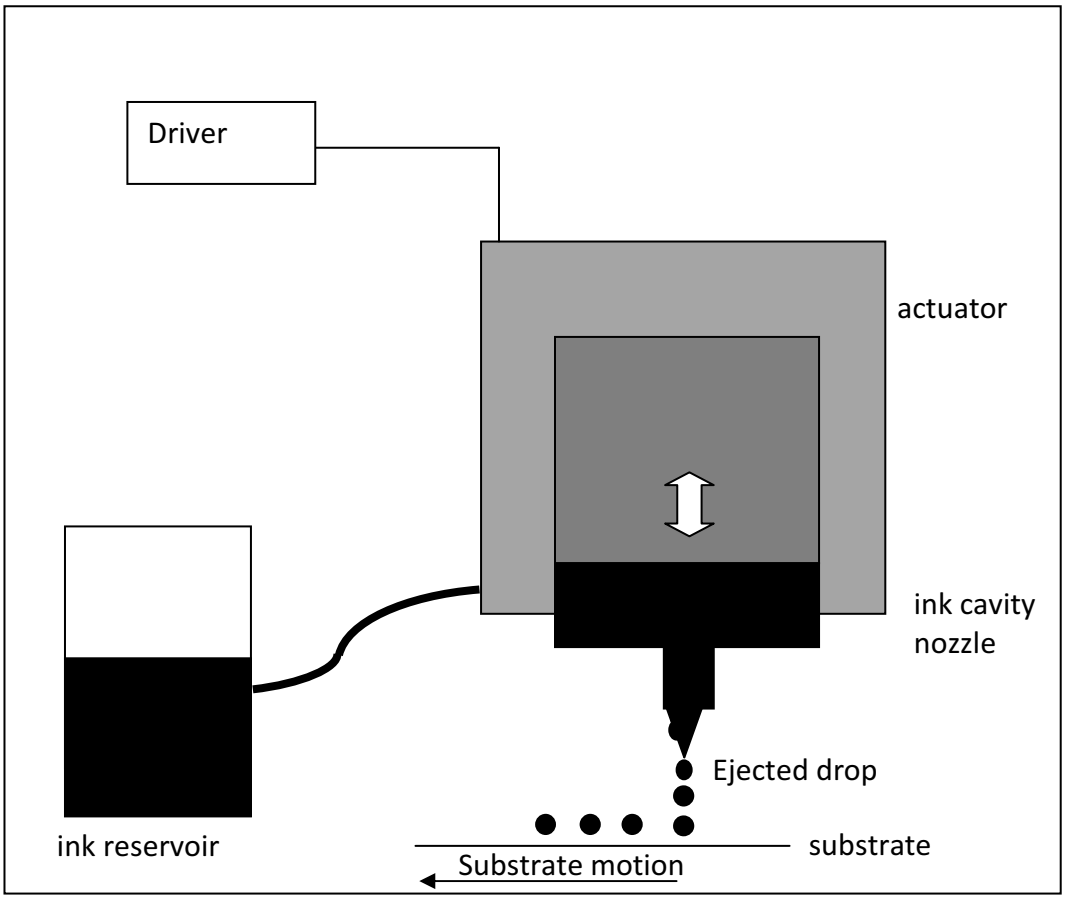

Figure 2.3 Schematic picture of a drop-on-demand ink jet printer

In piezoelectric inkjet, a piezoelectric element changes its shape as a result of an electronic pulse, inducing a mechanical pressure to a small amount of ink that will as a consequence be forced out of the printing nozzle. Respectively, in the continuous inkjet, a constant pressure is applied to the ink, producing a continuous flow of ink that is then controlled to produce differently sized ink droplets. Typically, the droplet sizes in inkjet printing are in the scale of 50 μm - 60 μm and the obtained resolution scan exceed 1400 dots per inch in home-market printers.

2.2.2 Working principle of piezoelectric printheads

When an electrical field is applied between opposite surfaces of piezo-ceramic plate, a pressure wave is induced into a fluid resulting in droplet formation and its emission from the

nozzle [27, 28]. The act of the pressure wave is to overcome the surface tension of the fluid retained at the orifice and to expel a stream of liquid from the nozzle. Typical print frequencies of DoD printers are in the range of 0.1 to 30 kHz. When a voltage is applied to the piezoelectric element, which is usually made from lead zirconate titanate, it expands and a pressure wave travels via the ink in nozzle and reservoir directions. A nozzle might be considered as a closed end due to its small diameter compared to the tube diameter, while reservoir acts as an open end. In this case, the pressure wave that arrives at the nozzle orifice is conserved and inversed when arriving at the reservoir [28]. The positive pressure wave is amplified by the driving waveform to get a large positive pressure peak at the nozzle, which consequently fires a drop. The reflection and propagation of acoustic pressure waves depend on the printhead design, nozzle orifice diameter, and properties of the materials.

The trapezoidal driving waveform, shown in figure 2.4 represents a typical waveform which is composed of voltage rising time t_r, dwell time t_d and voltage falling time t_f. It is substantial for successful droplet ejection to find a balance between the applied voltage over the piezoelectric element and the duration of the pulse [28].

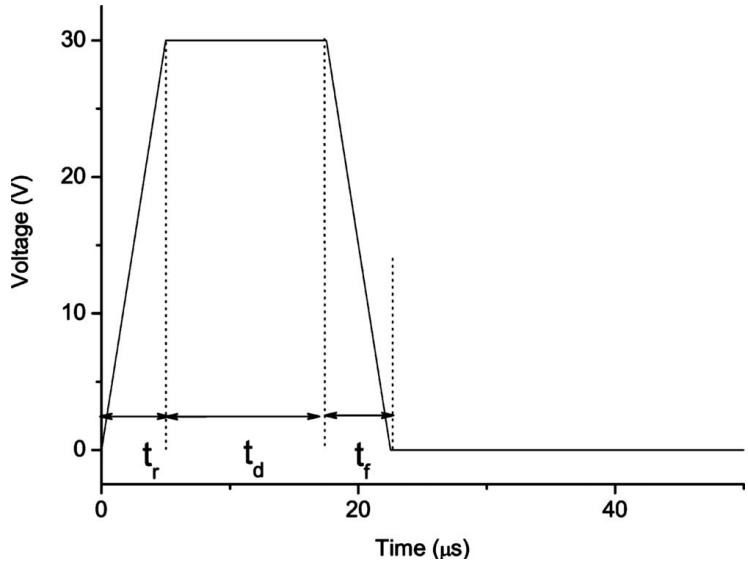

Figure 2.4 Typical waveform with settings of voltage and pulse width, taken from [29]

The settings of both, voltage and pulse width, have a large effect on the formation of a droplet. A minimum of voltage is necessary for droplet ejection. With larger voltage amplitude, a larger volume change of the piezoelectric element in the same amount of time is caused and a larger pressure wave is induced. As a result, an ejected droplet is larger in volume due to stronger fluid accelerations. The frequency is the rate at which the waveform, pictured in figure 2.4, is repeated and has a strong influence on the velocity of the ejected droplet [29]. Since the frequency affects the acoustic wave speed, it depends on the fluid properties, particularly its viscous properties [6].

2.2.3 Trends and challenges [6]

The pace of innovation in industrial inkjet is very fast. Increasing the print resolution, by decreasing the size of the drops and improving their accurately placing, was the main focus in the past. Current attention is directed to:

- Increase the jetting speed
- Improve printhead reliability (i.e., less nozzle clogging)
- Expand post processing techniques
- Achieving unique rheological behaviour of the ink
- Enhance the productivity

The smaller size of the printed feature enables the use of inkjet printing in functional application such as printed electronics [30-32]. It is much desired to develop technology that can produce small drop size, below 10 μm.

With reducing the size of the drops, their surface tension increases. In order to overcome this effect, the energy needed to eject them from the nozzle needs to be increased. Moreover, as a droplet gets smaller; its surface area to mass ratio becomes bigger and faster

deceleration is required that consequently reduces the flight path of the drop**.** To make it successful, the great deal of effort is going into designing print head and ink formulation.

Today, the smallest droplet size, possible to obtain is 20-50 μm in laboratory settings [31]. Decreasing the nozzle diameter in order to obtain a smaller size of the drop jet allowed inseparably integrate optimisation of the ink formulation and matching the ink – substrate complex.

Facilitating the adoption of inkjet technology is to increase the range of jettable fluids, such as pigment textile inks, ceramic inks, metallic nanoparticles inks, and of three dimensional (3D) plastic structures. That might be done by improving the physical properties of the ink.

Inkjet printing must be considered as a complete system, bringing together a number of disciplines, such as material science, engineering, software, and electronics. The main challenges apply to feature size, resolution, and productivity, and drop placement accuracy. Since there is no such a thing like a universal ink, number of ink's properties have to be taken into account, namely, functionality, print quality, drying time, adhesion, and jetting characteristic including viscosity, surface tension, particle size, and stability. Reducing the feature size might be achieved by joining the effect of surface treatment of the substrate and obtaining the unique rheology behaviour of the ink.

Accuracy of drop placement is still uncertain. To improve that, a number of factors have to be considered, such as jet-to-jet variation, sensitivity to nozzle straightness, nozzle and surface wetting, nozzle plate contamination, ink formulation, drop velocity, and ambient air flow.

2.3 Electrically conductive inks: preparation, requirements and properties

In inkjet printing technology, the major challenge is the ink formulation. Reducing the particle size to 50 nm or less is believed to improve image quality, resolution, and printhead reliability [30]. In order to achieve optimal performance and reliability of the printing system and to obtain the best printed pattern, the inks have to meet strict physicochemical properties (viscosity, surface tension, adhesion to a substrate, etc.). Typical ink suitable for inkjet printing has viscosity between 1 and 30 mPa s. Inks should behave as a true solvent (without component separation during high acceleration and to be stable at room temperature (for weeks without any sedimentation). The surface tension depends on the nature of the substrate that is going to be used. For the hydrophobic and hydrophilic substrates the surface tension varies between 25 Nm^{-1} to 50 Nm^{-1}.

In order to disperse particles and, at the same time, minimize nozzle clogging it is necessary to add a dispersing agent to the ink formulation. The amount of dispersant is a function of the effective surface area of the particles to be dispersed. For a given weight loading the effective surface area increases with the decrease of the particle size, and hence the larger the area to be covered by dispersant [6]. In other words, the smaller particles the more quantity of dispersant is needed.

In this section the basic matters that affect the overall performance of the ink will be discussed from the chemical point of view. That includes operation of the ink and its requirements and properties. As well as the ink properties after printing , since they are also to be taken into account while overall performance is considered, what is a desired structure of the film in terms of their physical strength and toughness, the adhesion attribute and the surface properties of printed features are discussed here.

2.3.1 Ink formulation

There are two major techniques used to produce nanofluids: the single-step method and the two-step method. In the two-step process, the preparation of the nanoparticles and the preparation of the nanofluid are separated. First nanoparticles are synthesised and dried. After that they are dispersed in liquid under stirring or ultrasonic vibration. Various physical treatment techniques are employed, including a stirrer, an ultrasonic bath, an ultrasonic disruptor or a high-pressure homogenizer to prepare nanofluids [33]. The biggest problem in the two-step method is the tendency of individual particles to quickly agglomerate before complete dispersion can be achieved.

The one-step method is based on the synthesis of nanoparticles directly in the fluid. A few methods have been found in literatures for the preparation of nanofluids using one-step method, for example thermal decomposition of an organometalic precursor in the presence of stabiliser [34], chemical reduction [35], and wet grinding technology with bead mills [36].

Akoh et al. [37] developed the single-step direct evaporation approach, so called VEROS (Vacuum Evaporation onto a Running Oil Substrate) technique. Further modification of this method was proposed by Wagener et al. [38]. They used high pressure magnetron sputtering for the preparation of Ag and Fe suspensions. The particles prepared with this method were small (around 2.5 nm) and characterised by rather narrow size distribution compared for instance to those obtained with gas evaporated particles. However particles were oxidised to a high degree. Zhu et al. [39] presented a novel one-step chemical method employing microwave irradiation for preparing copper nanofluids by reducing $CuSO_4*5H_2O$ with $NaH_2PO_2*H_2O$ in ethylene glycol. An advantage of the technique is the narrow particle size distribution with the mean particle size up to 20 nm, while the disadvantage is that some residues from the reaction could be left in a reaction vessel affecting the later fluid's properties.

2.3.1.1 Powder

Powder determines the characteristics of the final product as it is the only material left after the removal of solvent and organic residues. Mainly silver nanoparticles and gold nanoparticles are used in conductive inks due to their low electrical resistivity and high chemical stability. Copper and nickel particles are less chemical stable and tend to oxidise easier than silver and gold. Although the price of carbon nanoparticles is low they are difficult to prepare in an industrial process and their resistivity is higher than metal particles.

When the diameter of a particle is reduced, the ratio of particle's surface to its volume increases. As a result many metallic nanoparticles show a dramatic reduction in melting point, thus opening up the use of a wider range of substrates, including lower-cost plastics. It has been shown that gold nanoparticles with size around 2 nm melt at 100 ºC while melting temperature for bulk gold is 1000 ºC [40]. Decrease in melting point is very important for conductivity of the printed films. The film formed using naoparticles might be annealed at very low temperature resulting in the particles to fuse together. The higher concentration of the particles in the ink the better contact between particles is achieved, which consequently leads to well packed printed particles. As a result, the conductivity of the film obtained with smaller particles becomes closer to that of bulk than with large particles. Nanoparticles ink has a number of advantages over micro scale particles ink. Nano-sized particles conductive inks can be ink-jetted, without the risk of clogging nozzles, thus saving both material costs and production runs.

In recent years, production of nanoparticles has been investigated. Nanoparticles with the size smaller than 100 nm are often extremely stable in colloidal suspension which makes them possible to load in high mass. However, a significant decrease in particle size leads to stronger agglomeration between themselves due to high density and extremely high surface energy which in practise increases the difficulty to produce highly concentrated stable

dispersions. Therefore it requires the development of new dispersion procedures, including selection of appropriate dispersants and tools to obtain long-term dispersion stability.

Various techniques have been developed to synthesize the nanoparticles and they are discussed in more details in section 2.4.1.

2.3.1.2 Dispersant

When the particles in nanosize are placed in a liquid medium, the colloidal forces are more significant than the gravity force. As a consequence, nanoparticles tend to cluster and agglomerate if they are not prevented to do so. Particle agglomeration causes the system to change to the one with fewer and larger particles. Hence, it is necessary to modify the surface of the particles so that the agglomeration can be delayed. In order to prevent agglomeration of particles in a liquid medium, dispersing agents are used. Dispersing agents increase the repulsive forces between the particles to overcome the Van der Waals attractive forces. Moreover, the dispersant can promote the breakage of the hard agglomerates since it affects the rheology of the dispersion [41-43]. In addition, the presence of dispersants in colloids decreases the amount of solvent needed and hence increase the solid loading. The selection of dispersant depends mainly on the properties of the solutions and particles. Xuan and Li [44] used salt to increase the stability of transformer oil-Cu and oleic acid for water-Cu nanofluids. Oleic acid and cetyltrimethylammonium bromide (CTAB) surfactants were used to ensure better stability and proper dispersion of TiO_2-water nanofluids by Murshed et al. [45]. Hwang et al. [46] used sodium dodecyl sulfate (SDS) for the preparation of water-based multi-walled carbon nanotube. Common dispersants reported in literature to formulate stable Ag inks, include poly (*N*-vinyl-2-pyrrolidone (PVP) and polyelectrolyte [47]. It is a nature of the particles to be dispersed as well as the solvent that decides which dispersant will work the best in a given environment.

F127, a triblock co-polymer consisting of poly(ethylene oxide) (PEO)–poly(propylene oxide) (PPO)-poly(ethylene oxide) (PEO) segments arranged in an ABA structure, was for the first time used in the preparation of silver suspensions in the present research work. F127 micelles have demonstrated to enable encapsulating hydrophobic Fe_2O_3 nanoparticles inside their PPO cores and simutaneously the surface of the encapsulated nanoparticles was intrinsically covered by a layer of free PEO chains, which enabled the Fe_2O_3 particles to be colloidally stable [48]. Angelescu et al. [49] employed F127 as capping agent for the synthesis of Ag nanoparticles showing its good stabilising properties. They suggested that both moieties (PEO and PPO) may attach to the surface of the Ag particles, and as the entity, adopts several conformations. Firstly, the extended conformation of F127 along the surface takes place at the initial interaction with the Ag particles. The adsorbed polymer is subsequently replaced by the new polymers resulting in brush-like conformation which consists of entrenched PPO moiety on the Ag surface and stretched chains of PEO in the solution. Secondly and conversely, a polymeric hemi-micelle is formed when PEO chains are attached to the surface and PEO moieties exhibit hydrophobic interaction. From the kinetic point of view, such a surface coverage restrains adhesion of the particles due to the formed layer of trailing chains which is unfavourably compressed by the approaching particles [49].

2.3.1.3 Solvent

Traditionally organic solvents are chosen for the ink formulation, mainly due to their low cost and good compatibility with most of substrates due to low surface tension and being quickly dry on the surfaces. However in the use of organic solvents may cause the environmental problems in realistic industrial applications due to their high volatility. Additionally, due to being fast drying, the fluid can very easily block the print head nozzles. Most used solvents for silver ink preparation are toluene, tetradecane, and alfa-terpineol [50-52].

In more recent times techniques to cast water-based inks have been developed as an alternative [53, 54]. The advantage of using water-based inks is their low cost, environmental and healthy aspects, as well as easy attainment. However, the presence of water increases the surface tension of the ink which might decrease the adhesion to the substrate. Usually, additives such as wetting agent or treatment of the substrates are required to adjust the wetting properties of the ink to the substrate.

2.3.1.4 Dispersive techniques

Particle size reduction and their dispersion can be achieved with various techniques, such as ball milling or ultrasound methods. A ball milling technique consists of rolling a container containing the fluid and milling media (normally spherical ceramic balls). During rolling, the balls crush the powder and the energy of the impact breaks the agglomerates of the powder. Ultrasonic waves can be generated in a liquid suspension in two ways. The first, direct sonication is based on immersing an ultrasound probe into the suspension, reducing the physical barriers to delivering the power to the dispersion. In the second way, indirect sonication, the ultrasonic waves are propagated through a bath containing a liquid before they reach the sample container. Direct sonication is better than indirect sonication when the dispersing of dry powders is considered, as it yields a higher effective energy output into the suspension. Indirect sonication can be used to re-suspend the powder which has been pre-processed via direct sonication, or for particles that may be subject to unintended damage under direct sonication (e.g., cleavage of single wall carbon nanotubes). The total amount of energy (E) delivered to a suspension depends on the applied power (P) as well as on the total amount of time (t) that the suspension is subject to the ultrasonic treatment (equation (2.1)).

$$E = P\,t. \tag{2.1}$$

As a result, two suspensions treated for different times at the same power can show significantly different dispersion states. For a given system, optimal sonication conditions

must be determined by estimating the effect of a variety of sonication parameters on the dispersion state [55].

A new technique for ink dispersion is High Intensity Focused Ultrasound (HIFU) (figure 2.5), so far broadly used in medicine for cancer treatment, however in the present work, for the first time, it was used for ink preparation. The basic function of HIFU is disaggregation of particles, which is achieved by depositing large amounts of energy into the particle solution. The focused ultrasound is produced using a high power piezo-electric (lead zirconate titanate (PZT)) material (transducer) generating high frequency vibrations (750 kHz). HIFU introduces several novel aspects: (1) The high amplitude (up to 10^8 Pa) and frequency (~10^6 Hz) mean that as a beam propagates, it deforms, and can develop a "shock" wave front, i.e. the non-linear propagation effects; (2) Since the frequency of ultrasound is increased from ~10^4 Hz to ~10^6 Hz, the threshold value of strong micro scale transient cavitations is significantly increased. Therefore, the immense temperatures (approx. 5,000K) and pressures (approx. 2,000 atm) generated by cavitation bubble collapse could be alleviated. There's no distinct temperature increase at all [56]; (3) It avoids the possible contamination to the fluid due to bead breakage during ball milling and the prolonged ball milling process.

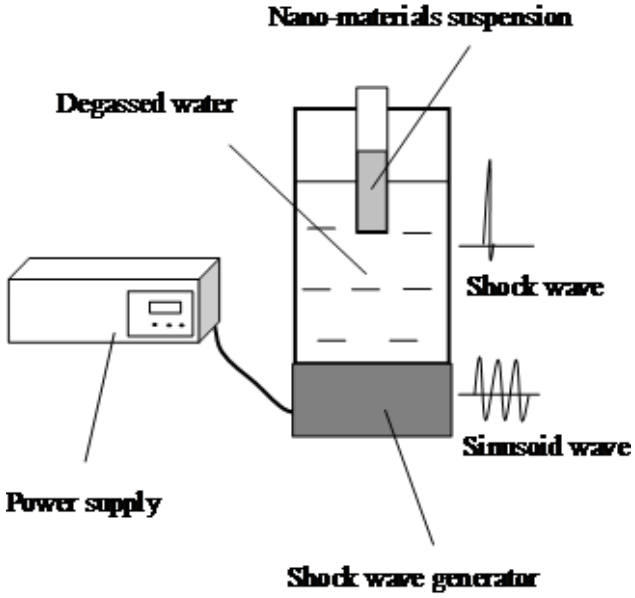

Figure 2.5 Sketch of HIFU method [56]

2.3.2 Dispersion characterisation

2.3.2.1 Rheological properties of nanfluids

Rheology is the study of the flow and deformation of matter under conditions of applied force [57]. The study of the rheological properties of the particle suspension is needed to understand their behaviour, to optimize dispersant amount needed for good particles stabilisation, it is also helpful to understand the ideal processing condition for inkjet printing.

The pioneers in the study of rheology are Newton and Hooke. Hooke observed that in a perfect elastic solid, the material deforms under the applied forces and it relaxes when the force is removed. The stored energy in the deformation perfectly returned during the relaxation. This phenomenon represents the elastic behaviour.

In Newtonian viscous fluid, deformation results in flow when the force is removed. Here, the energy is completely consumed as heat and this represents the viscous behaviour.

Kelvin and Maxwell proposed the theory which defines the behaviour of materials with both the elastic and viscous characters.

Figure 2.6 summarizes the categories of materials when a stress is applied at a time t_0. Deborah number (De) is a ratio of relaxation time (τ) and the experiment time t_0 (equation 2.2), which influence the behaviour of the fluid.

$$De = \tau / t_0 \tag{2.2}$$

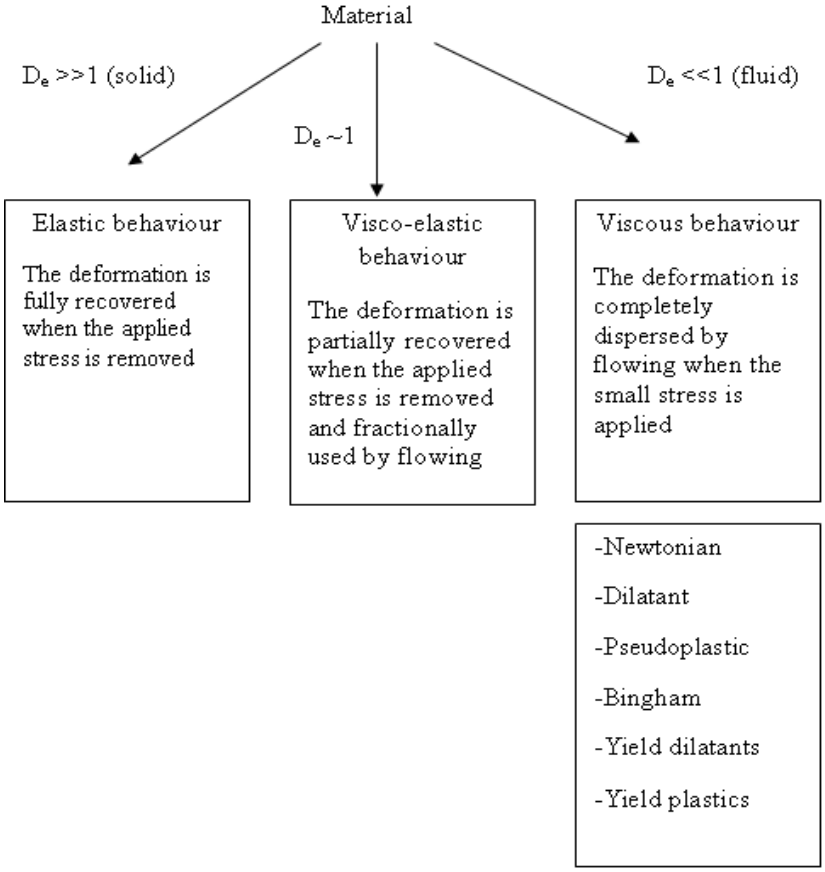

Figure 2.6 Classification of rheological behaviour of matter

The study of viscous materials (De<<1)

All fluids due to frictional forces between the molecules display a certain flow resistance which can be measured as a viscosity [58, 59]. Viscosity (η in Pa s) is a property of suspension which is being deformed by shear stress (σ in Pa).

$$\eta = \sigma / \dot{\gamma} \tag{2.3}$$

Where $\dot{\gamma}$ is the shear rate (in s^{-1}) and it is defined as the speed of the deformation:

$$\gamma = dy / dt \tag{2.4}$$

The shear stress is defined as:

$$\sigma = F / A \tag{2.5}$$

Where, F is the amount of force applied to the sample over a certain area (A).

To measure the viscosity of dispersion a rotational viscometer is used. The instrument can work either, in control of the input stress, or of the obtained stress. Two main parts form a viscometer, one of which is rotated, and the other stationary. The stress produced in a sample by the part in motion and is transmitted to the stationary one, at the end is recorded.

The most used geometries of the viscometer's part are, so called 'cup and bob' and the 'cone and plate' (figure 2.7). It is possible to measure the viscosity with different time, shear stress or shear rate.

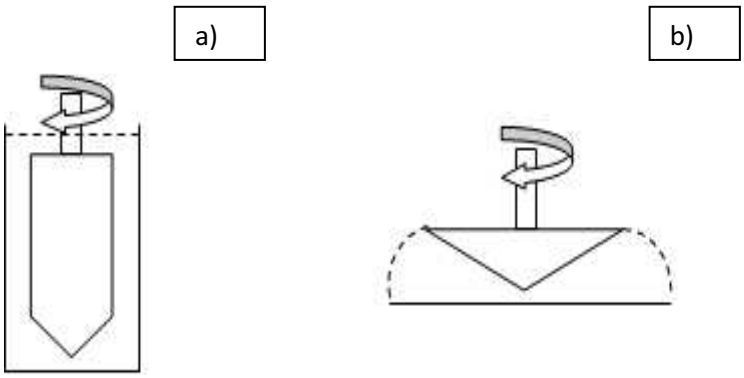

Figure 2.7 a) Cup and bob and b) cone and plate configurations

The flow behaviour of the fluid might be governed by complex interaction including hydrodynamic interaction between solid particles and the fluid, the attractive and repulsive force between the solid particles and the particle-particle interactions. The fluid can be classified as a Newtonian fluid or Non-Newtonian.

Newtonian flow behaviour

A fluid is said to be Newtonian if its viscosity remains constant with an increase in shear rate. Usually this kind of behaviour is observed in low molecular liquids such as, water or mineral oils. However, the presence of suspended nanoparticles is expected to cause more complex behaviour.

Non-Newtonian flow behaviour

When the viscosity of the fluid changes with an increase in share rate, the fluids are referred to as Non-Newtonian. There is a further classification of these fluids into shear-thinning and shear-thickening flow behaviour.

Shear thinning behaviour

In this case the shear viscosity decreases with an increase in shear stress. This behaviour can be explained by a gradual change from a disordered to an ordered structure while a shear rate is increased. When the stress exceeding a yield value is applied, the aggregated structure is broken into smaller pieces and shear becomes easier resulting in lower viscosity. As the attractive forces will tend to dominate bringing back the original aggregates structure, the apparent viscosity measured is the balance of the shear forces and the attractive forces. At a very small shear rate the Brownian movements of the particles dominate and the system is in disorder. With increasing the shear rate, the Brownian movements lose their importance as the particles will rearrange following the flow and at the sufficiently high shear rate, the viscosity will not vary considerably with shear rate. The plateau will be reached.

Shear thickening flow behaviour

In the phenomenon of shear thickening, the viscosity of the sample increases with an increase in shear stress. This can be explained by the fact that at low shear rate, the particles are kept in a layered, closely packed structure where the viscous shear forces are weaker than the

repulsive forces. With increasing the shear rate the layer structure will be destroyed and as a result more and more particles collision will occur. This friction creates a resistance to flow which is measured as higher viscosity.

Figure 2.8 presents the summary of the rheology behaviour of a suspension resulting from interactions of their particles.

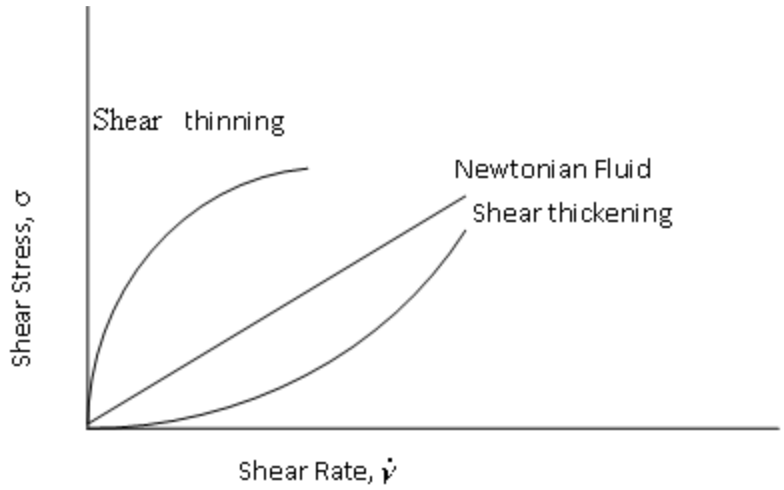

Figure 2.8 Rheological behaviour of suspension

Rheological measurements can provide some information about aggregation in dispersion. The rheological yield values reveal the strength of the agglomerations which can be damaged by shear. The viscosity is related to the volume of the fluid which aggregate**s at the shear rate used. The rheology behaviour of a suspension is influenced by particle interaction, particle concentration, particle size distribution, particle morphology, and properties of the medium. The higher volume content of powder in a suspension the more particle interaction becomes an important factor influencing viscosity. When the particles agglomerates trap some liquid the suspension behaves like it has apparent higher solid content. Hence it is possible to use the viscosity measurement to determinate the best amount of dispersant to be added to a suspension. With the increasing concentration of dispersant the** viscosity of the dispersion usually decreases up to certain concentration followed by increasing viscosity above that concentration.

Influence of the particles content on viscosity

Einstein's [59] theory of the relative viscosity (η/ηs) for small, spherical, monosized particles, at very low concentration, highlights the importance of the volume fraction of the particles in influencing the viscosity.

$$(\eta/\eta_s) = 1+2.5\ \varphi \tag{2.6}$$

Where η is the viscosity of the suspension, η_s is the viscosity of the pure medium (at zero particles concentration), and φ is the volume fraction of particles. At the very low concentration of particles the particle/medium interactions are important. As the forces act on the upper and the lower hemisphere of the particle the spherical particle rotates with the same velocity as the medium flow velocity. The rotation will be resisted by viscous forces round the surface of the particles. As the overall flow is kept constant the stress must be increased, hence the viscosity is increased by the added particles. The viscosity change might be caused by increased interaction between particles when their concentration is enhanced in a suspension. Krieger-Dougherty in equation (2.6) shows that for spherical particles the rheological properties of the suspension are directly related to the volume occupied by the particles [60, 61].

$$\eta=[1-(\varphi/\varphi_m)]^{-[\eta]} \tag{2.7}$$

Where φ is the volume concentration of particles in the dispersion, φ_m the maximum packing fraction, which is 63% for random close packing, [η] is the intrinsic viscosity, or effective hydrodynamic shape factor, which for spherical particles is equal to 2.5.

From the Krieger-Dougherty equation the viscosity of the nanoparticle suspension can be calculated if the viscosity of the medium and the concentration of the particles are known, and the maximum packing of the particles is determined.

2.3.2.2 Surface tension

The surface tension plays an important role in any droplet creation technique including inkjet printing. The ink suited for inkjet printing should have appropriate viscosity and surface tension in order to facilitate drop formation.

Surface tension is a property of the surface of a liquid and is caused by cohesion energy (the attraction of molecules to like molecules) present at an interface. The interactions of a molecule in the bulk liquid are balanced by equal attractive forces and each molecule is bound with a characteristic binding energy in all directions. The liquid phase of the molecules on the surface is replaced by air that gives weak interaction due to the low density of the air. The interactions of molecules with the air are significant and hence binding energy is reduced. As a result the presence of free energy at the surface is observed. The excess energy is called surface free energy which is equal to the number of missing bonds multiplied by the binding energy per bond [61].

Surface tension *(γ)* is defined as the ratio of the surface force *(F)* to the length *(d)* along which the force acts:

$$\gamma = F/d \tag{2.8}$$

The chemical composition of the fluids is an important factor to determine its surface and interface tension. Water and other polar liquids have strong intermolecular interactions and consequently high surface tension. Water has the highest surface tension (because of the hydrogen bonding), hydrocarbons have lower and fluorinated fluids have the lowest surface tension (as the fluorine atom does not share electrons very well).

Principles of the surface tension measurement:

In the stalagmometric method, the liquid's drops are produced from a thin glass pipette under a little pressure. They are all in spherical shape and grow up to the same size. The force that causes the particle to come away is its weight (P), while the force that let the drop stay at the

outlet of the pipe is a particle's surface tension. Initially the force comes from the weight of the drop is lower than the force that comes from a particle's surface tension and the particles stays at the outlet. As the particle's size grows the weight of the drop increases and becomes equal to the surface tension forces resulting in broke away from the pipette under the influence of gravity.

The surface tension (Γ) of liquid can be calculated from the equation 2.9.

$$\Gamma = \gamma_1 * m_2/m_1 \quad (2.9)$$

Where, γ_1 is surface tension of water [$72*10^{-3}$ mN/m], m_1 mass of water's drop at break-away and m_2 mass of measured liquid's drop at break-away, respectively.

2.3.2.3 Stability

Preparation of stable fluids is a key matter in nanofluid research. Stability of nanofluids concerns a few aspects [61],

- *Thermodynamic stability.*

Since nanofluids are multi-phase systems with high surfaces energies, they are thermodynamic unstable.

- *Kinetic stability*

Nanoparticles in the nanofluids possess strong Brownian motions. Nanoparticles mobility can compensate the sedimentation caused by the gravitation.

- *Dispersion stability*.

Because those nanoparticles can form aggregates, their dispersion in fluid may worsen with time.

- *Chemical stability*

No chemical reactions either between nanoparticles and base fluid or nanoparticles themselves are desired.

Three kinds of forces act on the suspended particles in the liquid: gravitational force, tending to settle or raise particles depending on their density relative to the solvent; a viscous drag force which arises as a resistance to motion, and the kinetic energy of particles which causes Brownian motion. For spherical particle of radius *r* the viscous drag force must be equal to the gravitational force thus the settling velocity, *V*, the viscous drag force is given by:

$$F_{drag} = 6\pi rV\eta = 4\pi r^3 g(\rho_p - \rho_L)/3 = F_{gravity} \quad (2.10)$$

where, η is the viscosity of the water, ρ_P is the density of the particles and ρ_L is the density of the medium and g is the acceleration rate of the gravity. Clearly, from those two forces acting on small particles, it will take a very long time to settle the particles and they will be stable. In fact, the third force caused by Brownian motion, together with the attractive and repulsive forces between particles determines the stability of the nanofluids. The speed of the Brownian motion can be characterised by mean displacement (x) and can be expressed with the equation (2.11).

$$x^2 = 2Dt \quad (2.11)$$

where *D* is the Einstein's Brownian diffusion coefficient and *t* is the diffusion time.

It is possible to express the diffusion coefficient with Einstein equation:

$$D = \frac{kT}{3\pi\eta r} \quad (2.12)$$

Where *k* is the Boltzman constant, *T* temperature, *η* viscosity of the medium, and *r* is the particle size. Based on equation (2.11) and (2.12), it can be said that displacement caused by Brownian motion increases with decreasing particles size and hence the nanoparticles tend to move around approaching other nanoparticles. The attractive forces between the particles will lead to their collision and cause the growth of large aggregates, which will consequently settle them out as, with particle growth, the gravitational forces start to dominate particle's

behaviour [62]. Although the Van der Waals forces acting between molecules will always act to coagulate dispersed colloids, it is possible to generate an opposing repulsive force of comparable strength. As smaller particles have higher surface energy that increases the possibility of the agglomeration of nanoparticles, they must be stabilized by surfactant or capping reagent in their dispersed medium [62].

The dispersion stability of the nanoparticles is determined by the interaction (attraction and repulsion) between the dispersed particles. The repulsion between particles comes from different sources. One is induced by the electrical double layer on the surface of the nanoparticles (electrostatic stabilization). Another might be caused by the adsorbed layer of polymer molecules on the surface of the particles (steric stabilisation).

2.3.2.3.1 Electrostatic stabilization

The intensity of the repulsion between the particles in electrostatic stabilization is determined by the magnitude of the surface charge. The particles in a dispersion medium are stabilized with the forces of electrical double layer; they acquire surface charge by the dissociation of surface groups or by the addition of an electrolyte which causes coagulation; a consequence of ion adsorption on the surface of particle. The development of this charge at the particle surface affects the distribution of ions in the surrounding interfacial region. The formation of an electrical double layer is a result of increase in the concentration of counter ions close to the surface of particle. The electrical double layer consists of two parts, first an inner region (Stern layer) where the ions are strongly bound and an outer (diffuse) region where they are less strongly associated (Gouy- Chapman layer). Within the diffuse layer there is a boundary inside which the ions and particles form a stable entity. When a particle moves, ions within the boundary move with it. The ions beyond the boundary stay with the bulk dispersant. The experimental estimation of potential at this boundary (surface of hydrodynamic shear or

slipping plane) is difficult and it is normally approximated with the electrokinetic potential in colloidal system (called zeta potential) (figure 2.9) [63, 64].

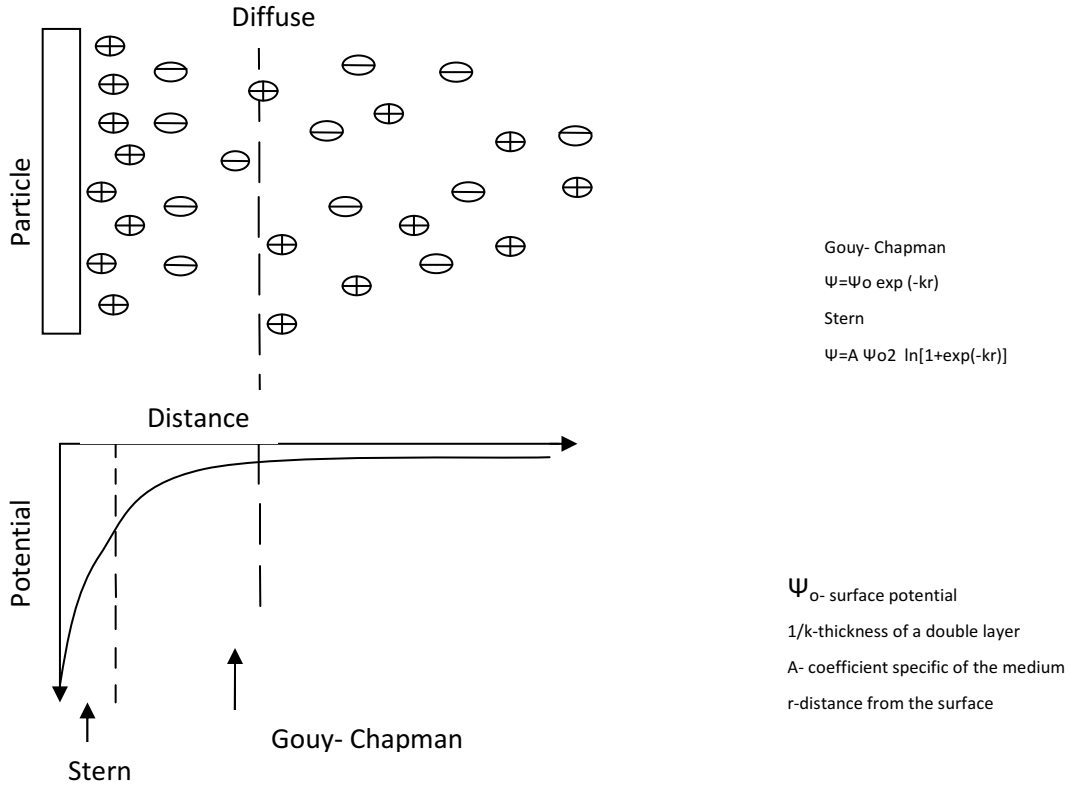

Figure 2.9 Schematic pictures of the diffusion double layer and potential profile according to the Gouy-Chapman and the Stern mode

The Derjaguin, Landau, Verwey and Overbeek (DLVO) theory

Using DLVO theory, it is possible to determinate the stability of suspensions and help predict long-term stability by means of the zeta potential [65-66]. When two charged particles in a dispersive medium approach each other, double electric layers overlap, the repulsion takes place as a result of increased ion concentration. The basis of DLVO is to use the sum of the repulsive force (V_R) and attractive (V_A - van der Waals forces) to calculate the particle interaction potential.

$$V_T = V_R + V_A \tag{2.13}$$

In figure 2.10 the total interaction potential (V_T) is plotted against the distance (r) between particles. Four curves are drawn referring to attractive and repulsive parts of the potential. Curve A shows the potential between particles when the repulsion forces are very small, hence the particles quickly collapse in a primary minimum. Curve B represents a maximum of potential which prevents the particles from coagulation in the primary minimum. A secondary minimum of this curve is an effect of weak flocculation. In curve C there is no primary minimum and the energetic barrier to get the secondary minimum is very high hence this case represents a stable system. Curve D outlines the system independent dispersion.

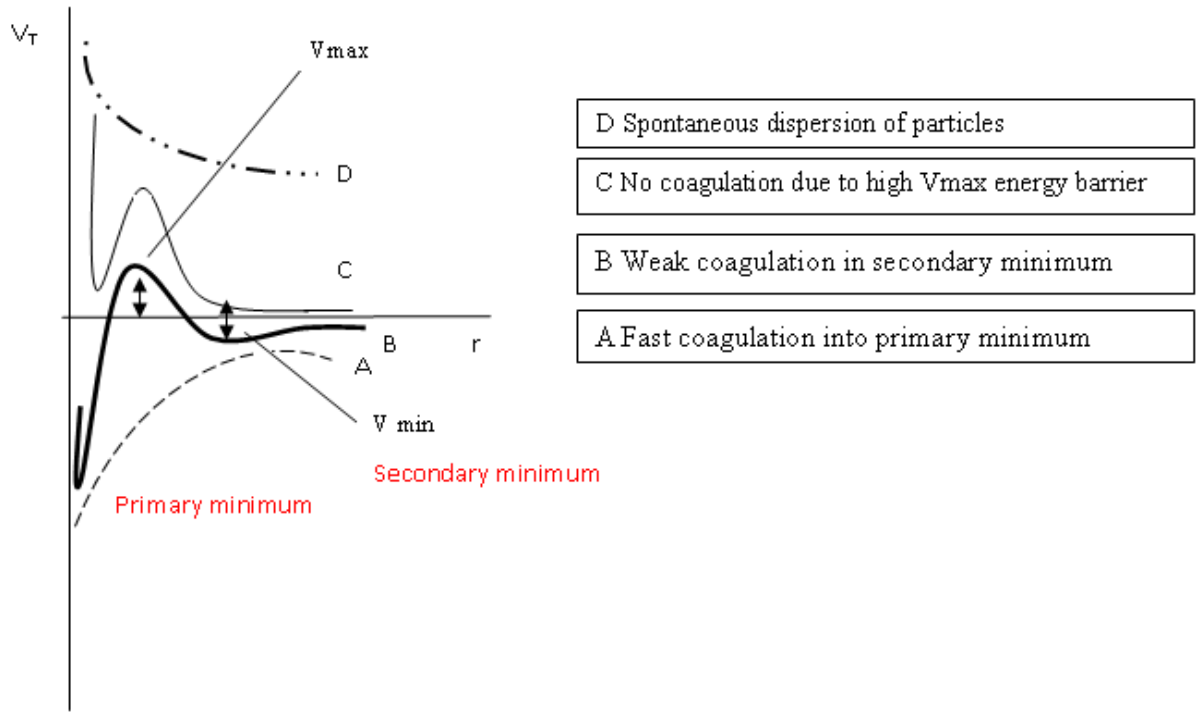

Figure 2.10 Potential energy versus particle distance, adapted from [66]

Decreasing the primary minimum and maximum will promote flocculation of particles. Practically, the greater the minimum, the stronger the cohesive tendency of the flocs and the higher the energy needed to break them down. The smaller the maximum, the easier the particles overcome its energy barrier, and fall into a minimum.

2.3.3 Steric stabilisation

Two mechanisms can be used to assure steric stabilization. The metal centre is surrounded by sterically bulky layers of material, such as polymer [67] or surfactant [68, 69], preventing the particles coming close enough for Van der Waals forces to cause irreversible attraction (see figure 2.11b) A non adsorbing polymer can be located among the particles preventing their aggregation (figure 2.11d). However the presence of polymers added to the dispersion medium can cause the flocculation when polymers do not completely cover the particles (figure 2.11a) and another case where non absorbing polymer can be evicted from the area between two surfaces, creating a gradient of concentration (figure 2.11c).

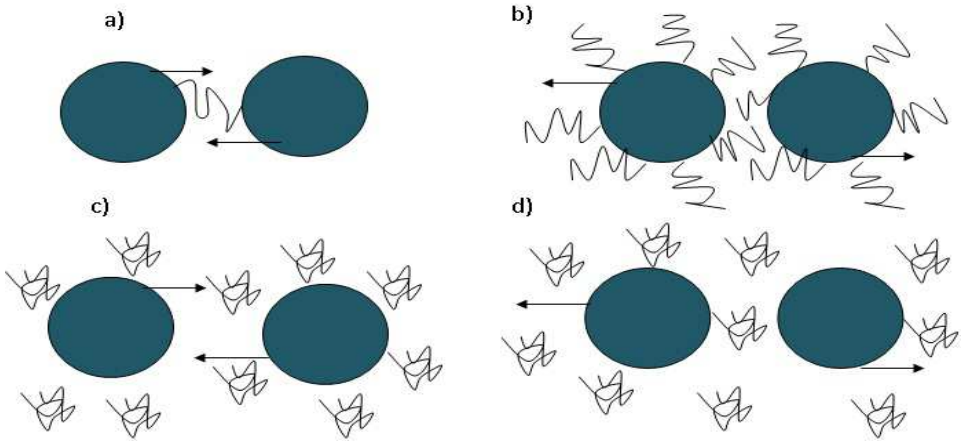

Figure 2.11 Schematic representation of polymer behaviour on the surface of particle: a) bridging flocculation, (b) steric stabilisation, (c) depletion flocculation, and (d) depletion stabilisation

2.3.4 Fluid dynamic

As it was mentioned before, the main concern for inkjet printing is that fluid must fit the physical and rheological requirements of fluid flow in the printhead, in order to be successfully ejected. In a piezoelectric inkjet printing process, the generation of drops is based on pressure wave that is electromechanically induced [70]. When a voltage is applied, the piezoelectric material changes shape, which generates a pressure wave in the fluid forcing a droplet of ink to be ejected from the nozzle. That happens only when the kinetic energy of the ink is sufficient to overcome the surface energy interactions.

If the viscosity of the ink is too high then a large pressure pulse is needed to generate a droplet. Whereas if the ink has very low surface tension, the printhead will generate the desired droplets accompanied with satellites, which reduces the resolution of the final as-printed features.

There are three dimensionless numbers, namely, the Reynolds (*Re*), the Weber (*We*) and the *Z* numbers (*Z*), which have been proved in recent studies [71] to be representative for analysis of a drop formation and to determine the possibility of the fluid to be ejected. The *Reynolds* number represents a dimensionless ratio of the inertial forces against the viscous stress within a droplet:

$$Re = \frac{\rho d v}{\eta} \tag{2.14}$$

Where ρ is the density, d the orifice diameter, v the velocity and η the viscosity of the droplet.

The *Weber* number is a dimensionless ratio of inertia forces versus the interfacial stress, describing the kinetic-surface energy conversion governed by both the speed of the jet and the surface tension:

$$We = \frac{\rho d v^2}{\gamma} \tag{2.15}$$

where γ is the surface tension of the liquid. Both numbers affect the droplet impact and spreading. Typically for inkjet print process, both the *Reynolds* and *Weber* numbers are

relatively low and in the order of 1-100, as the velocity and the size of the droplets are relatively small, which usually prevents splashing of the deposited droplets on the surface.

The *Z*-number, which is the inverse of the *Ohnesorge*number (*Oh*) can be written as a function of both dimensionless *Re* and *We* number:

$$Z = Oh^{-1} = \frac{Re}{\sqrt{We}} = \frac{\sqrt{\rho d v}}{\eta} \tag{2.16}$$

A droplet can be ejected by a DoD printer if Z is in the range 1-10 and that the droplet volume increases as the value of *Z* increases. The lower limit (Z < 1) is determined by the viscosity and usually high pressure is required to eject a droplet whereas the upper limit (Z > 10) represents the formation of satellite droplets [72] (figure2.12).

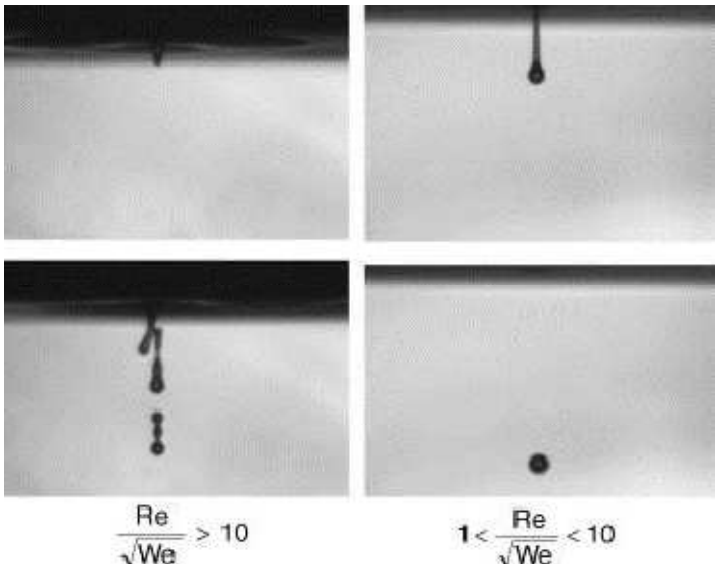

Figure 2.12 Images of ejected droplets of inks with Z > 10 (left) and 1 < Z< 10 (right). From [73]

2.3.5 Ink on substrate

2.3.5.1 Adhesion

Adhesion describes the work necessary to separate the atoms or molecules at the interface. Two surfaces can be held together by Van der Waals's forces, electrostatic forces or chemical bonding forces.

The surface tension of an ink and the surface energy of a substrate have a profound effect on the way in which the liquid wets the substrate and on the strength of the adhesive bond between the substrate and the dry film. If the surface tension of the ink is greater than the surface energy of the substrate then the fluid will not spread out forming a continuous film. Decreasing the surface tension of the ink (for example by adding a surfactant into a formula) will result in easier wetting of a substrate by an ink and consequently better adhesion. The surface energy is only one aspect of controlling the complex phenomenon that we refer to as adhesion. Adhesive testing involves the application of force to remove the film from the substrate. The aim is to measure the force needed to overcome the forces of adhesion between film and substrate. There are several methods of quantifying the adhesion of a film to a substrate. Mechanical method includes Scotch tape test [74], abrasion test [75] or stretch test [76]. In mechanical method adhesion is measured by applying a force to film-substrate system. The applied forces cause a mechanical stress at the interface, which on an appropriate level causes the removal of the film from the substrate [77]. The load at which a separation of film and substrate take place is called a critical load and is taken as a measure of adhesion [78].

2.3.5.2 Hardness

According to Braun a harness is the resistance to local non-homogeneous deformation caused by line-shaped force centres [79]. Hardness tests measure the resistance to damage with a specified amount of deformation, principally the deformation leading to damage. For film on a hard substrate, the resistance to deformation increases with decreasing layer thickness. This means, in order to measure an actual hardness of the film, the thicker film the better.

The purpose of the hardness testing is to analyse the behaviour of the film on the substrate subjected to practical conditions. The properties of the film will influence the performance of a device under various conditions.

The most common method for testing the mechanical properties is nanoidentation. The technique was developed in the mid-1970s and is based on subjecting the sample to forces, usually by the action of a hard tip whose mechanical properties are known. The load placed on the indenter tip is applying to the surface of the film at progressively greater load until the user-defined value. The area of the residual indentation in the material is measured and the hardness, *H*, is calculated from equation (2.16).

$$H=P_{max}/A_r \tag{2.17}$$

where P_{max} is a maximum load and A_r is a residual indentation area.

Hardness also can be defined as a function of depth. During a test, a load and depth of penetration can be measured, and then the area of the indent is determined using the known geometry of the indentation tip. These values can be plotted on a graph to create a load-displacement curves. These curves can be used to deduce mechanical properties of the sample.

2.3.5.3 Resistivity

The conventional technique

Electrical resistivity (ρ) is a measure of how strongly a material resists the flow of electrical current and it is the inverse of conductivity (σ). The following procedure is usually applied when the resistivity is to be evaluated. A conductive ink is printed in a simple pattern and then sintered at a given temperature. The next step involves the resistance measurement using a 4-point probe. The sample height (h) needed to calculate the resistivity is determined by direct measurement, for example using a microscopy or Dektak instrument. Finally the resistivity is calculated using equation (2.18).

$$\rho = RA/l \tag{2.18}$$

where *A* is the conductive cross-sectional area and *l* is the conductive path length. In the SI system, the unit of resistivity is the ohm*meter (Ωm).

The resistivity of pure metals at room temperature extends from 1.68×10^{-8} Ωm for silver, the best conductor, to 135×10^{-8} Ωm for manganese, the poorest pure metallic conductor. As the temperature decreases toward absolute zero, resistivity drops down to a very low residual value for some metals. At some temperature above absolute zero the resistivity of other metals suddenly changes to zero, and they become superconductors.

The resistivity values reported in literature for printed features using commercial silver based inks are higher than that of bulk silver. This can be due to incomplete particle-to–particle contact, residual porosity and a presence of organic additives.

The van der Pauw technique

The advantage of the van der Pauw (vdP) technique for resistivity measurements is that it allows to take a measurement without knowing exact sample geometry. Initially, the technique was developed in order to measure the resistivity and the sheet resistance of thin and flat samples of semiconductors, but it can also applied to the case of conductors.

Figure 2.13 shows an example of contact disposition on the edge of a sample in the van der Pauw technique. To make a measurement, a current flows along one edge of the sample (for instance, I_{AB}) and the voltage across the opposite edge (in this case, V_{CD}) is measured. Using equation (2.19) resistance of the sample can be calculated and later the resistivity is obtained from equation 2.21.

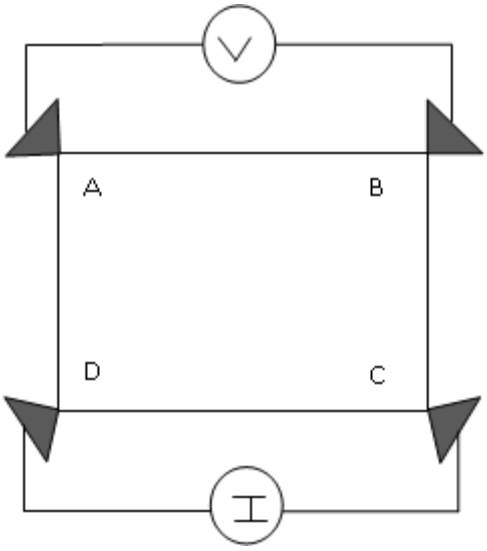

Figure 2.13 Example of contact disposition on the edge of a sample, in the van der Pauw technique

$$R_{AB,CD} = \frac{VoltageA-B}{CurrentC-D} \tag{2.19}$$

for a square printed area

$$R_{AB,CD} = R_{BC,\,DA} \tag{2.20}$$

and f = 1

$$\rho = \frac{\pi d}{ln\,2}\,(R_{AB,CD} + R_{BC,DA}/2)\,f\,(R_{AB,CD}/R_{BC,DA}). \tag{2.21}$$

where d is the film thickness.

L.J. van der Pauw [80] showed that the resistivity of a certain sample of arbitrary shape without knowing the current pattern can be determined when the following conditions are satisfied:

1. The sample must be homogeneous in thickness

2. The sample must not have isolated holes

3. All four contacts must be located at the edges of the material

4. The area of contact should be sufficient small. In principal, an order of magnitude smaller than the area of the entire sample

The resistivity values reported in literature vary with the size of particles and ink formula, as well as the sintering method and time used. Lee et al. [81] obtained a resistivity value of 16 μΩ cm while using water-diethylene glycol based Ag ink which was sintered at 260 ºC for 3 minutes. Fuller et al. [82] studied silver ink containing 5-7nm particles dispersed in α-terpineol, the obtained resistivity was found to be 3 μΩ cm after sintering at 300 ºC for 10 min. Perelaer et al. [52] applied microwave radiation to a dispersed nanoparticles (5-10 nm) in tetradecane and obtained resistivity of 30 μΩ cm.

2.3.5.4 Transparency. Transparent Electrode materials

Transparency is a physical property of allowing the transmission of light through a material. Transparent materials possess bandgaps with energies corresponding to wavelengths which are shorter than the visible range of 390 nm to 750 nm. As such, photons with energies below the bandgap are not absorbed by these materials and thus visible light passes through. Materials with high electrical conductivity and optical transparency are important components of many electronic and optoelectronic devices such as liquid crystal displays, electronic paper, solar cells, and light emitting diodes [83-85]. The most extensively used material for transparent electrodes is indium tin oxide (ITO). However there has been a quest to look for materials with improved bending, lower cost and higher transmittance that can replace ITO. Towards this objective, various types of new materials have been developed by different groups, among which carbon nanotube (CNT) films [86] and, more recently, grapheme [87,88] have been successfully used as the transparent conductive electrodes (TCE) in organic light emitting diodes [89] and solar cells [90]. However, their performance in terms of sheet resistance and transparency is still lower than of the ITO. Two research groups [91] employed Ag nanowires to fabricate TCEs with better performance which were further successfully used in organic solar cells [92, 93].

2.3.5.5 Morphology of the printed pattern.

One of the challenges of printing conductive materials is to obtain desired morphology and geometry of the pattern. The ability of controlling the geometry of the printed features is very important in determining its electrical resistivity and mechanical adhesion. For conductive tracks, ideal printed lines should be straight and smooth. Additionally, in order to optimize the electrical performance of the printed features, defects such as discontinuity of the deposit, spreading of the ink or edge irregularities have to be avoided.

In order to control the morphology of the film on the substrates, various actions can be taken. One is to adjust the dot spacing parameter. The dot spacing is the centre-to-centre distance between two adjacent droplets. Figure 2.14 shows the various dots spacing during printing. When chosen dot spacing between two droplets on the substrate is larger than the droplets themselves and the continuous film will not be formed, in either *x*- or *y*-direction. The dot spacing in one of the two dimensions smaller or equal to the droplet diameter at the substrate will result in the formation of lines. When the dot spacing in two dimensions is equal to or smaller than the droplet diameter, a continuous film will form.

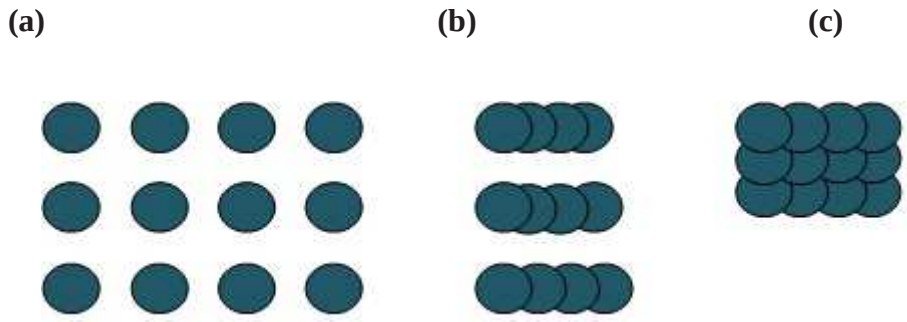

Figure 2.14 Schematic representation of concept of varied dot spacing

The other way to control the morphology of printed features is related to ink's properties, where those properties are viscosity, surface tension, and wetting. In order to limit the mobility of the ink on the substrate, and in the same time to avoid the spreading of the ink, the phase-change inks, such as alumina-filled wax suspensions [72, 94] can be used. In

this case, the ink is kept in a liquid phase (using high temperature) before jetting. By using much cooler substrate; the landed drop can rapidly solidify, thus controlling spreading and feature geometry. However, a few problems associated with using wax-based inks were recognised. Namely, the additional step is required to remove the solidified carrier fluid which can cause shrinkage-related anisotropy in the final product [95] and the risk of losing the resolution of the pattern is high as following layers of ink will melt the underlying deposits at the moment of impact, when the fabrication of three-dimensional structures is used.

Pereler et al. [96], in order to control the geometry of inkjet printed features on a substrate, used the block copolymer $PVME_{612}$- b -$PVOBA_{38}$ in their ink formula and printed an aqueous TiO_2 nanoparticle ink above a certain temperature, where the solubility of the polymer was limited and gel was formed. Obtained droplets and lines with improved morphological control were achieved using this thermal gelation effect.

The other way to control the ink behaviour on the substrate is to modify the surface energy of a substrate [97]. Pre-pattering is an approach based on creating patterns composed of varying surface energies on the substrate, which direct the printed ink into regions of preferential wetting. For example, Sirringhaus et al. [98] used a water-based polymer and pre-patterning to obtain straight line width of 5 micrometers. Disadvantages of this approach include increased processing time due to a need of pre-patterning the substrate and complication of the process as some of the patterns require the use of lithography masks to produce surface energy patterns.

Another and more reasonable approach is the use of hot-embossing or nano-imprinting method [99,100]. The hot embossing process involves master being pressed for a few minutes into a substrate. Using a thin film of a thermoplastic polymer that has been heated above its glass transition temperature a very fine sized structure, for example, circular

features with diameters of 25 nm has been fabricated [101,102]. Once the substrate is structured, it can be filled with inks using capillary forces.

2.4 Synthesis of silver nanomaterials

2.4.1 Synthesis of silver nanoparticles

Silver is a soft, transition metal with the highest electrical and thermal conductivity of any metal and the lowest contact resistance. Silver can be found in nature as an alloy with gold and other metals, and in minerals such as argenite and chlorargyrite. It is stable in pure air and water; however it routine when it is exposed to air or water containing ozone or hydrogen sulphide [103].

The properties of material depend strongly on their size due to a greater surface area per weight. The size and morphology determine their application potential.

There are generally two approaches for fabrication of nanomaterials: top down and bottom up. Top-down is characterized by the production of nanoproducts by reducing the dimensions of the original. It can be made by applying specific machining and etching techniques such as lithography, ball milling, cutting, grinding, etc., giving rise to electronic devices, quantum well lasers, computer chips and high quality optical mirrors.

The bottom-up approach is related to the controlled assembly of atomic and molecular aggregates into larger systems. These generally fall into two categories: condensation from a vapour and chemical synthesis.

Condensation from vapour is a method used to make metallic and metal oxide ceramic nanoparticles. It consists of evaporation of a solid metal followed by rapid condensation to form nanosized clusters that settle in the form of powder. Well known variations of this method are vacuum evaporation on running liquids (VERL) and chemical vapour deposition (CVD). Synthesis of nanoparticles in the gas phase for electronic, optical

and magnetic applications was shown very well in the review of ref. [104]. The chemical synthesis approach seems to be a more effective technique for controlling the final shape of the particles than vapour condensation [105]. The typical example is a sol-gel approach, or microemulsion. This technique is based on growing nanoparticles in a liquid medium composed of various reactants. The desired size is reached by choosing chemicals that either form stable particles, or stop growing at a certain size.

Several methods have been developed to chemically synthesize silver nanoparticles. For example, citrate synthesis (the Turkevich method) [106], Borohydride method [107], water-organic two-phase synthesis [108], organic reducing agent (Tollens reaction) synthesis [109], inverse micelles synthesis [110], Laser ablation method [111], photolysis [112], and biosynthesis [113].

In recent years, silver nanoparticles (AgNPs) have received increasing attention with the rapid development in the field of electronic devices. AgNPs found their applications also in the treatment of diseases that require maintenance of circulating drug concentration or targeting of specific cells or organs [114]. For example, Ag NPs have been shown to interact with the HIV-1virus and inhibit its ability to bind host cells in vitro [115].

2.4.1.1 Super critical carbon dioxide method (sc CO_2)

The supercritical fluids (SCFs) are substances at a temperature and pressure above its critical point (figure 2.15). Their viscosity, density and diffusivity can be modulated by small pressure and temperature variations, as a result, they are considered as liquid-like or gas-like, depending on the conditions and the application.

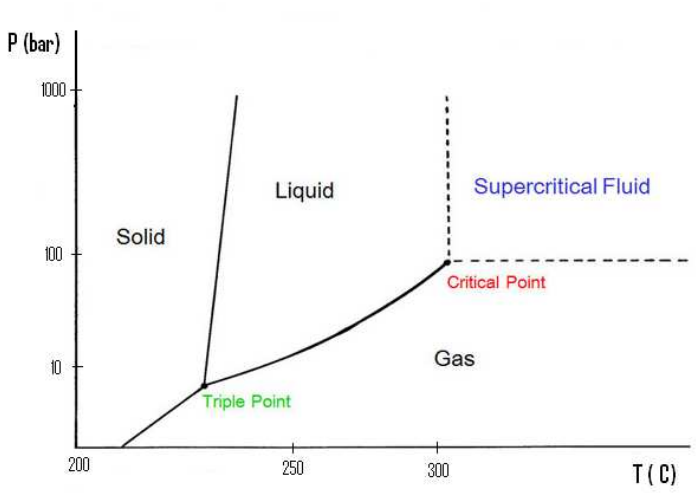

Figure 2.15 Carbon dioxide pressure-temperature phase diagram

The density of supercritical fluid is similar to that of liquids but viscosity and diffusivity are closer to that of gases. These features let supercritical fluids penetrate into the porous structure and extract the solute from the solid. Methods using supercritical fluids allow the creation of ultra fine powders, by controlling the size and shape of the nanoparticles produced.

There are many supercritical fluids which are generally flexible, more simplified and with a reduced environmental impact that can be used in the preparation of a great variety of nanomaterials, such as CO_2, water, propane, acetone, N_2O, trifluoromethane, ethanol, acetone, ammonia, dimethyl sulfoxide (DMSO) and N-methyl pyrrolidone (NMP).

Several variants, for example, solvent, solute, reaction media, antisolvent and emulsion phase, in SCF technology that allow the creation of the desired products by control of its size and morphology can be found in literatures. Table 2.2 shows common methods in terms of the played role by supercritical fluid CO_2.

Table 2.2 Supercritical methods in terms of the role played by $scCO_2$

The role of $scCO_2$	Methods	Nanomaterials	Ref.
As a solvent	RESS- The rapid expansion of supercritical solution	(PbS)	[116]
	RESS-SC (Rapid Expansion of a Supercritical Solution-Solid Co-solvent)	phenytoin	[117]
	RESOLV- The rapid expansion of a supercritical solution into a liquid solvent	Ag	[118]
As an emulsion phase	water-in-CO_2microemulsion	Ag, CdS, ZnS	[119],[120]
As an antisolvent (cooprecpant)	GAS - Gas Anti Solvent (operated in batch)	Lysozyme	[121]
	SAS (Supercritical Anti Solvent) operated in semi-continuous mode	Fullerene	[122]
As a reactant.	Supercitical hydrothermal synthesis	TiO_2, ZrO	[123,124]

The methods used in the present work consist of two modes, RESS and GAS/SAS. Both methods are described below.

RESS

This method consists of the saturation of the supercritical fluid with a solid substrate and rapidly depressurising this solution through a heated nozzle into a low pressure chamber, causing an extremely rapid nucleation of the substrate in highly dispersed material. The

morphology of the resulting solid material, crystalline or amorphous and size distribution depends on the chemical structure of the material and can be controlled by the RESS parameters (e.g. temperature, pressure drop, impact distance of the jet against a surface and nozzle geometry) [125]. The advantage coming from this method is the absence of organic solvent; however the limitations lay in the requirement of products that present reasonable solubility in supercritical carbon dioxide which is the widely used in SCF.

GAS/SAS

In this method a liquid solution contains the solute, insoluble in SCF, to be micronized, while the supercritical fluid is completely miscible with the liquid solvent. As a rule, SC-CO_2 is used. Therefore, contacting the liquid solution with the SCF induces the formation of a solution and produces supersaturation and precipitation of the solute. The process can be operated in batch or in semi-continuous mode. In the case of batch operation the process is called GAS (Gas Anti Solvent, CO_2 plays role as a precipitant) where a given quantity of the liquid solution is placed in a precipitation vessel and the supercritical antisolvent is added until the final pressure is obtained. In the case of semicontinuous operation the process is called SAS (Supercritical Anti Solvent) and then the supercritical anti-solvent and the liquid solution are continuously delivered to the precipitation vessel in co-current or counter-current mode. In this method, several factors play important roles. One is the liquid solution injection device and another is the high-pressure vapour-liquid equilibrium (VLE) and mass transfer between the liquid and the SCF. Particularly, VLEs of the ternary system solute solvent-antisolvent and the position of the operating point in SAS processing with respect to these VLEs can be crucial for the success of the process.

Various solvents that have affinity with SC-CO_2 can be used, which increases the possibility of applying the technique to several compounds with different properties. The chosen solvent also has an influence on the final product.

The most used solvents are DMSO and NMP, methanol (MeOH), acetone, toluene and ethyl acetate (EtAc). Ethanol (EtOH), due to its chemical structure and the possibility to easily form hydrogen bridges, is used less often as it interacts strongly with the solid compound dissolved in it and modifies the VLE solvent-antisolvent-solute in an unpredictable way. Water cannot be used as solvent because of its relatively low solubility in SC-CO_2.

2.4.1.2 Wet chemistry method

Wet chemistry method belongs to bottom-up approach which refers to the build-up of a material from the bottom: atom-by-atom, molecule-by-molecule, or cluster-by-cluster. The advantage of this method is the potential to produce quantities of the final product. Moreover it is a very convenient way to control the size and shape of the particles [126]. The method is based on reduction of metal salts in the presence of suitable capping agents to generate metal particles. Generally speaking the main parameters in wet chemistry method are the type and concentration of reagents, their redox potentials and rate of addition, type and concentration of protective agents, temperature, and pH [127]. The difference in the redox potentials of the reagents (ΔE) is the driving force of the ion metal reduction process (mOx^{n+} + Red = mOx^{0} + Red^{mn+}). It correlates with the Gibb's free energy of the reaction at standard conditions:

$$\Delta G = -nF\Delta E + RTlnK \qquad (2.22)$$

(where K = equilibrium constant, n = the number of electrons in a reaction equation, F = Farady's constant).

The reduction process is thermodynamically possible only if the redox potential of the reducer is more negative than that of the oxidizer (in this case metal precursor) and, consequently, ΔE is positive. This difference should be larger than 0.3–0.4 V; otherwise the reduction will proceed too slowly and may not result in the formation of nanoparticles [138].

Particle size distribution depends on the interaction between nucleation and particle growth processes that occur during preparation. By influencing the relative rates of these processes the particle size can be determined. In order to control the growth of particles a number of parameters can be adjusted, such as temperature and concentration of the metal precursor, the nature of stabilizing or reducing agent. Using a fast reduction agent results in the formation of many silver seeds at the beginning of the synthesis process. This high amount of silver seeds will shorten the growing time of silver seeds and prevent the formation of larger nanoparticles. If the solution is homogenous there is a high chance that particles end within a narrow size distribution [129].

2.4.2 Synthesis of Ag nanowires

Ag nanowires (AgNWs) received a great interest due to their unique optical, thermal and electrical conductivity. Moreover, they can serve as a template to generate other nanostructures, usually hard to obtain, e.g gold nanotubes [130].

Over ten years a number of research groups investigated strategies for the synthesis of size – controllable Ag NWs. There are generally two approaches for the fabrication of AgNWs: the vapour deposition which mainly utilizes physical methods such as an electron beam, and the second, liquid phase growth approach. The liquid phase synthesis has the advantage of possibly using a range of solvents, simple monitoring technology, and low cost.

Polyol method

Polyol process was originally developed by Fievet et al. [131] for synthesis of metallic nanoparticles. Xia et al. [132] developed further this method for obtaining Ag NWs by the injection of $AgNO_3$ and PVP solutions drop-by-drop into ethylene glycol (EG) solution heated to 160 ºC. In this process AgNWs are obtained by self-seeding process where EG acts as both solvent and reducing agent. The necessary factors that influence the formation of

nanowires are: low precursor concentration, slow addition rates, and right molar ratio between the repeating unit of PVP and $AgNO_3$.

Salt-mediated polyol processs

The same research group, developed a salt-mediated polyol process that is based on polyol process but the reaction takes place in the additional presence of at race amount of salt, such as NaCl, $Fe(NO)_3$, $CuCl_2$, CuCl [133,134]. The salt-mediated method is a simple and effective process when the mass synthesis of AgNWs is needed. For instance, they obtained high yield of AgNWs by reducing $AgNO_3$ with EG heated to 148 ºC in the presence of PVP and NaCl. In another experiment, in order to obtain AgNWs, Xia et al [132] used polyol process with the addition of CuCl or $CuCl_2$ salts. Based on the obtained results, they suggested that the trace amount of Cl^- plays important role in the polyol process for Ag NWs synthesis. Cl^- ions supports the electrostatic stabilisation for the silver seedsthat are primarily formed. Presented Cl^- ions in a solution react with Ag^+ ions forming AgCl, which reduces concentration of Ag+ in a solution and allows slow release of Ag+ which consequently enable the formation of high yield thermodynamically more stable metal particles which are further needed for wire growth.

Seed-mediated growth method

AgNWs have also been synthesised by solution–phase method where $AgNO_3$ is reduced in EG, in the presence of $PtCl_2$ at a high temperature using oil bath [135]. It was suggested that the formation of AgNWs is via two steps. In the first step, 5 nm Pt nanoparticles are formed by reducing $PtCl_2$ with EG. The second step involves nucleation and growth of Ag NWs by adding $AgNO_3$ and PVP solutions into the reaction medium. At high temperature silver nanoparticles with larger sizes are able to grow at the expanse of smaller ones through Ostwald ripening [135]. This is a spontaneous process which is based on dissolving small

crystals or sol particles, and their redeposit onto larger crystals or sol particles. Larger crystals are more energetically favoured than smaller crystals. Although the formation of many small crystals is kinetically favoured (i.e. they nucleate more easily), they are energetically less stable than the ones already well ordered and packed in the interior. This is due to larger surface area to volume ratio molecules on the surface of small crystals. Large crystals are thermodynamically favoured and with their greater volume to surface area ratio, they represent a lower energy state. Thus, many small crystals will attain a lower energy state if transformed into large crystals.

Chapter 3

Experimental methodology

In this chapter the experimental procedures and review of the characterisation methods are described. The first part of this chapter will present the preparation and characterisation of the Ag particles using wet chemistry and $scCO_2$ method and synthesis of nanowirers by polyol process. The second part of this chapter concerns preparation and characterisation of the nanofluids. The final part of this chapter explains the deposition methods for film preparation and the method for their characterisation.

3.1 Synthesis of silver powder

3.1.1 Silver particle synthesis using $scCO_2$ technology

Figure 3.1 shows scCO2 equipment with all the parts for both, Supercritical Anti Solvent (SAS) and Rapid Expansion of Supercritical Solution (RESS) modes.

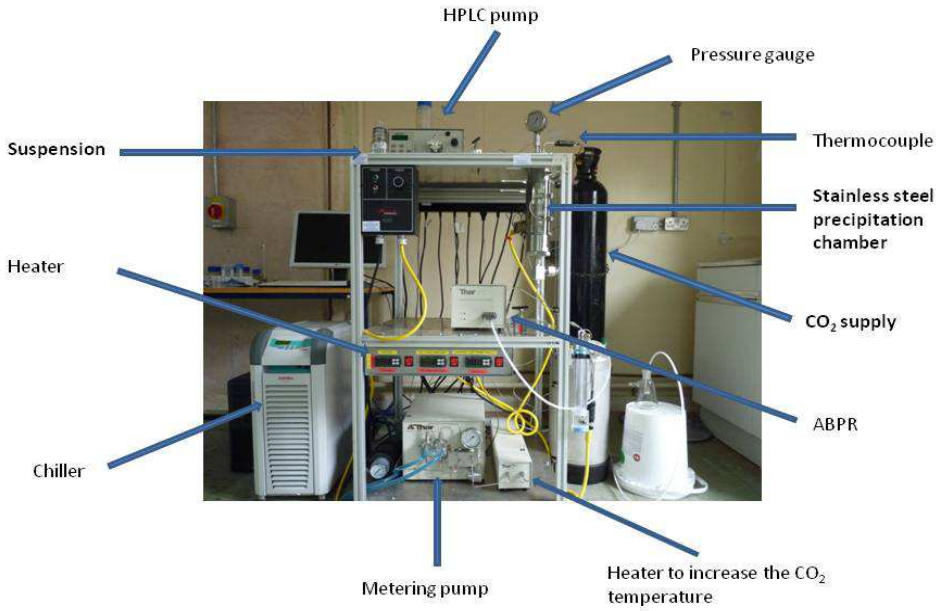

Figure 3.1 Picture of the $scCO_2$ setup used

The equipment consists of CO_2 bottle with liquid CO_2 which is during the process pressurized to the desired pressure using a CO_2 pump, and preheated to extraction temperature through a heat exchanger. Reaction vessel is made with steel, equipped with heating jacket to control the temperature and the lid with attached stirrer, and connected at the bottom with a collection vessel through the still pipe finished with a nozzle. ABPR pump which adjusts the fit of the attached needle, repeatedly closing and opening slightly as it attempts to maintain pressure, and High-Performance Liquid Chromatography (HPLC) pump for introducing the solution sample into the reaction vessel.

For the nanoparticles synthesis experiment only RESS apparatus was used. Figure 3.2 shows schematically the parts involved in the experiment.

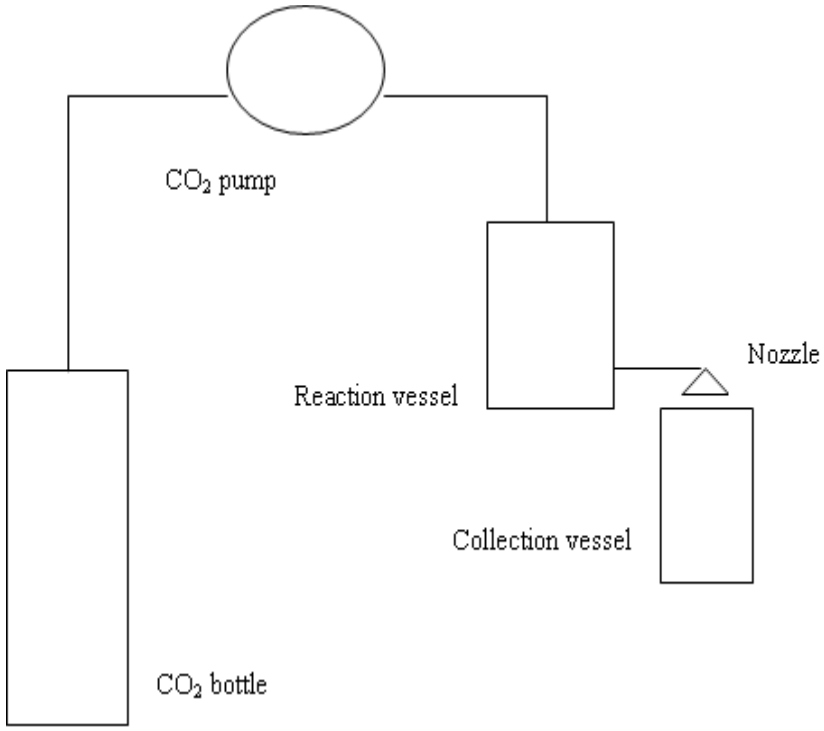

Figure 3.2 Schematic diagram of RESS mode equipment in supercritical fluid method

Nanoparticle synthesis in supercritical environment followed by a rapid expansion was conducted. 0.04g of $AgNO_3$ and 2.5 g of PVP were dissolved in 30 ml ethylene glycol followed by stirring for 20 min. Then 20 ml of so prepared solution was placed into a reaction

vessel with a maximum volume of 500 ml. When reactor was closed, CO_2 was then charged into the cell by up to 10-25 MPa using the CO_2 pump. The mixture of CO_2 and $AgNO_3$ solution was stirred by rotating agitator at 200 rpm. The temperature and pressure for the process were maintained for required time (a range between 1 hr and 3 hrs)**.** The dissolved polymer/dispersed silver particles mixture was sprayed through a capillary nozzle (0.8 mm in diameter), into container with solvent (for a 10 s) by opening a valve. The nozzle was maintained at 40 ºC with an electric heater to avoid plugging by solutes precipitation. Once the pressure was decreased sharply by opening the valve, the particles were formed and precipitated in a collection vessel.

Two different pressures were analysed at various temperatures and reaction time. The produced powder was collected on a stainless steel located at the bottom of the vessel.

3.1.2 Silver particles by wet chemistry method

Ag nanoparticles were synthesized by a new approach developed in this work. All chemicals were used as purchased. Figure 3.3 shows the synthesis route to produce silver nanoparticles with controllable size.

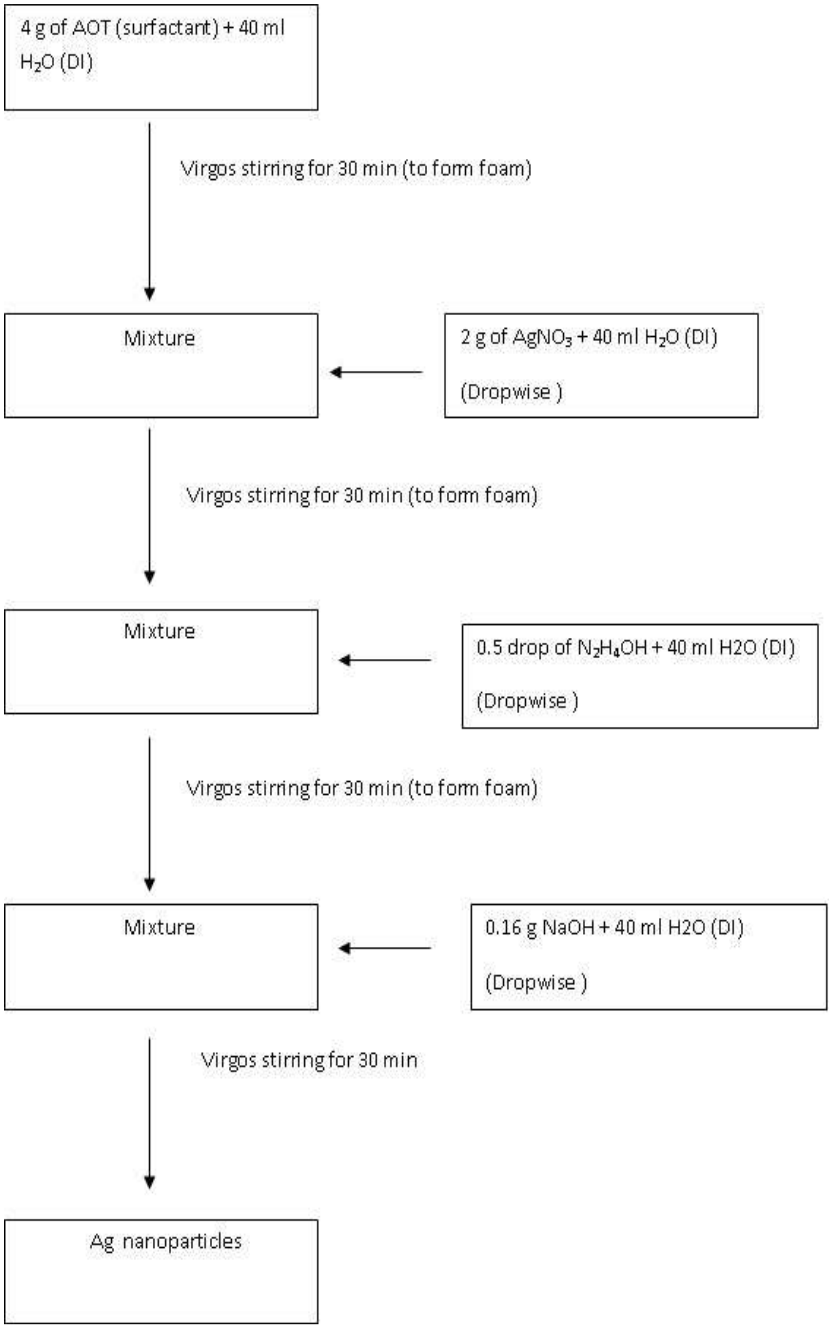

Figure 3.3 Schematic illustration of the possible formation process of the silver nanoparticles

Silver nitrate (2g) used as Ag precursor and surfactant dioctyl sodium sulfosucinate (AOT, 4g) as a capping agent were separately dissolved in water, forming 0.03M and 0.02M solutions respectively and then two solutions were mixed by adding the surfactant solution to the metal salt one. The mixture was kept stirring to form a foam. 40 ml of hydrazine, N_2H_4OH (1.5 mM) was then added to the solution. To complete the reaction 40 ml of 0.1M

NaOH aqueous solution was added to precipitate out Ag nanoparticles. The silver particles in the collapsed foam solution were collected, washed by isopropanol or acetone.

3.1.3 Synthesis of Ag nanowires by polyol process

Ag nanowires were synthesized by polyol process in the presence of Pt nanoparticle seeds using polyvinyl pyrrolidone (PVP, *M*w = 40 000) as the protecting agent. The procedure is described as follows: 15 ml ethylene glycol (EG) was refluxed in a round flask with condenser at 160° for 1 h, and then 1.5 ml EG solution of $PtCl_2$ (1.5 mM) was added quickly. After the reaction lasted for 4 min, 7.5 ml of an EG solution (0.12 M) containing$AgNO_3$was added and then, 15 ml EG solution (0.001 M) of PVP was added into the refluxing solution dropwise. When the addition ended, the reaction mixture was further heated at 160° for 60 min. The system was then cooled to room temperature, and the sample was washed with acetone and dried in air.

3.2 Powder characterisation

In order to characterise the final products, several techniques were used which include:

- X-ray diffraction (XRD, D5005 Siemens) – It is a non-destructive analysis technique provides information on the microstructureof materials. This technique is carried out by observing the scattered intensity of an X-ray beam while hits a sample as a function of incident and scattered angle, polarization, and wavelength. The powder was placed on carbon tape attached to a glass slide. The scans were carried on in the range 20-60 2θ with a step size of 0.05° and a time per step of 1 s.
- Scanning electron microscopy and particle size analysis (SEM, SFEG XL30 FEI) - provides information regarding the morphology and size of particles. A conductive carbon tape was stuck to an aluminium tip and the powder was placed on top of the tape. The

SEM parameters used for imaging were: through lens detector (TLD), spot size was 2 nm, working distance was 5 mm, , and acceleration voltage was10 kV.

- Zeta potential (Malvern Zetasizer series) - these measurements provide information on the surface charge of a material and its isoelectric point. The size measurement of particle and molecule can be from one nanometer to several microns. The measurement is based on using dynamic light scattering, zeta potential and electrophoretic mobility of the particles. Samples were made up in 18.2 MΩ deionised water at a concentration of ~0.5 mg/ml and were sonicated for 15 minutes before zeta potential measurements were taken. The pH of the solution was manually adjusted by the addition of 0.1 M HCl or NaOH to ca. 10-15 ml of the suspension before the zeta potential was measured.
- Thermogravimetric analyses (TGA) - This test determines changes in weight of the sample in relation to change in temperature. This analysis has a high degree of precision in three measurements: weight, temperature, and temperature change. In TGA process heat and stoichiometry ratios is utilized to determine the percent by mass of a solute. Analysis is based on increasing the temperature of the sample gradually and plotting weight (percentage) against temperature. Maximum reached temperature was 800 ºC. The experiment was performed with Setaram Setsys Evolution 16/18 apparatus at a heating rate of 10 ºC in air.
- Nanoparticle tracking analysis (NTA) (Nanosight LM20) - It's an innovative system for sizing particles from about 30 to 1000 nm, with the lower detection limit being dependent on the refractive index of the nanoparticles. This technique combines laser light scattering microscopy (DLS) with a charge-coupled device (CCD) camera, which enables the visualization and recording of nanoparticles in solution. The NTA software is then able to identify and track individual nanoparticles moving under Brownian motion and relates the movement to a particle size according to the well known Stokes-Einstein equation.

- Ultraviolet–visible spectroscopy (UV-Vis) It is qualitative and quantitative analyses tchnique using light in the visible and adjacent (near-UV and near-infrared (NIR)) ranges which corresponds to electronic transitions of different origins.The absorbance data from the measurement can be related to the concentration of the sample by using Beer's Law. Samples were prepared by dispersion of known amount of sample (very diluted) and then 3 ml of the prepared solution was placed in a cuvette and submitted to the measurement.

3.3 Ink development

3.3.1 Inks formulation

In a first part of the work two types of silver inks (AG1 and AG2) were developed and used in this work. The effect of various silver content (0.1-0.5 wt % and 10-40 wt % for AG1 and AG2 respectively) and dispersant (0.1-1 wt %), were checked on fluid properties such as viscosity, surface tension, aggregates formation and stability.

Two different ways were adopted to mix the ink components. The ink AG1, using silver nanoparticles prepared by the method described in section 3.1.2 with final washing by IPA, was formulated in the following optimised way: 0.5 g of Ag powder was dispersed in 5 g of an aqueous medium containing 0.6 wt% Pluronic F127. Pluronic F127 was utilised as a dispersant. Pluronic F127 is a nonionic, triblock copolymer (PEO 106 - PPO70 - PEO 106) surfactant terminating in primary hydroxyl with an average molar mass of 10,000. The solution was then treated by High intensity focused ultrasounds (HIFU) (figure 3.4) for 60 min.

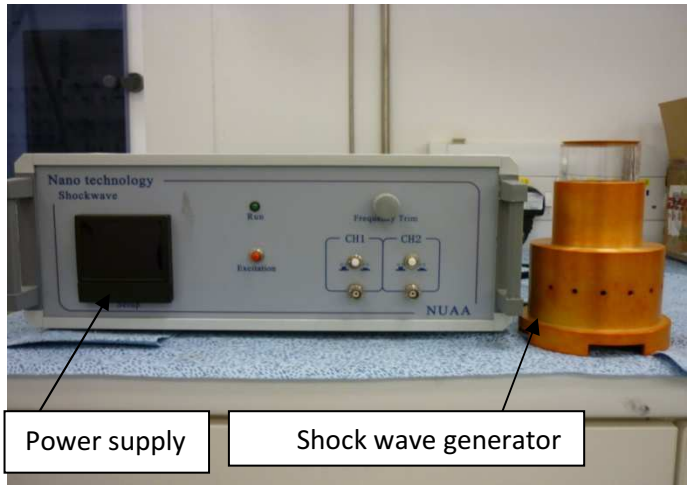

Figure 3.4 HIFU equipment

A second ink, AG2, using silver nanoparticles prepared by the same method as AG1 but treated with acetone in the final step, was prepared in the following optimised way: 6 g of Ag powder were mixed in 9.6 g of an aqueous solution having 0.5 wt% Pluronic F127. HIFU treatment is not needed as this powder disperses spontaneously.

In a second part of the work silver nanowires ink was formulated. The effect of five different surfactants in various solvents on stability and film uniformity of the AgNWs dispersion was investigated. Water and methanol were chosen as a dispersion medium and the AOT, CTAB, PVA, and F127 were chosen as dispersing agents. For this purpose known amount of Ag NWs was dispersed in 6ml of methanol with addition of each surfactant and was analysed with UV-Vis spectrophotometer.

3.3.2 Physicochemical properties of silver nanofluids

3.3.2.1 Rheological properties of silver inks

Rheological properties of both inks (AG1 and AG2) were characterized using a Bohlin CVO rheometer (Bohlin Instrument, Ltd.). The viscosity of the colloidal aqueous suspensions containing silver particles and copolymer F127 was measured at 25 ºC in the range of shear rate (1-1000/s) using a cup and bob configuration (C14 DIN 53019). Before this

measurement, on a 3 ml sample, a pre-shear of 200 s^{-1} was applied for 30 s, and followed by an equilibration time of 60 s.

3.3.2.2 Surface tension measurement

Surface tension measurement was based on the weight of the drop of the fluid (Stalagmometric method) prepared using the method described in section 3.3.1. Firstly the weight of 50 drops of deionised water was measured and then 50 drops of sample were weighted.

The surface tension (Γ) of liquid was calculated from the equation 3.1.

$$\Gamma = \gamma_1 * m_2/m_1 \quad (3.1)$$

where, γ_1 is a surface tension of water [$72*10^{-3}$mN], m_1 mass of water's drop and m_2 mass of measured liquid's drop.

3.3.2.3 Stability studies

To evaluate the stability of nanofluid streated by HIFU with the presence of F127 copolymer, the viscosity of nanofluids, containing 5 wt% Ag nanoparticles, 0.6 wt% dispersant and treated by HIFU for 60 min, was measured against the time over 20 days. The rheometer (Bohlin Instrument, Ltd.) was used to conduct the measurements with varying shear rate. The same measurement was performed for AG2 ink containing 40 wt% silver nanoparticles and 5 wt % of F127.

3.3.2.4 Extractability properties of the dispersants

First, a calibration curve was prepared and the concentration of Ag NWs dispersed into the solution was determined. For this purpose a number of solutions of the Ag NWs each of accurately known concentration were prepared. Then for each solution, measure the absorbance at the wavelength of strongest absorption was measured. Subsequently a graph of

that absorbance against concentration was plotted to obtain a calibration curve and the corresponding concentrations for AgNWs samples were read from the graph.

Dispersions were analyzed with UV–vis spectroscopy and the maximum extractable concentration of Ag NWs (at 0.25 wt% surfactant concentration) was determined for each of the surfactants. The baseline correction was carried out using pure 0.25 wt% solutions of the four surfactants so that their absorbance values got subtracted from that of Ag NWs dispersions.

In order to find the optimum Ag NWs-to-F127 ratio, a concentration of F127 was varied from 0.05 to 0.25 wt%, keeping the amount of Ag NWs constant, using methanol as a solvent. Constant Ag NWs concentrations used in these experiments were the maximum extractable concentrations of Ag NWs chosen from the first turn of experiments for 0.25 wt% surfactant concentration. Constant Ag NWs concentrations were selected to be 7 mmol and again, the samples were analyzed using UV–vis spectroscope.

3.4 Characterization of deposited films

3.4.1 Ink jet printing

Inkjet printing was carried out with a DoD Fujifilm Dimatix DMP-2831 ink jet printer (figure 3.5). Silver inks prepared as described in sections 5.3.1 were used to print at room temperature and typically into a pattern of one line with a length of 5mm.

The inks were printed on three different substrates, 520 µm thick silicon substrate, 480 µm alumina, and 810 µm LTCC tapes.

Disposable cartridges (DMC-11610) used in this work are equipped with 16 silicon nozzles located at 254 µm spacing; the orifice size of each nozzle is approximately 21 µm. The ink droplets ejection was achieved by applying a 25 V pulse lasting 15 s at a frequency of 1000 Hz. The substrate temperature was varied from 20 to 60°C.

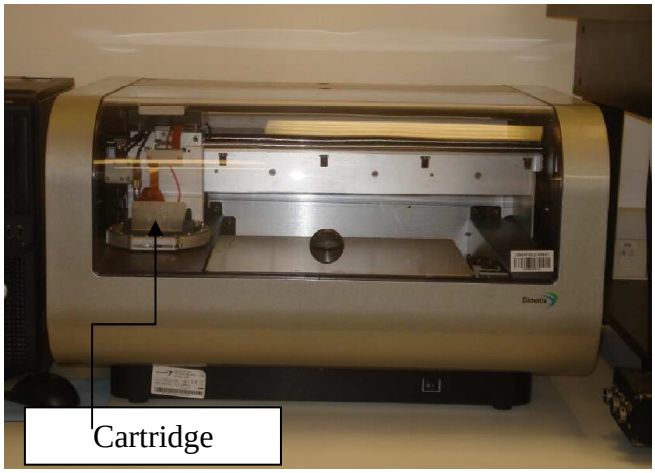

Figure 3.5 Fujifilm Dimatix DMP-2831 ink jet printer

In printing process several parameters were examined to determine their influence on the print quality. The drop spacing (DS) was varied between 5 and 60 µm. A printed pattern were composed of a square of 10x10 pixels and 5 mm long line varied in width between 200 and 300 µm, both were printed a CPH of 0.35 mmand at a voltage of 25 V.

3.4.2 Meyer rods

In order to determine conductive and transparency properties of the Ag NWs, AgNWs films were deposited on the previously glass and plastic substrates using Meyer rods.

The ink utilised for this purpose was a AgNWs dispersed in methanol with addition of 0.7 wt% of F127. Prior to the deposition, the glass was washed with acetone and isopropanol and then heated for 30 seconds at 200°C in order to evaporate any residual solvent. The organic components were removed by heating the wafer at 120 ºC for 10 min. The films were built up by depositing several layers of the Ag NW ink.

To deposit AgNWs film on a substrate, AgNWs ink was dropped on a plastic or a glass substrate. Then, a Mayer rod was pulled over the solution (figure 3.6) leaving a uniform layer of the AgNWs ink on a substrate with the thickness dependent on the used rod wires

distribution as shown in Figure 3.6. Different Ag NW films were obtained in terms of resistivity and transparency properties by depositing 1, 2, or 3 Ag NWs layers.

Figure 3.6 Meyer rod coating setup for Ag NW coating on plastic substrate

3.4.3 Characterisation

The morphology of printed lines was measured by a reflective light optical microscope (Nikon Optiphot 2) scanning electron microscopy (SEM, SFEG XL30 FEI). A confocal scanning laser microscope (Olympus Lext OLS3100) was used to check surface topography (profile) and roughness. The thickness of printed silver tracks was measured with a Dektak instrument.

3.4.3.1 Conductivity measurement

Conductivity measurements of printed tracks on substrates were performed using a four probe technique. The printed film was firstly heated for 10 min in a range of temperature between 200 and 700 ºC. After cooling down the samples to room temperature the resistivity of the film was measured.

3.4.3.2 Adhesion studies

Adhesion study involves investigating incorporation of a nanosized silica fume as an adhesion promoter within the ink silver. Adhesion tests were first carried out using a

conventional scratch tester (model ST-3001) but it was found that films failed at the minimum available load (1N). Following this, trials have been carried out using a nanotest nanoindentak model 600 nano-indenter in scratch test mode. In these measurements the stylus is scanned over the sample three times: the first and third with minimal force to measure the initial and final topography, and the second with a pre-defined load applied to test film adhesion. In the tests a maximum load of 200 mN was used in a scan across a ~ 2μm thick, ~300 μm wide Ag track (printed onto alumina tape and sintered at 350 °C for 10 minutes) In results has been showed that 200 mN was not enough to scratch the film with addition of silica. Hence, in order to test the effect of various content of silica in silver ink on adhesion of the film to the substrate, a peel off test was employed. In this case, tapes with various force of adhesion were used indicated by different colours, blue with lowest adhesion (strength σ), yellow with higher adhesion and green with highest adhesion.

3.4.3.3 Hardness measurement

The hardness of the printed films was measured with an indenter (nanoindentak model 600 nano-indenter)**.** This technique has the advantage of being able to measure properties such as hardness and elastic modulus without removing a film from the substrate.

Silver thick films of 10 mm^2 dimensions were prepared by inkjet printing technique on an alumina substrate. The printed patterns were allowed to settle for 10 min, and then dried at different temperature varied from 350 ºC to 700 ºC for 10 min. The load placed on the indenter tip was applied to the surface of the film at progressively greater load until the user-defined value. The area of the residual indentation in the material was measured.

3.4.3.4 Transparency

Optical transmission spectra of AgNWs films on either PET or glass were obtained using a UV-Vis spectrometer with either bare PET or glass as the reference. Transparent materials

possess bandgaps with energies corresponding to wavelengths which are shorter than the visible range of 200 nm to 750 nm. As such, photons with energies below the bandgap are not collected by the tested materials and thus visible light passes through.

Ag films were obtained by depositing AgNWs ink on glass and plastic substrates using Meyer rods (method described in section 3.4.2). Then the films were dried at 120 ºC for 10 min.

3.5 Printing onto embossed structures

The micro-channels were formed by embossing of the silicon wafer and by laser machine on alumina tape and Low Temperature Co-fired Ceramic (LTCC) substrates. The embossing process involves a master being pressed for a few minutes into a thin film of an alumina substrate. Once recessed topography structures have been formed, a silver nanoparticle ink was dispensed over the as-formed microchannels using an inkjet printer (Dimatix), described in section 3.4.1.

Chapter 4

Synthesis and characterisation of silver nanomaterials

4.1 Introduction

Small and spherical Ag particles are required for the development of an ink suitable for ink jet printing. Powders should have diameters less than 1/100 the size of the nozzle diameter that is usually in a few or a few tens of micrometers, otherwise nozzle clogging would normally occur. Such a small size gives the particles unique properties which directly relate to their dimensions and to the fact that a large ratio of the atoms in the particle is in the surface of the particle. One of the advantages coming from the nano-size of material is a dramatic reduction in melting point. Moreover, the optical, electronic and magnetic properties of particles improve with the size reduction.

For the preparation of nanoparticles, small size is not the only requirement. For any practical application and especially ink formulation, the processing conditions needs to be controlled in such a way that resulting material characterised with uniform size distribution, identical morphology, chemical composition, and crystal structure of particles. Additionally, the particles, in liquid medium should be individually dispersed or mono dispersed, so that no agglomeration occurs. Hence, it is very important to choose the most appropriate and efficient method, while the application of obtained particles aims for ink formulation.

Several studies [136,137,138] including both top-down and bottom-up approaches, have been developed and applied for the synthesis of nanoparticles. Top-down techniques including milling, repeated quenching, and lithography can result in nanoparticles size ranging from a couple of tens to several hundreds nanometer in diameter. However, nanoparticles produced by for instance milling technique have usually a relatively broad size

distribution and varied particle shape. In addition, they may contain a significant amount of impurities from the milling balls which can affect the final product.

Repeated quenching approach can also break down a bulk material into small aggregates, if the material has a very small thermal conductivity. However this process is difficult to design and control and also to produce the desired particle size and shape.

Bottom-up techniques including physical and chemical methods, such as chemical reduction, electrochemical techniques, and photochemical reduction [129] are more popular due to better results in size uniformity and shape of particles. It has been reported that the size, morphology, stability and properties of the metal nanoparticles are strongly influenced by the experimental conditions [129].

All synthesis methods or techniques can be grouped into two categories: thermodynamic equilibrium approach and kinetic approach. In the first one, synthesis process consists of (1) generation of supersaturation, (2) nucleation, and (3) subsequent growth. In the kinetic approach, formation of nanoparticles is achieved by either limiting theamount of precursors available for the growth or confining the process in a limited space.

In this chapter, the particle will be synthesised through thermodynamically equilibrium approach. The design of synthesis methods in which the size, morphology, stability and properties can be easily controlled is proposed.

The results of the experimental investigation of silver nanoparticle synthesis using wet chemistry and supercritical carbon dioxide ($scCO_2$) will be discussed in details.

Wet chemistry is a cost effective, time saving and environmental friendly method. High yield and uniform particles are possible to obtain using this technique. On the other hand $scCO_2$ is a very promising and above all, enviromental friendly method. Comparision of those two techniques for silver preparation is presented including analysis of the influence of process parameters on the particles' size and morphology.

4.1.1 Objectives

The objectives of this portion of the study were:

1. To develop new chemical methods for the syntheses of silver nanoparticles
2. To identify the influential factors in the synthesis of Ag nanoparticles
3. To optimize the best conditions of the synthesis and achieve the ultimate goal of a small (< 100 nm), uniform Ag nanoparticlecs in high high yield (1 g from synthesis in a laboratory scale)

4.2 Study of wet chemistry parameters on size and morphology of silver particles

4.2.1 Effect of the silver nitride concentration

Ag nanoparticles have been synthesized by the wet-chemical method described in section 3.1.2 which is a simple and efficient synthesis procedure. The starting point of the synthesis is dissolution of silver nitrate in water, where metal salt splits into a positive silver ion (Ag^{+}) and a negative nitrate ion (NO^{-3}). In order to turn the silver ions into solid silver, a stoichiometric amount of hydrazine aqueous solution is added. Hydrazine as a fast reducing agent enables to achieve small particles. Using a fast reduction agent results in the formation of many silver seeds at the early stage of the synthesis process, and prevents the formation of larger nanoparticles. The chemical reaction may be written:

$$2AgNO_3 + 4N_2H_4OH \longrightarrow 2Ag + 5N_2 + 10H_2O \qquad (4.1)$$

When the silver seeds are formed it starts to grow continuously until the equilibrium between the final nanoparticles and the (Ag^{+}) of the solution is reached [139].

The effect of silver nitrate concentration on the size and shape of Ag particles was determined by preparing different concentration of metal salt solutions. Figure 4.1 shows SEM images of particles synthesized with different precursor concentration. Three different concentrations of the salt precursor were used in this study. Concentration of $AgNO_3$ was

varied from $5*10^{-4}$ to $3*10^{-2}$ M and hydrazine concentration from $1.25*10^{-4}$ to $7.5*10^{-3}$ M. It was found that the concentration has great influence on particle size. The particle size distributions became narrower and the average particle sizes decreased with decreasing concentration of silver nitrate.

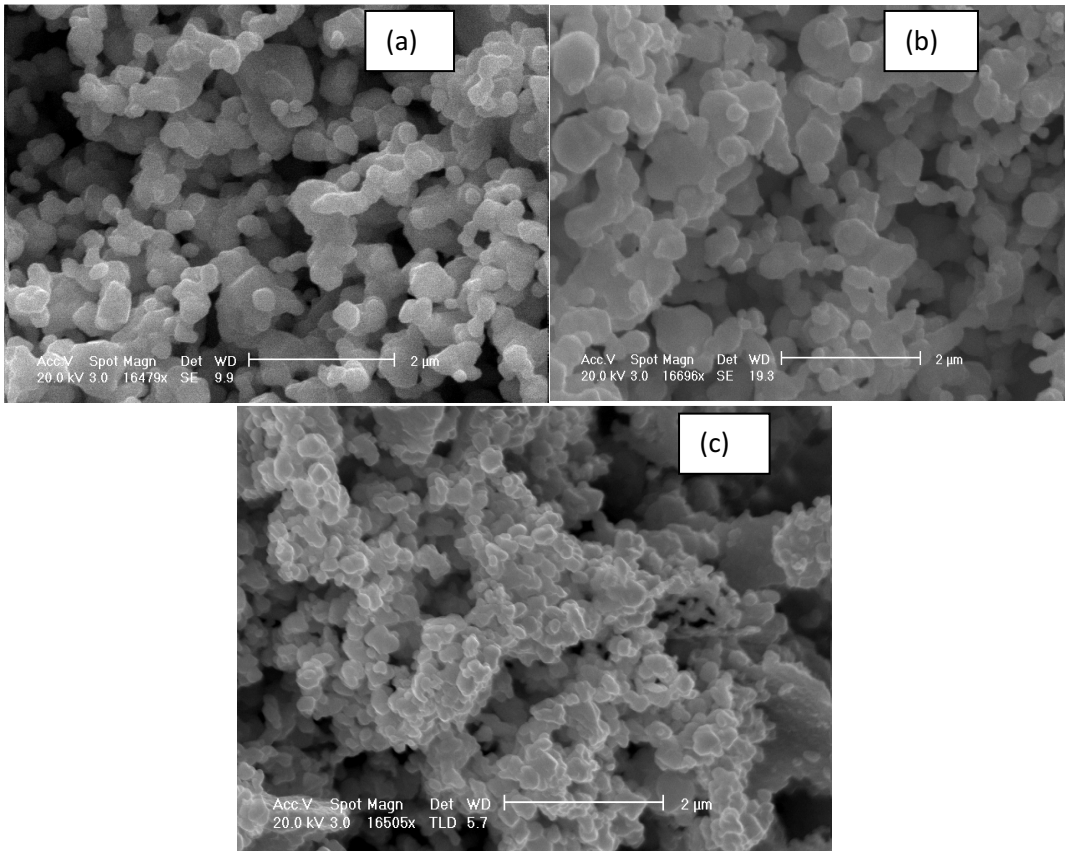

Figure 4.1 SEM micrograph of silver nanoparticles synthesised from (a) 0.05M, (b) 0.03M, and (c) 0.0005M solution of $AgNO_3$

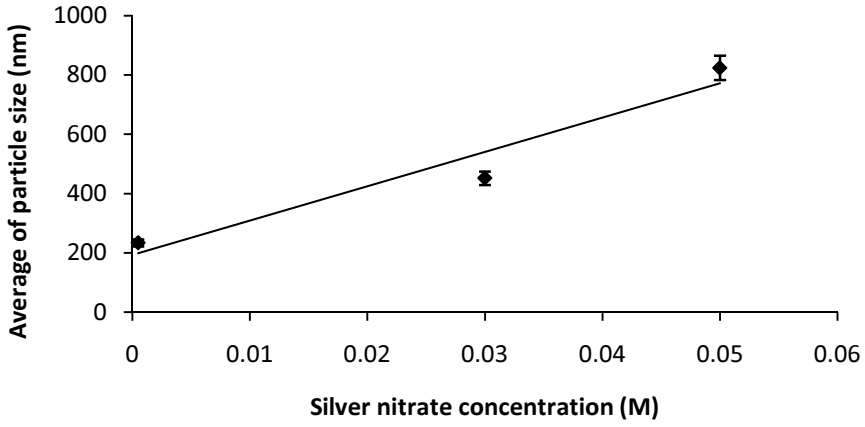

Figure 4.2 Graph showing the size dependence on precursor concentration of the samples shown in figure 4.1

At lower concentrations, the diffusion rates decrease and reduced number of ions is reduced, as a result, smaller particles form. While at higher concentrations more silver ions are available for reaction and the diffusion rates are higher. The ions react to form Ag which nucleates instantaneously, and then with further availability of ions, the nuclei grow into larger particles rather than causing fresh nucleation [129].

The XRD patterns of spherical Ag nanoparticles with size between 200-800 nm are shown in figure 4.3 All of the three characteristic peaks for silver (2θ = 38.2°, 44.4°, 64.5°, 77.5° and 81.6°), corresponding to Miller indices (111), (200), (220), (311) and (222), are observed. The decrease of Ag nanoparticle size results in the decrease in the intensity of these peaks. The appearance of those peaks reveals that the resultant particles are pure face centred cubic (fcc) silver.

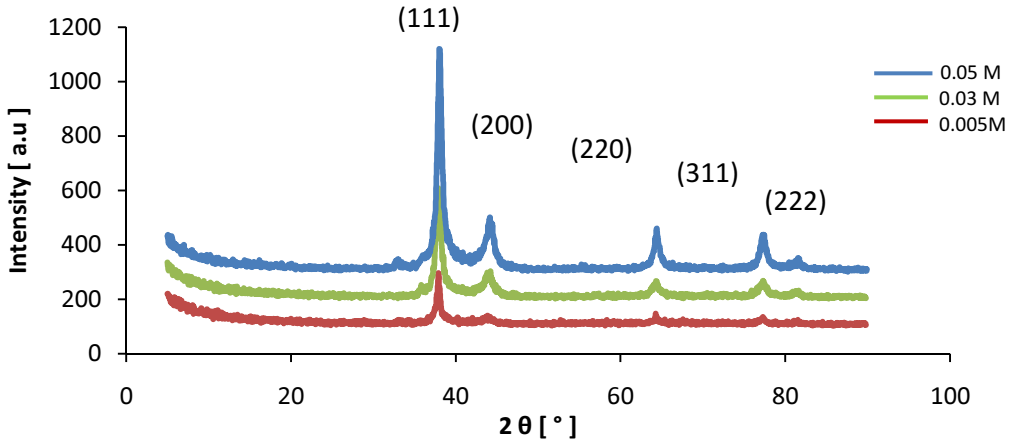

Figure 4.3 XRD pattern of silver particles prepared with various concentration of $AgNO_3$ solution.$AgNO_3$

Reduction by hydrazine gave size of silver particles between 200 nm and 800 nm depend on silver salt concentration. Although the size of silver particles was reduced by means of decreasing its precursor concentration the particles still remained aggregated.

4.2.2 Effect of different capping agent on the formation of silver nanoparticles

The next step in attempt of decreasing the size of particles was introducing the capping agent that would prevent further growth of particles. The purpose of surfactant or polymer is to preventing particles from agglomerating by producing a protective shell around the forming particle. The important condition is that the stabilizer molecules are dissolved in a good solvent. A large number of polymers is commercially available. In our experiment, as a first the PVP polymer was chosen as it has good reducing properties and forms easily complex with silver ions [140].

PVP as a silver capping agent was introduced to $AgNO_3$ and hydrazine solution. The molar ratio between PVP and $AgNO_3$ was 1:1. Figure 4.4 shows the possible PVP protection mechanism.

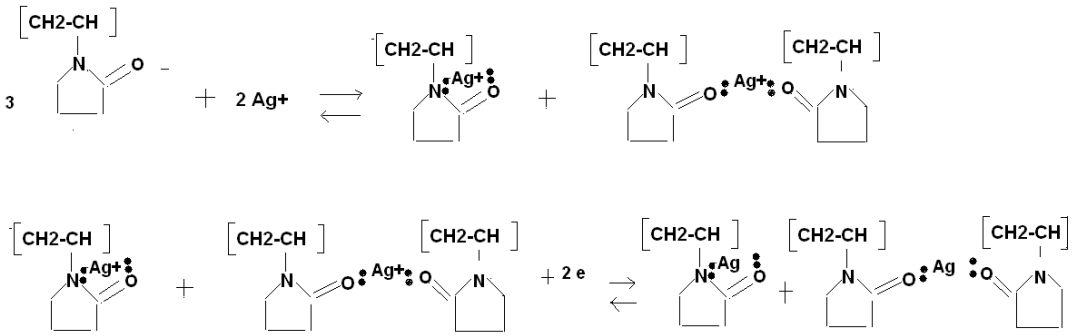

Figure 4.4 PVP protection mechanism of Ag nanoparticles

The PVP donates a lone pair of electrons of oxygen and nitrogen to sp orbitals of silver ions which results in forming Ag-ions-PVP complexes. The Ag ions mix more electronic clouds with PVP than from water as a result the silver ions in a complex with PVP are more easely reduced by hydrazine. Additionally, because of the PVP steric effect the aggregation and grains growth are prevented [141].

Figure 4.5 shows SEM image (a) and XRD pattern (b) of silver particles prepared with a presence of PVP protecting agent. The addition of PVP considerably reduced the size of particles resulting in spherical silver nanoparticles as small as 20 nm.

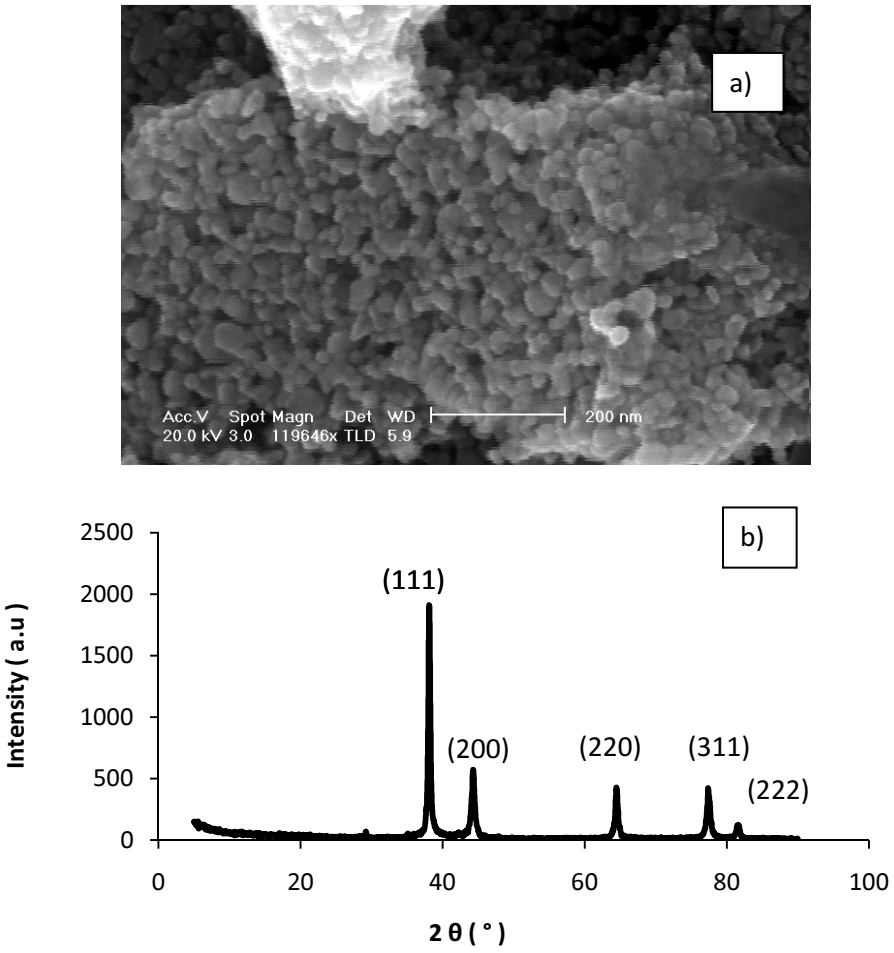

Figure 4.5 SEM micrograph (a) and XRD pattern (b) of silver particles prepared in presence of PVP

The XRD patterns reveal the presence of Ag nanoparticles in obtained samples. All of the five characteristic peaks for silver (2θ = 38.2°, 44.4°, 64.5°, 77.5° and 81.6°), corresponding to Miller indices (111), (200), (220), (311) and (222), are observed. The particle size could be calculated from the Ag (111) diffraction line using Scherrer's formula,

$$t = k \lambda / \beta \cos \theta \qquad (4.2)$$

where t was the mean dimension of the crystallites, β was the full width at half maximum of the diffraction peak, θ was the diffraction angle, λ was the wave length of Cu Kα radiation

(0.1540 nm), and k was a constant (0.89). The calculated size of silver nanoparticle protected by PVP was about 20 nm which is in a good agreement with the value obtained from SEM. Although the size and shape of obtained particles with a presence of PVP were desired, there was a problem with separation of particles from the solution. With a view of improving this disadvantage the surfactant sodium bis (2-ethylhexyl) sulfosuccinate (AOT) was used as an alternative capping agent and a new simple procedure was described for the synthesis of silver particles.

Reaction mechanism

The aqueous foam was formed after an aqueous solution of AOT was added to an aqueous solution of $AgNO_3$. Ag^+ ions were bonded electrostatic with AOT molecules at the air bubble-solution interface. The silver ions were reduced in the foam by hydrazine and results in the formation of silver nanoparticles stabilized by the anionic surfactants (figure 4.6).

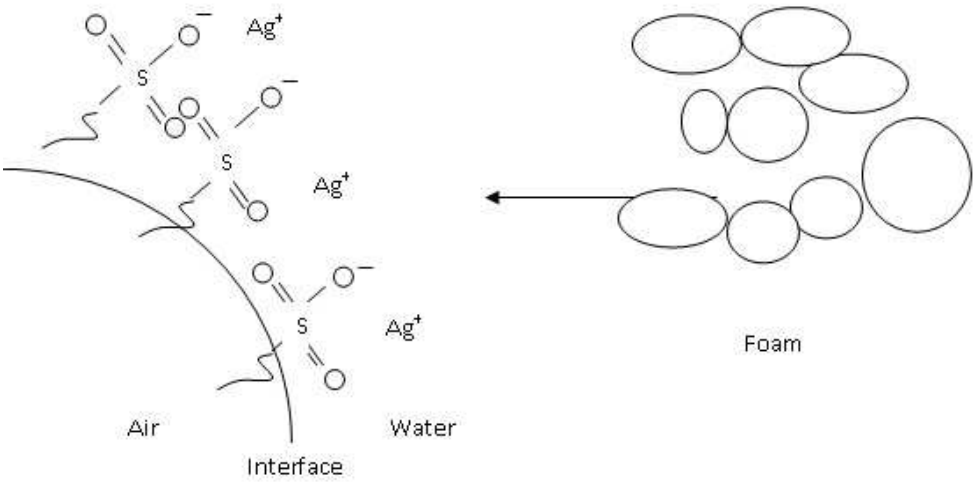

Figure 4.6 Schematic diagram of silver particle synthesis mechanism

Foam provides a high surface area of air bubbles dispersed in a liquid. The surfactant adsorbs at the gas-liquid interface stabilizing the bubbles of the foam. As a result the surface provides a high concentration of nucleation centres from which silver particles to grow. The surface therefore acts as a good template for crystallization. Silver ions are kept and spatially separated preventing the formation of large silver particles when reduced to silver metal.

The high yield of synthesised silver particles was obtained, indicating that a foam-based method for the synthesis of nanomaterials shows that the large internal surface area of the foam can be utilized to synthesize large amounts of nanomaterials in a single step.

Figure 4.7 presents SEM (a) and XRD (b) pattern of Ag particles prepared in the presence of AOT stabilizing agent. The five diffraction peaks at 2θ of 38.2°, 44.4°, 64.5°, 77.5° and 81.6° respectively could be indexed as (111), (200), (220), (311) and (222) Miller indices reflection of the face-centred cubic (fcc) structure of silver. The calculated size values for Ag samples protected by AOT, by Scherer formula at 2θ of 38.2º are general approximations to those of SEM observation which is 20 nm. Although silver is easily oxidized to oxides, some possible oxides such as (AgO, AgO_2) are not observed in the XRD profiles. It might be due to the presence of a surfactant that forms a protective layer preventing oxidation of metal. It indicates that the presented synthetic method for Ag is feasible in achieving metallic silver structure as taking into account the fact that the samples have been exposed to the air and water for a long time during the synthesis, still remaining the absence of silver oxides.

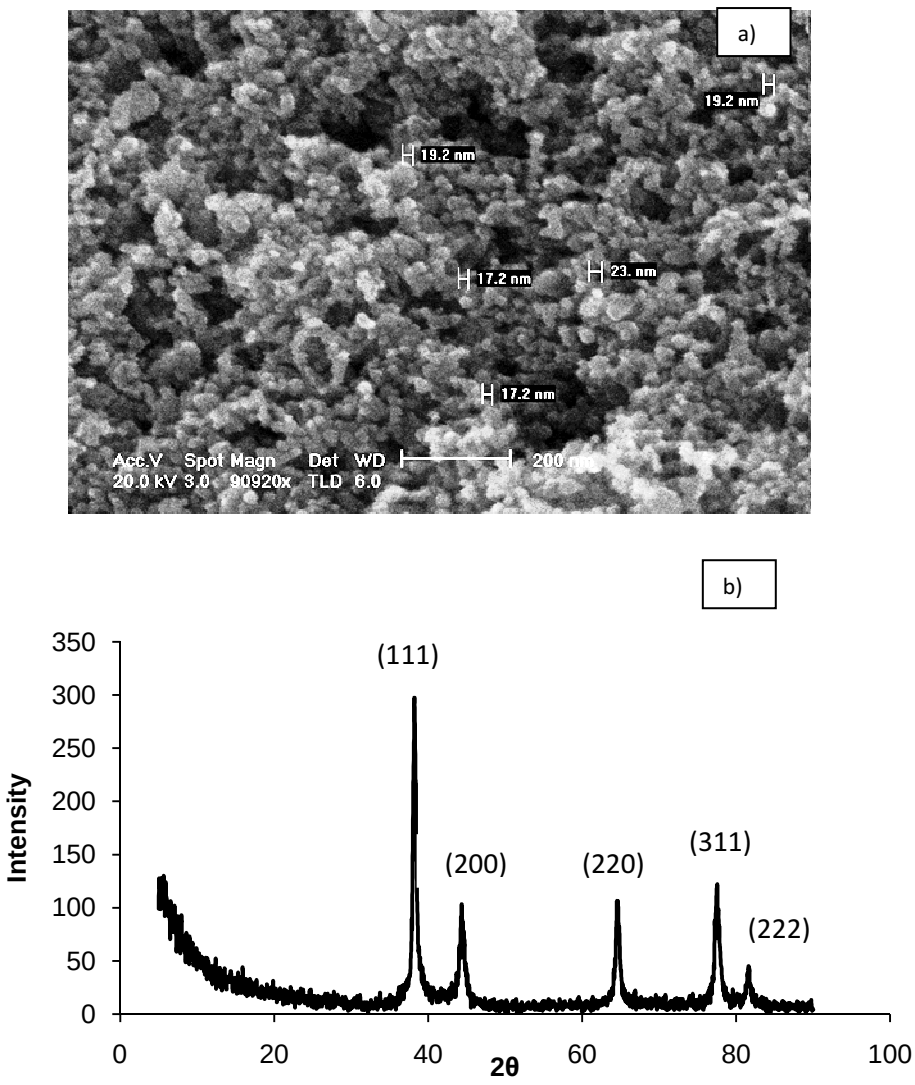

Figure 4.7 SEM micrograph (a) and XRD pattern (b) of silver particles prepared with a presence of AOT

Unlike the silver particles prepared with PVP, AOT protected silver particles were easily separated from the solution. That might be due to high solubility of PVP in water. As a result low yield of particles protected by PVP was obtained. For this reason AOT was chosen to be used in further processes.

It should also be mentioned that although polymer stabilizers play a very important role in the synthesis of metal nanoparticles, the synthesis without using any polymer stabilizers can be prepared as well. [142]. Yin et al. [143] synthesised silver nanoparticles through tollens process without adding any stabilizing reagent, as synthesized aqueous

dispersion of silver nanoparticles of 20–30 nm in size was found to be very stable due to electrostatic stabilization mechanism. However, the particle size is sensitively dependent on the synthesis temperature and any variation of temperature would results in a significant change of metal nanoparticles size.

4.2.2.1 The effect of AOT concentration on particle size

The appropriate amount of present surfactant in the solution is very important for the well working protection mechanism. From the thermodynamic point of view, the interaction between two approaching and fully covered by stabilizer particles will occur when the distance (d) between the particles becomes shorter than twice the thickness (L) of the stabilizer layer on the particles. In this case, the Gibbs free energy will increase and the particles repel each other. However, when there is not enough a stabilizer present to cover the surface, the polymer tends to interpenetrate into the other polymers in order to reduce the unoccupied space between them resulting in decreasing the Gibbs energy, hence causing further agglomeration [129]. This reduces the entropy of the system.

Equation 4.3 expresses the change in Gibbs free energy

$$\Delta G = \Delta H - T\Delta S > 0 \quad (4.3)$$

where, ΔG is the change in Gibbs free energy; ΔH is the change in enthalpy, T is is the temperature and ΔS is the change in entropy.

Equation 4.4 describes ΔH:

$$\Delta H = U_{sys} + PV \quad (4.4)$$

Where U_{sys} is the energy of the system, P is the pressure and V is the volume.

If the change in energy for the system of the two particles approaching each other comes to zero then ΔH can reach zero. Taking this into account, it can be said from the equation 4.3 that two particles covered with stabilizer will repel each other. Hence, the

distance between the particles must be ≥2L [129] in order to prevent the aggregation of the particles.

Based on the results of the previous tests, a surfactant AOT was chosen to study the effect of its concentration on particle size and shape. It was carried out by preparing solutions of AOT with different concentrations, ranking from 4 mM up to 0.01 M. The prepared solutions were used in Ag synthesis, while the other conditions were kept the same.

Figure 4.8 shows nanoparticles tracking analysis (NTA) of Ag NPs prepared with various AOT concentrations (4 mM (a), 7 mM (b), 9 mM (c), and 0.01 M (d)). The results revealed that the size of Ag nanoparticles can be tuned by concentration of AOT. The average diameter of Ag nanoparticles from NTA was 80 ± 36 nm when concentration of AOT was 4mN. Increasing the concentration of AOT up to 7mM, led to the average diameter of Ag nanoparticles of 70 ± 10 nm. When the concentration of AOT was further increased to 9 mM, the average diameter of Ag nanoparticles was 60 ± 12 nm. When the concentration of AOT was increased to 0.01 M, the average diameter of obtained Ag nanoparticles increased to 110 ± 36 nm.

Summarizing the experimental results, particle size decreased as the amount of surfactant was increased. This might be explained by the fact that the smaller droplets have more collisions and therefore need more surfactant to stabilize the particles. During particle nucleation, the better colloidal stabilizer in the initial stage of particle growth in batch will lead to smaller final size of particles [144].

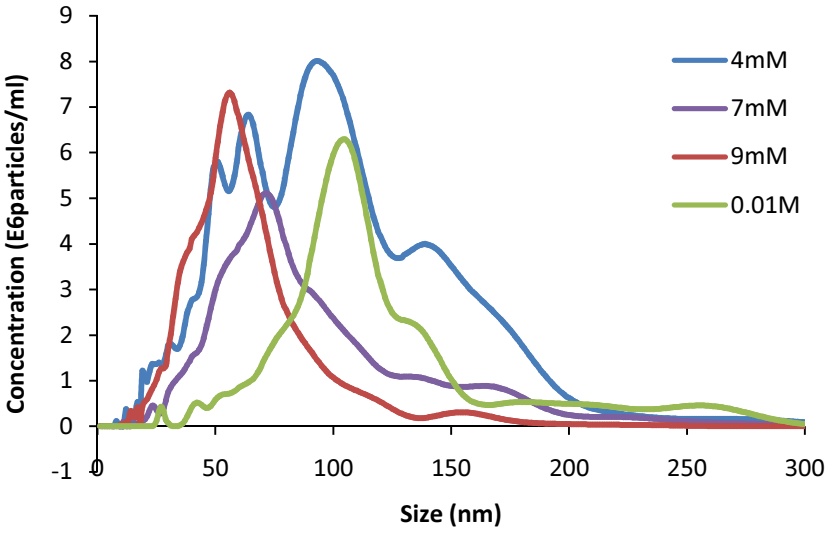

Figure 4.8 NTA analyses of Ag particles prepared with different AOT concentration

However based on obtained results it might be said that a further increase in surfactant concentration will not necessarily lead to a dramatic reduction in particle size. More surfactant in a solution can also lead to the presence of free surfactant micelles.

Figure 4.9 presents SEM pictures of Ag particles obtained from the 4 mM (a), 7 mM (b), 9 mM (c), and 0.01 M (d). The morphology of all obtained particles was spherical.

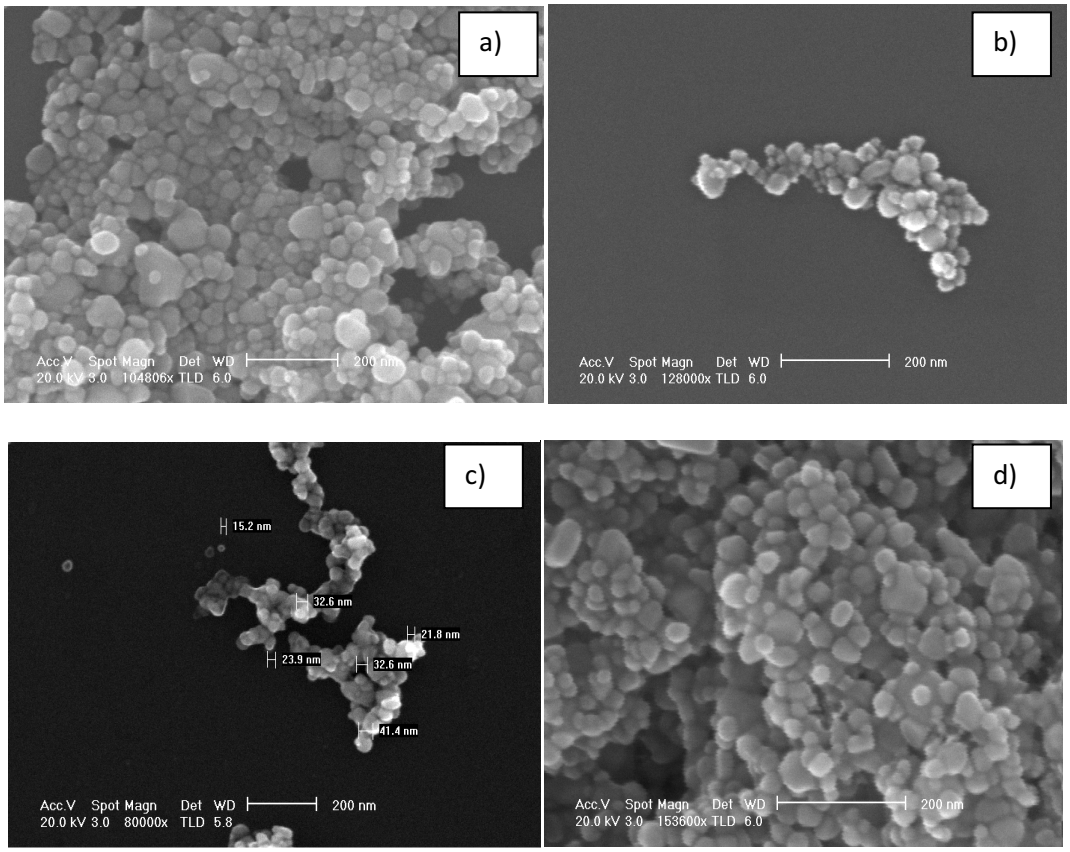

Figure 4.9 SEM micrographs of Ag particles obtained at (a) 4mM, (b) 7mM , (c) 9mM, and (d) 0.01M AOT

The average size of particles obtained with AOT at the SEM picture is smaller than those obtained with NTA analysis. This is due to stretching of the AOT molecules away from the Ag particles while suspended in a liquid solution. Since the NTA measurements are performed on the nanoparticle solution, the diameter of the particle will be measured as two times the thickness of the AOT layer plus the diameter of the actual particle. On the other hand, during SEM measurement, the particle is placed on a wafer and the solvent is removed, as a result AOT layer on the particle will collapse on its surface. This means that the diameter will decrease compared to that measured by NTA, however it is still bigger than the actual particle.

4.2.3 Effect of NaOH concentration

The role of NaOH on the size and morphology of final particles was studied by varying its concentration. At the end of the synthesis process NaOH was added. It has been found that addition of NaOH increases the production yield, reduces the size of particles and improves the morphology of the Ag particles. Additionally, When the concentration of sodium-hydroxide solution is high (0.3 mol) the obtained morphology was the spherical nanoparticles while no presence of NaOH causes irregular shape of the particles (figure 4.10). Different concentration of sodium hydroxide resulted in various morphology and size of final particles (figure 4.11). The size and the morphology of the samples were investigated by SEM. Images in figure 4.10 shows spherical Ag nanoparticles (a-c) with the average size between 80 and 400 nm depends on the NaOH concentration. Figure 4.10 (d) shows the disks shape silver structures with average size of 250 nm.

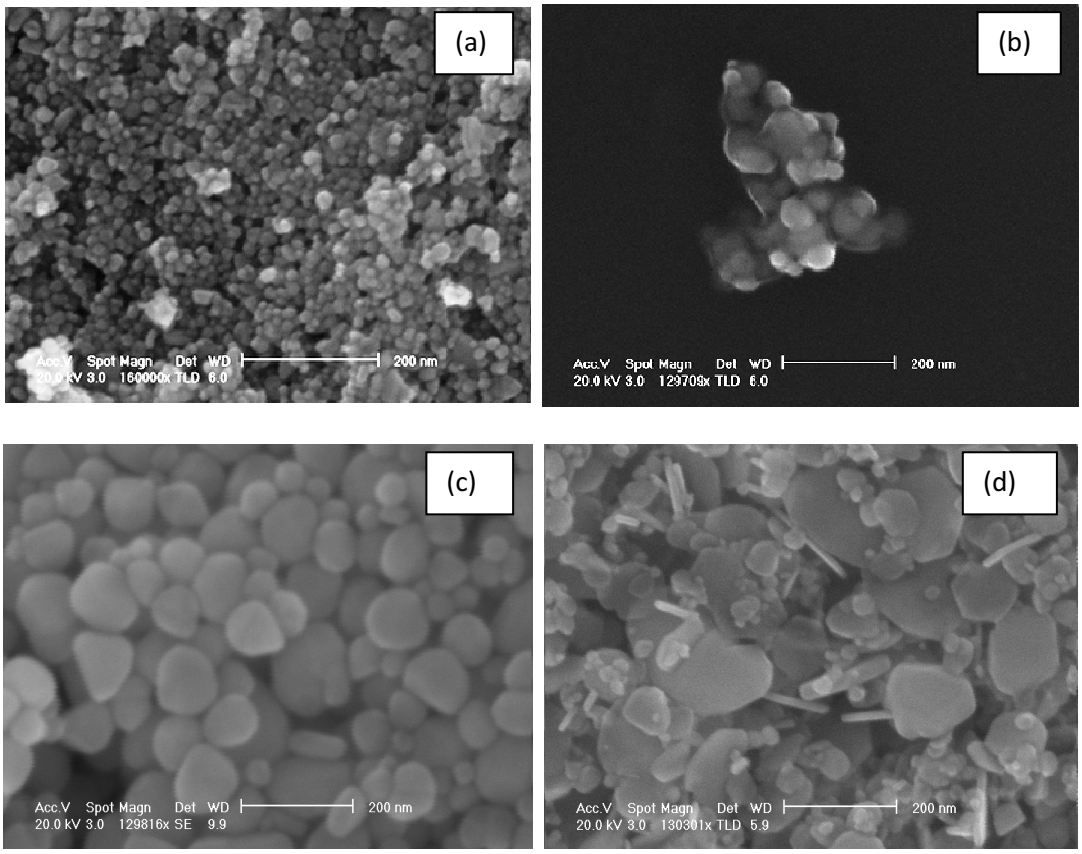

Figure 4.10 Ag nanoparticles prepared with NaOH concentration of (a) 0.005 mol, (b) 0.125, (c) 0.025 mol and (d) without addition of NaOH

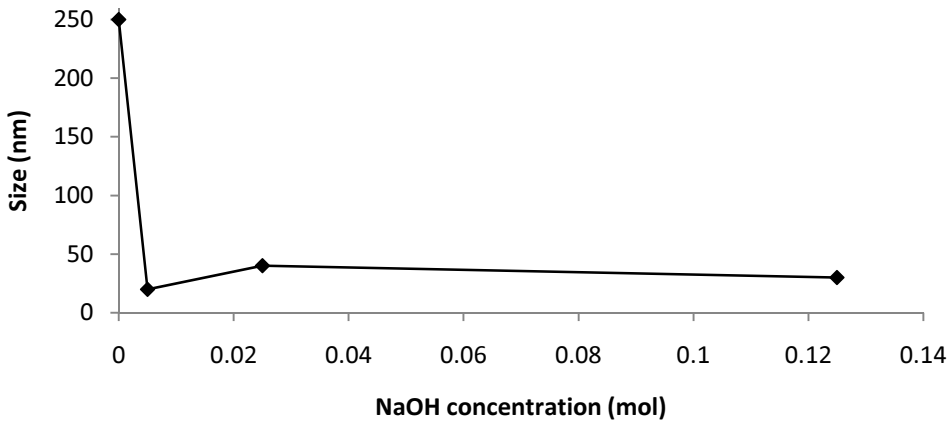

Figure 4.11 Graph showing the size dependence on NaOH concentration of the samples shown in figure 4.10

The XRD patterns of spherical Ag nanoparticles with size between 20-250 nm areshown in figure 4.12 All of the three characteristic peaks for silver (2θ = 38.2°, 44.4°, 64.5°, 77.5° and 81.6°), corresponding to Miller indices (111), (200), (220), (311) and (222), are observed. The intensity of these peaks decreased as the size of the particles decreases.

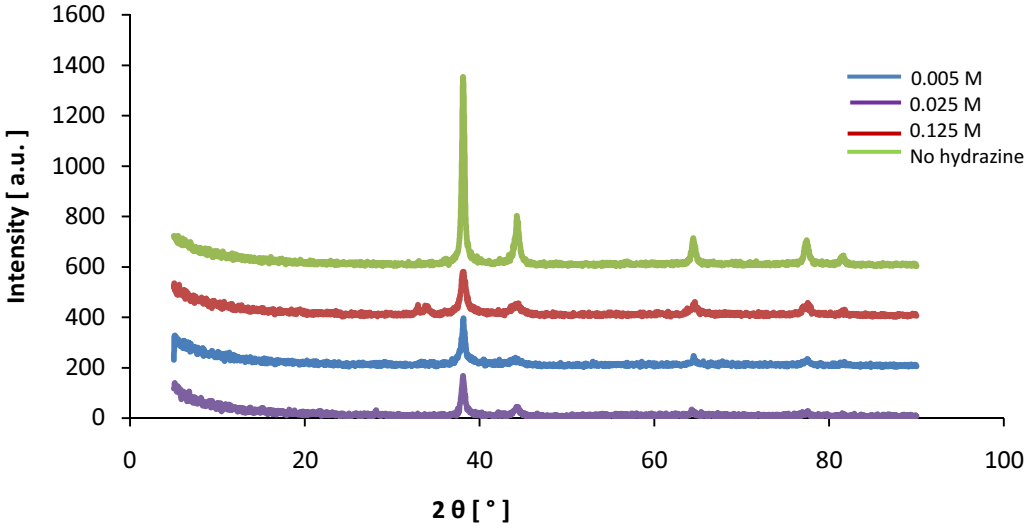

Figure 4.12 XRD pattern of silver particles prepared with 0.005 mol, 0.025 mol 0.125 mol, and without addition of NaOH

4.3 Study of $scCO_2$synthesis parameters on size and morphology of silver particles

A $scCO_2$ as a second method to be investigated for synthesis of Ag nanoparticles was prompted by the advantageous properties of supercritical fluids that bring the benefits of broad process application. $ScCO_2$ combines properties of liquid such as high solubility and high density as well as those of gases, like low viscosity. More over is not-toxic, and easy to recover. Its dissolving properties can be widely varied by alteration of pressure and temperature.

UV-Vis analysis

To check the effect of various factors, such as time, pressure and temperature, on final product, UV-Vis spectrophotometer was used. In metal nanoparticles such as silver, the conduction and valence band areoverlapped so that the electrons can move freely. Due to the collective oscillation of electrons of silver nanoparticles in resonance with the light wave [147], the free electrons give rise to a surface plasmon resonance (SPR) absorption band [148-150]. The electric field of an approaching wave causes a polarization of the electrons with respect to much heavier ionic core of silver nanoparticles, resulting in that a net charge difference occur which in turn acts as a restoring force. This forms a dipolar oscillation of all the electrons in the same phase. A strong absorption takes place, when the frequency of the electromagnetic field becomes resonant with the coherent electron motion. This absorption strongly depends on the size of the particles, dielectric medium and chemical surroundings [151, 152]. The absorption peak (SPR) for silver obtained with $scCO_2$ is in the visible range at 410 nm.

4.3.1. Effect of reaction time on particles growth

The reduction of silver nitrate in ethylene glycol (carry out in a reaction vessel) might be written as follows:

$$HO\text{-}CH_2\text{-}CH_2\text{-}OH \longrightarrow 2\ CH_3CHO + 2\ H_2O \quad (4.5)$$

$$2\ CH_3CHO + 2\ Ag^+ \longrightarrow CH_3CO\text{-}OCCH_3 + 2\ Ag + 2H^+ \quad (4.6)$$

The mass transfer of $scCO_2$ diffuses effectively into reaction solution to promote the synthesis of particles [145]. The high diffusivity of $scCO_2$ reduces the viscosity of the ethylene glycol and penetrates the entire solution to promote the contact frequency of silver ions (Ag^+) and electrons (e^-) [146].

The reaction was carried out for 1 and 3 hours at various pressures and temperatures. Figure 4.13 shows the Uv-Vis spectrum of Ag particles synthesised at 200 bar and 80 ºC for 1 hr. It can be noticed that shorter time of reaction resulted in a low absorbance value of 0.14, moreover after a three days the absorbance value for silver dispersion increased up to 0.21. That indicated that in the obtained sample some amount of $AgNO_3$ was presented and its further reduction with ethanol took place. The same has been done for the other temperatures and pressures values and the results are shown in Table 4.1. Based on the results, it was decided to perform all reactions for 3 hours. To complete the reaction, either high temperature, or high pressure was required.

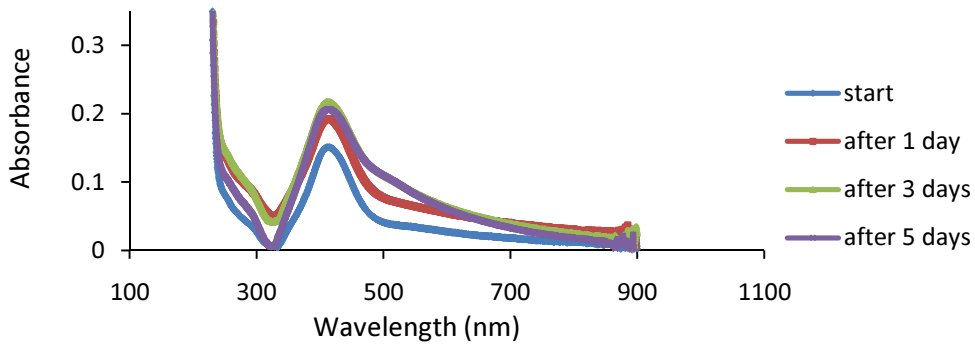

Figure 4.13 UV-vis spectrum of Ag nanofluid made at conditions: 200 bar, 80 ˚C and 1hrs.

Table 4.1 The presence of $AgNO_3$ in a receiving fluid from synthesis of silver particles at different pressure, temperature and time

Pressure [bar]	Temperature [°C]	Time [hour]	Presence of $AgNO_3$ in a collected solution
160	50	1	Yes
		3	Yes
	60	1	Yes
		3	Yes
	80	1	Yes
		3	**No**
180	50	1	Yes
		3	Yes
	60	1	Yes
		3	Yes
	80	1	Yes
		3	**No**
200	50	1	Yes
		3	Yes
	60	1	Yes
		3	Yes
	80	1	Yes
		3	**No**

4.3.2. Effect of temperature on particles growth

The particles synthesized by chemical reduction are consisted of two steps; the nucleation that forms new particles and growth of grain that increases the particles' characteristic length. Faster nucleation relative to the grain growth produces a smaller particle size and this process is very sensitive to temperature [153]. Figure 4.14 shows UV-Vis absorption spectra of the synthesised Ag nanoparticles at 200 bars and 50, 60, and 80 ºC. The absorption peak of silver is obtained in the visible range at 410 nm.

For the lower temperatures the peaks are broaden, owing to the smaller size of the particles.

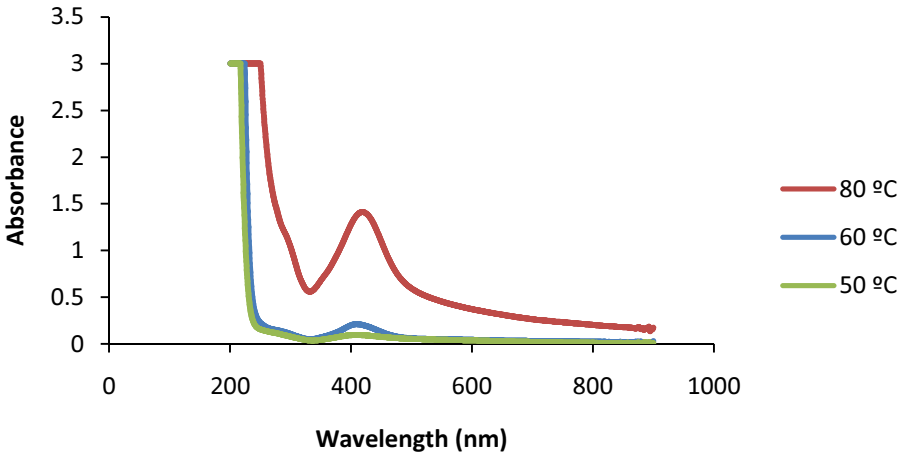

Figure 4.14 UV–Vis spectrum of Ag ink made at 200 bar and different temperatures, for 3 hrs

Figure 4.15 presents SEM images of the as-synthesized Ag nanoparticles. It was found that they are spherical, and 30, 50, and 100 nm in diameter at 50, 60, and 80 °C respectively, carrying out the reaction at 200 bars. It may be that at higher temperatures the rate of particle growth increases and possibly leads to the formation of larger Ag particles. However, a lower reaction temperature resulted in a smaller value of absorbance, indicating that the energy is not big enough for ethylene glycol to transfer aldehydes into ketones, producing electrons to form Ag nanoparticles via the supercritical CO_2 process.

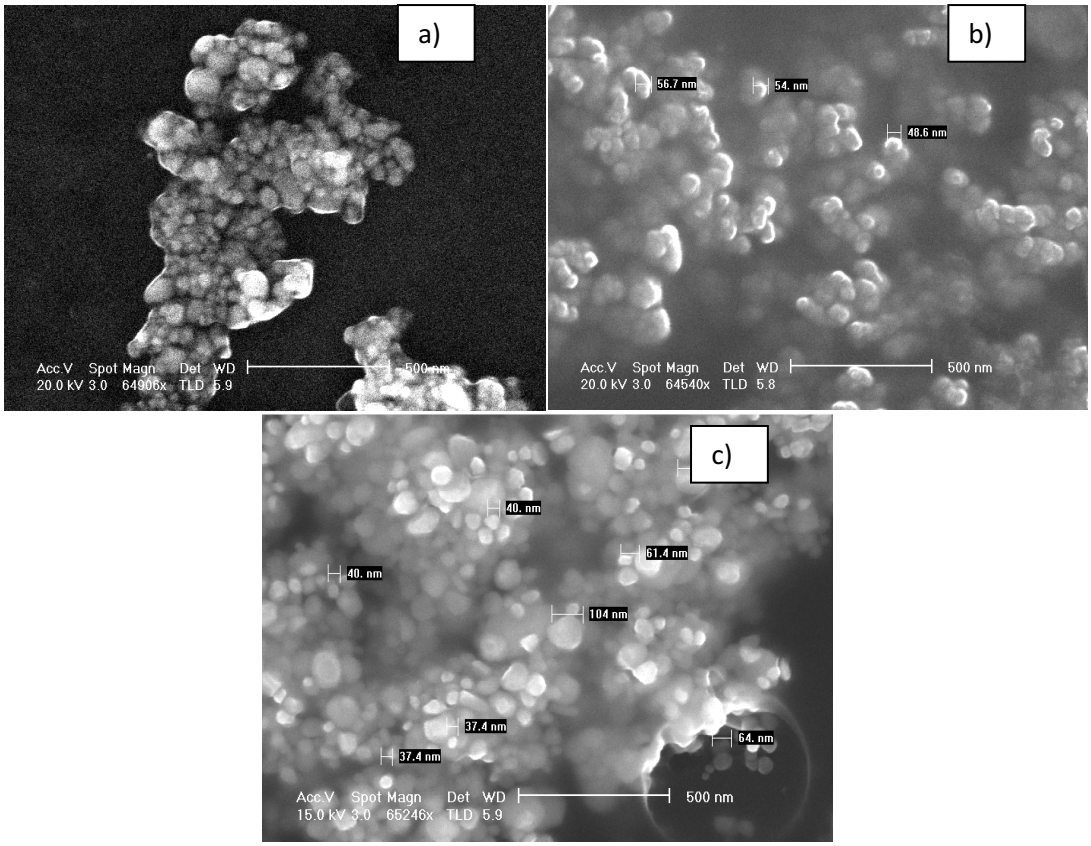

Figure 4.15 SEM micrographs of Ag particles prepared at (a) 50 ºC, (b) 60 ºC, and (c) 80 ºC

4.3.3. Effect of pressure on Ag particles growth

The pressure variable is of the same importance as temperature and chemical composition for synthesis of nanoparticles.

The energy barrier ΔG^* forms a spherical nucleus described by [154, 155]

$$\Delta G^* = 16\pi\gamma^3 / 3\Delta G_v^2 \tag{4.7}$$

whereγ is the interfacial energy, $\Delta\mu$ is the difference in chemical potential, ρ is the number density and ΔG_v is the difference in Gibb's free energy per unit volume. The variation of the energy barrier with pressure can be formulated as

$$\left(\frac{\partial \Delta G^*}{\partial P}\right)_T = \left(\frac{3\Delta G^*}{\gamma}\right)\left(\frac{\partial \gamma}{\partial P}\right)_T - \left(\frac{2\ \Delta G^*}{\Delta G\ v}\right)\left(\frac{\partial \Delta G v}{\partial P}\right)_T$$

(4.8)

The pressure variation of interfacial energy is very small and can be ignored when compared with ΔG_v. With increasing the pressure, the energy barrier of nucleation step is lowered; as a

result, the nucleation rate is stepped-up. According to the phase transition theory, the lower ratio of growth rate to nucleation rate causes the decreased size of particles. Therefore, when the pressure increases, the particle size decreases. Figure 4.16 shows the UV-Vis absorption spectra of silver nanoparticles.

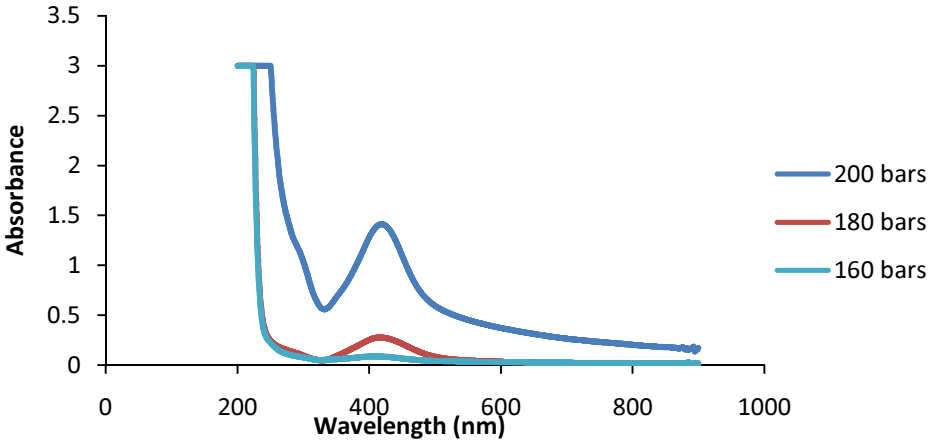

Figure 4.16 UV-Vis spectrum of Ag ink made at 80 ˚C, 3hrs, at various pressures (160, 180, and 200 bars)

The results show that, the intensity of absorption peak, at about 410 nm increases with the increase of pressure. That indicates that the higher yield can be obtained with a higher pressure. Figure 4.17 presents SEM images of the Ag nanoparticles synthesised at 80 ºC at 160, 180, and 200 bars. The Ag nanoparticles are clearly small and have a uniform dispersion due to increased solubility of CO_2 to ethylene glycol obtained by increasing pressure [156, 157]. With increasing the pressure, density and mass transfer increased and hence efficiency of supercritical CO_2 enhances the solubility of supercritical CO_2 to ethylene glycol, which makes the reactive solution rapidly reach super-saturation. In the same time it can increases the nucleation rate to affect instantaneous formation of Ag nuclei.

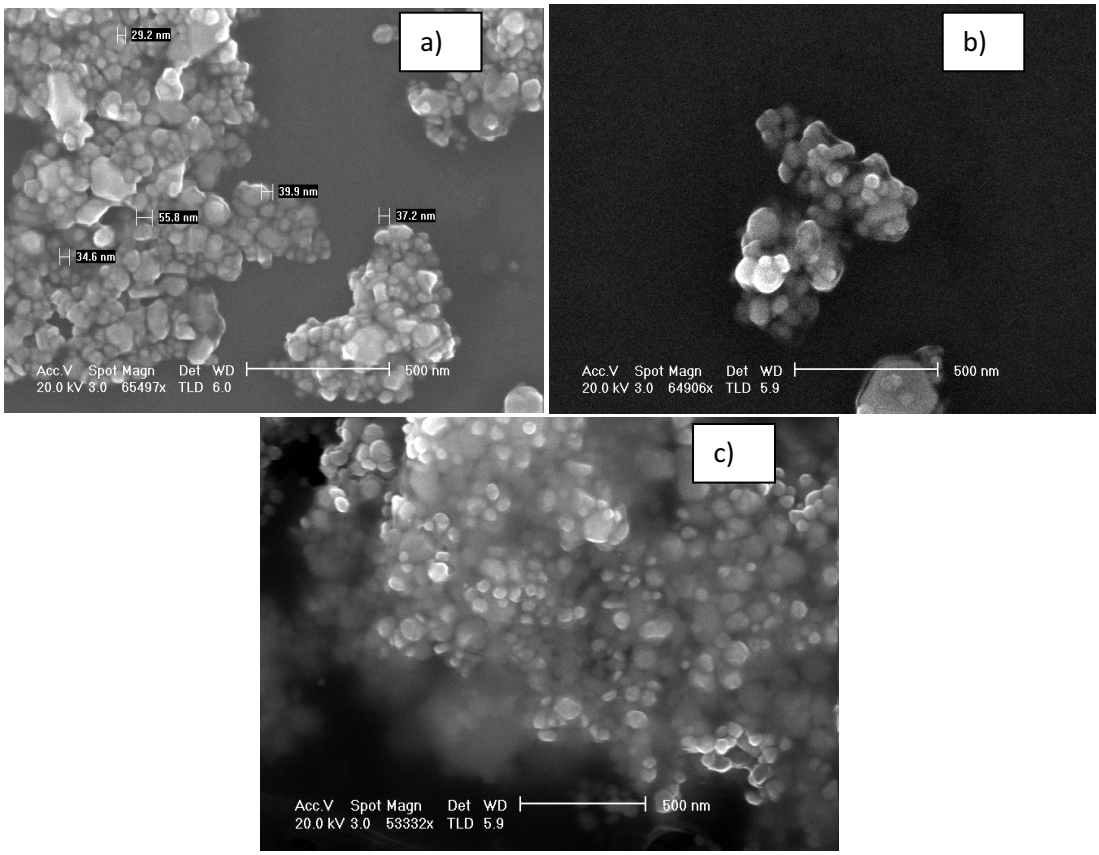

Figure 4.17 SEM micrographs of Ag particles prepared at 80 ºC and (a) 160, (b) 80, and (c) 200 bar, for 3 hrs

Figure 4.18 presents the SEM picture of Ag nanoparticles obtained at a ratio of PVP (MW 10,000)/$AgNO_3$ = 1 in the presence of ethylene glycol using a supercritical CO_2-assisted process at 180 °C and 200 bar for 3 hrs. Those were the best conditions optimized for synthesis of Ag particles in $scCO_2$.

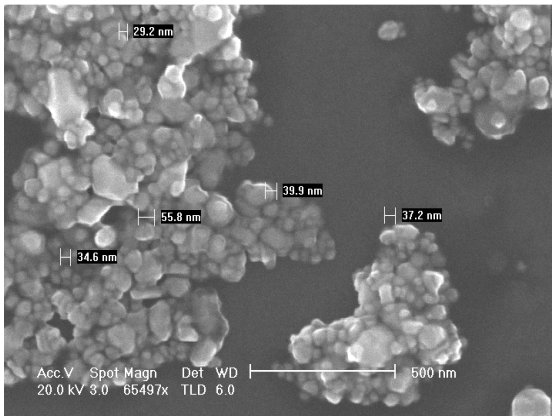

Figure 4.18 SEM micrograph of silver particles prepared in $scCO_2$ at 200bar and 80 °C for 3 hrs

4.4 Summary

An objective of this part of study was to develop a method that would allow the creation of large numbers of particles easily separable from the solution and capable to contribute to the formation of stable ink.

The wet chemistry method was developed and various reaction conditions were analysed. The morphology and dimensions of the product were found to strongly depend on reaction conditions such as type of capping agent, concentration of $AgNO_3$, AOT and NaOH. The initial concentration of $AgNO_3$ had to be lower than ~0.3 M; otherwise the final product reaches the size of 700 nm with irregular shapes. Using AOT as a stabilizer the size of obtained particles was 20 nm, they were much easier separated from the solution compared to using PVP. The molar ratio between AOT and $AgNO_3$ was set as 2:1 resulting in the smallest size of particles, changing it to 1:2 or 1:0.5 the particles size increased. Hence, the particle size decreased as the amount of surfactant was increased. However based on obtained results it might be said that a further increase in surfactant concentration will not necessarily lead to a dramatic reduction in particle size as more surfactant in a solution can lead to the presence of free surfactant micelles. Addition of NaOH was required to obtain the spherical and small particles in high yield.

Another chosen method for Ag particles synthesis was $scCO_2$. It is a very environmental friendly approach as the organic solvents are replaced by supercritical fluids with low toxicity.

The influence of $scCO_2$ pressure and temperature on silver size was investigated. The size of obtained particles decreased with increased $scCO_2$ pressure and its temperature. 200 bars and 80 ºC was the conditions under which the smallest size of particles was obtained. The time of reaction was investigated as well, showing that with longer time processing, the higher yield was possible to obtain. However there was still, compared to wet chemistry

method, not enough powder for further processing. Additionally, the wet chemistry method offers better stabilization of nanoparticles from agglomeration, easier extraction of nanoparticles from solvent, simpler control processing and enables a mass production.

For these reasons the wet chemistry method was chosen to make Ag particles for formulating the silver inks. The characterisation and application of these particles will be described in the next chapters.

Chapter 5

Development of high loading silver ink

5.1 Introduction

The preparation of metal inks requires the use of metal particles that have extremely small size to avoid the clogging of printer head. A significant decrease in particle size increases the difficulty to produce highly concentrated stable dispersions due to the stronger agglomeration and extremely high surface energy, and therefore it requires the development of new dispersion procedures, including selection of appropriate dispersants and tools to obtain long-term dispersion stability.

Once the stable dispersion of nanoparticles is obtained, the ink formulation must be adjusted according to the given specification regarding the dimension of the patterns as well as a required resolution. Additionally the rheological behaviour must be adapted to reach the process requirements.

The conductivity of printed tracks increases with the thickness of the tracks. In order to achieve thick conductive tracks with few printed layers, high solid content has to be loaded in the ink. The more concentrated the ink is, the thicker film is possible to obtain with better conductive properties, which would save time and reduce the costs of the process, otherwise more layers are required to lay down on the substrate by repetitive printing procedure. Plus higher content of solid in ink also increases the resolution of printed features since less liquid is deposited with one drop of ink.

This chapter focuses on the development and characterisation of high loading and stable Ag inks.

5.1.1 Objectives

The objectives of this portion of the study were:

1. To formulate and optimise silver inks suitable for ink jet printing application
2. To identify the optimum dispersant for the Ag inks
3. To evaluate the performances of obtained inks including study the rheology, surface energy, stability and electrical properties of the Ag inks
4. To reduce the number of layers in the silver nanoparticles film processing by increasing the thickness of a single layer with the goal of obtaining a dense 1 µm thick and conductive film (as close as possible to the bulk value, 1.58 µΩ cm).

5.2 Ag inks formulation

The inks for inkjet printing were prepared with different silver particles. They were synthesised by the wet chemistry method described in section 3.1.2, but treated with different solvents, either 2-propanol (IPA) or acetone after the synthesis. It has been found that the subsequent aggregates of Ag particles have various sizes and the inks prepared using these particles behave differently (figure 5.1). It has been observed that acetone-treated Ag NPs could be better dispersed in aqueous-based solvent, probably due to the formation of a more hydrophilic surface. Figure 5.1 (a) shows nanoparticles tracking analysis (NTA) of Ag NPs treated with two solvents. NTA is an innovative system for sizing particles from about 30 to 1000 nm, with the lower detection limit being dependent on the refractive index of the nanoparticles. This technique combines laser light scattering microscopy (DLS) with a charge-coupled device (CCD) camera, which enables the visualization and recording of nanoparticles in solution. The NTA software is then able to identify and track individual nanoparticles moving under Brownian motion and relates the movement to a particle size according to the well-known Stokes-Einstein equation.

The results show that the average size distribution of particle agglomerates treated with acetone is 80 nm and more uniform compared to those treated with IPA.

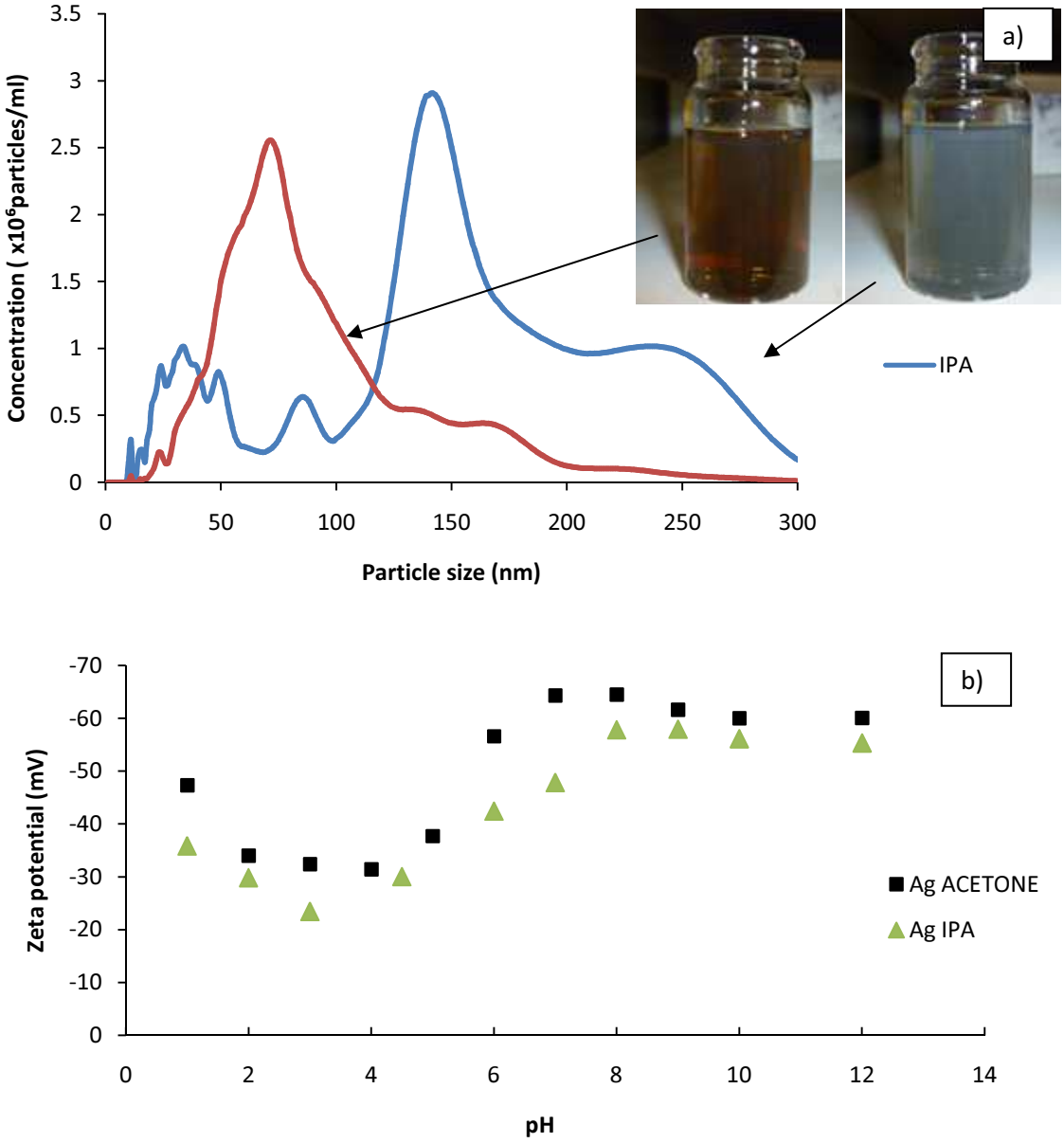

Figure 5.1 (a) nanoparticles tracking analysis (NTA) of Ag NPs treated with two solvents, and (b) zeta potential measurement of dispersed Ag nanoparticles in water

From the obtained results, the agglomeration state was also determined by the colour of the dispersed nanoparticles in solution. When the diameters of the nanoparticles increased, the maximum absorbance wavelength shifted towards the red which is visually observed in

colour of the dispersion. It can be seen in the inset of figure 5.1 (a) that a dilute solution of Ag NPs treated with acetone presents a yellow-brown colour while the solution with the particles treated with IPA shows a grey colour indicating the presence of bigger agglomerates.

Different behaviour of particles in aqueous medium indicated that their surface charge density vary from each other. To assure the well dispersed and electrostaticly stable dispersion of particles, the strong repulsive forces have to be generated on their surfaces. In order to compare the surface charge of the particles treated with acetone and IPA, the zeta potentials of two silver aqueous suspensions at different pH values were measured and they are presented in figure 5.1 (b). For both silver dispersions, the zeta potential is at the minimum when pH is between 2 and 3, indicating that the force of electrostatic repulsion between particles is weaker than it is at other pH values, and precipitation occurs. When pH is in the range of 3 to 8, the electrostatic repulsion force between particles increases and becomes sufficient to prevent particles from coagulating and settling. At pH ~ 8, the zeta potential shows the highest value which indicates that the electrostatic repulsion force between particles are the strongest so the dispersion stability of Ag nanoparticles at this pH is the best. Particles treated with acetone reached a value of zeta potential of -70 mV.

Figure 5.2 (a) and (b) show the SEM and XRD of synthesized Ag NPs treated with acetone. Ag NPs are well crystallized evidenced by XRD and some agglomerates can be observed in the SEM image, but compared with the particles treated with 2-propanol, (described in section 4.2.2.1) the sizes of these agglomerates are much smaller.

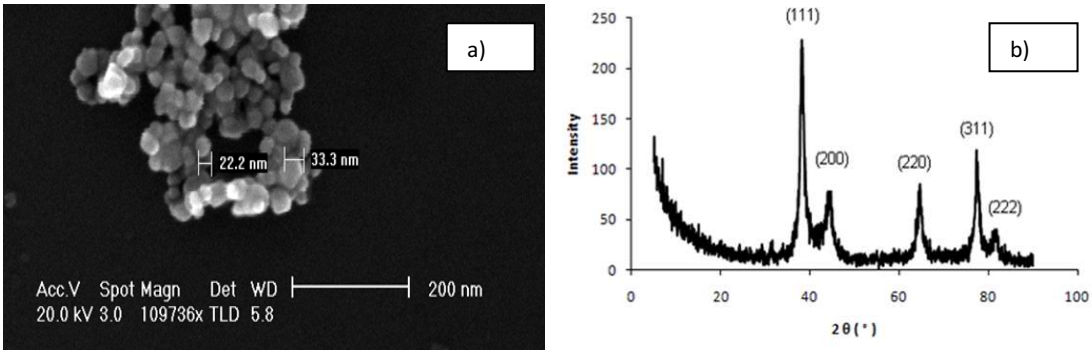

Figure 5.2 (a) SEM micrographs and (b) XRD pattern of Ag particles treated with acetone

The average size of the obtained particles at the SEM pictures is around 20-30 nm. This is smaller than obtained with NTA analysis (80nm). This is due to stretching of the AOT molecules away from the Ag particles while suspended in a liquid solution. Since the NTA measurements are performed on the nanoparticle solution, the diameter of the particle will be measured as two times the thickness of the AOT layer plus the diameter of the actual particle. On the other hand, during SEM and TEM measurement, the particle is placed on a wafer and the solvent is removed, as a result AOT layer on the particle will collapse on its surface. This means that the diameter will decrease compared to that measured by NTA, however it is still bigger than the actual particle size.

The possible maximum loading of the particles treated with IPA was 5 wt% using combination of F127 and HIFU technique. While using Ag particles treated with acetone it was possible to obtain 45 wt% Ag dispersion. Table 5.1 presents the formulation of Ag inks.

Table 5.1 Ag inks formula

Ink	Solvent		Powder		Dispersant	
	Name	**wt%**	**Name**	**wt%**	**Name**	**wt%**
A1	Water	92.9	Ag/IPA	5	F127	2.1
A2	Water	52.9	Ag/Acetone	45	F127	2.1

Two inks will be separately described below in terms of their properties, printability and post annealing characterisation.

5.3 Physicochemical properties of silver nanofluid, and the effect of F127 and HIFU on its properties – AG1 formula

5.3.1 Rheologiccal behaviour of silver nanofluid

The important characteristic of inks for inkjet printing is their rheological behaviour. During inkjet printing, the high shear is applied to the nozzle; hence it is important to observe the rheological property of the ink to get an idea about behaviour of the ink during printing.

On rheological parameters, such as viscosity and yield stress, a solid content has an influence. Figure 5.3 presents the change in viscosity of the aqueous Ag suspensions against shear rate. The suspensions contain Ag particles with different solid concentrations (1, 3, and 5 wt %). It can be seen, as expected, that the viscosity rises with increasing silver content in a fluid. The viscosity value for 1wt% of silver in ink is 1.6 mPa s and it increases up to 2.1 mPa s when silver loading increases to 5 wt%. That is due to the increase of the interaction between silver particles when solid content increases. The rheological behaviour of the

suspension containing nanoparticles depends mainly on the interaction between the nanoparticles. When two suspended particles approach each other, the double layer on each particle overlaps and repulsive forces on each other are generated. These repulsive forces are partly influenced by an attractive force due to the van der Waals interaction between the approaching particles, as well as on the medium they are dispersed [66].

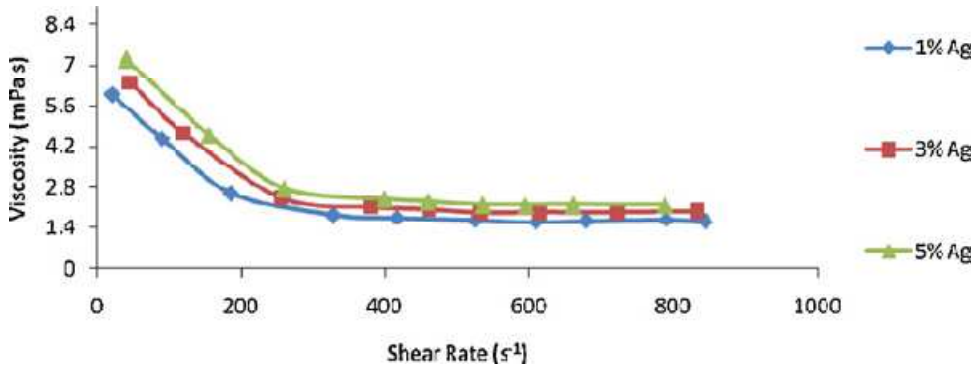

Figure 5.3 Rheological behaviour of ink with different silver contents. The ratio of Ag: F127 is fixed at 1:0.6 by weight

The yield stress is the minimum stress value needed to be applied before the fluid flows. Yield stress values (τ_0) were calculated by Bingham (equation (5.1)) and Casson (equation (5.2)) models [158],

$$\tau = \tau 0 + \eta \tag{5.1}$$

$$\sqrt{\tau} = \sqrt{\tau 0} + \sqrt{\eta + \gamma} \tag{5.2}$$

where τ is the shear stress (Pa), τ_0 the yield stress (Pa), η the viscosity (Pa s)when the shear rate, γ (s^{-1}), reaches an infinite value.

The above Bingham model only studies the linear part of the curve of shear stress as a function of shear rate, while the Casson model studies the entire curve. The correlation factor (R^2) for the two models was always close to 1, indicating that both models approximate the viscosity curves. Table 5.2 shows the yield stress values and correlation coefficient for Ag fluid with various solid concentrations.

Table 5.2 Parameters and correlation coefficient for Ag inks

Sample	Ag concentration	Bingham model		Casson model	
N°	(wt%)	τ_0 (Pa)	R^2	τ_0 (Pa)	R^2
1	1	0.25±0.001	0.996	0.08±0.01	0.998
2	3	0.41±0.0008	0.992	0.12±0.02	0.997
3	5	0.63±0.001	0.995	0.21±0.01	0.998

When silver content increases from 1% to 5%, yield stress increases from 0.25 to 0.63 Pa for a Bingham model and from 0.08 to 0.21 Pa for Casson model.

Based on obtained results, one can say that the fluid displays a Bingham plastic behavior. In this model, fluid has linear shear stress which requires a finite yield stress before fluid flows. After this point the flow rate increases steadily with increasing shear stress (figure 5.3). The physical reason for this behaviour is that the liquid contains particles which interact, creating a denser structure and a certain amount of stress is required to break this structure. Once the structure has been broken, the particles move with the liquid under viscous forces [158].

5.3.1.1 Dispersant amount optimization

It is important to determine the optimal amount of dispersant in a particle suspension as an insufficient amount of dispersant would result in the flocculation of some particles while excessive amount of dispersant would increase the viscosity, and either of these is causing destabilisation of the suspension.

The well-known method for dispersant amount optimisation is the measurement of viscosity. When the particles agglomerates trap some liquid the suspension behaves like it has apparent higher solid content. Hence it is possible to use the viscosity measurement to

determinate the best amount of dispersant to be added to a suspension. With the increasing concentration of dispersant the viscosity of the dispersion usually decreases up to certain concentration followed by increasing viscosity above that concentration.

Plotting the viscosity versus amount of added dispersant results in the curve where the minimum of the viscosity value corresponds to the optimum amount of dispersant. This point indicates that the particles are covered with a layer of dispersant which enables stabilisation of particles in liquid media.

Figure 5.4 shows the influence of dispersant concentration on the particle size of 1 wt% Ag aqueous suspension, at different HIFU times.

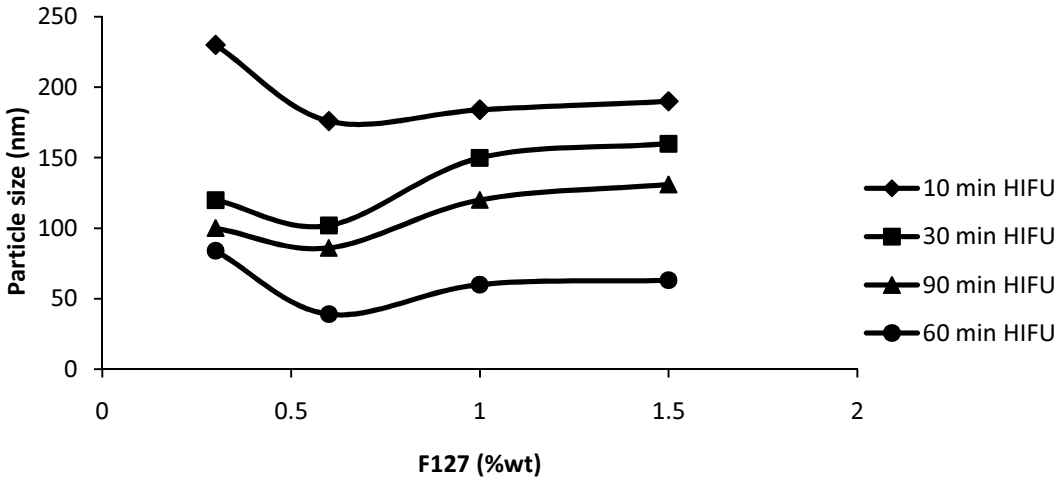

Figure 5.4 Effect of different amounts of copolymer added to1 wt% of Ag suspension on the particles size at different HIFU treatment times

It can be seen that the average particle size is reduced with the increase of dispersant (F127) amount and reaches the minimum at the concentration of 0.6 wt% at any given HIFU time. However, at a given dispersant concentration the average silver particle size firstly decreases with the time of HIFU treatment up to 60 min, and then increases to larger value at HIFU treatment for 90 min. The minimum particle size was obtained in a silver suspension with 0.6 wt% F127 after 60 min HIFU treatment. Increasing the time of HIFU treatment leads

to finer particles and thus increases the surface area, which needs more dispersant to cover the fresh surface. The amount of dispersant at tested F127 wt% may not be enough therefore leading to the reagglomeration. It is known that the adhesive forces of nano particles increase rapidly and become the dominant factor.

Figure 5.5 shows the change of viscosity against the concentration of dispersant at 1 wt% Ag concentration suspension. The HIFU treatment time was varied from 10 to 90 min for each sample. As can be seen, the viscosity values at any given HIFU treatment time decrease gradually with increasing concentration of dispersant and reach a minimum at the concentration of 0.6 wt%. Further addition of dispersant raises the viscosity of the suspension. This specific amount of copolymer is related to the size and the surface area of the particle to be covered: smaller particle size means higher surface area and hence higher amount of dispersant is needed.

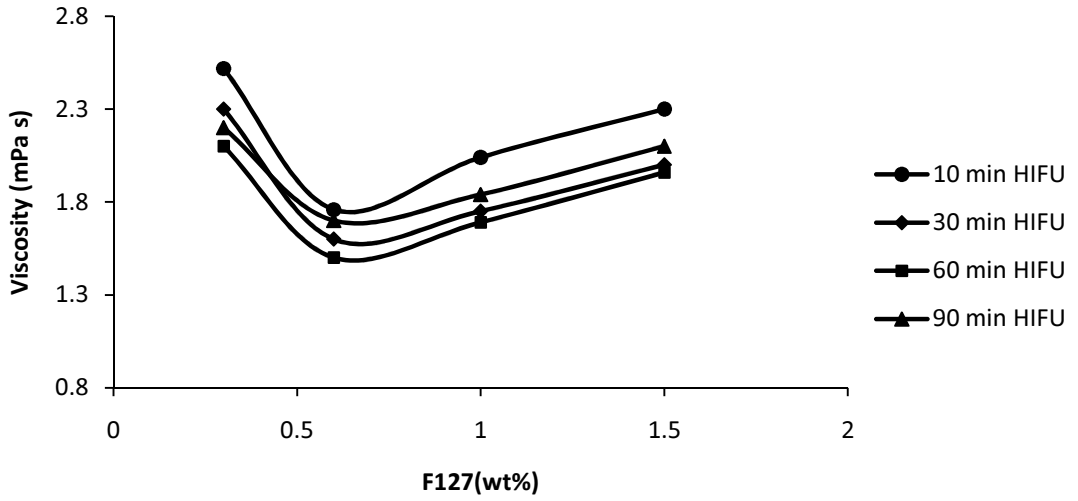

Figure 5.5 Effect of copolymer concentration on the viscosity of 1% Ag aqueous suspension at different HIFU treatment times

These results shown in Figures 5.4 and 5.5 indicate that the amount of F127 required for monolayer coverage and the amount required for reaching the minimum viscosity correlate very well.

5.3.1.2 Investigation of dispersing method

Particle size reduction and their dispersion can be achieved with various techniques, such as ball milling or ultrasaounds methods. In present work, for the first time, HIFU technique has been investigated as a potential method for preparing particle dispersion. As a top-down technique, and in comparison with conventional ultrasonic agitation and ball milling methods, HIFU introduces several novel aspects [56]: (1) The high amplitudes (up to 10^8 Pa) and frequency (~10^6 Hz) mean that as a beam propagates, it deforms, and can develop a "shock" wave front, i.e. the non-linear propagation effects; (2) Since the frequency of ultrasound is increased from ~10^4 Hz to ~10^6 Hz, the threshold value of strong micro scale transient cavitations are significantly increased. Therefore, the immense temperatures and pressures and the extraordinary heating and cooling rates generated by cavitations bubble collapse could be alleviated. There's no distinct temperature increase at all [56]; (3) It avoids the possible contamination to the fluid due to bead breakage during ball milling and the prolonged ball milling process.

Figure 5.6 illustrates the change of average particle size against HIFU treatment time for different Ag contents at a given dispersant concentration. With the increase of the HIFU treatment time up to 60 min, the particle size decreases in each sample. When the dispersion has low content of Ag particles the effect of HIFU treatment is better resulting in the smaller size of the particles. Although the minimum size is possible to obtain in the suspension with 5 wt% Ag (60 min HIFU treatment), the increase of silver content up to 10 wt% in a suspension slows down the disaggregation process.

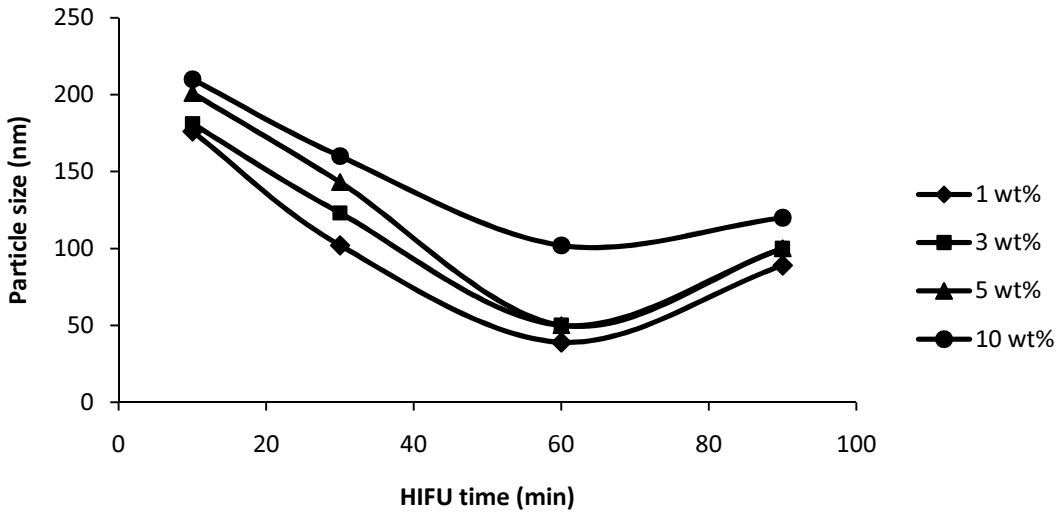

Figure 5.6 Particle size as a function of HIFU treatment time at different solid loading

5.3.1.3 Stability

The nanopartricles dispersion should be stable to aggreagtion and precipitaion in order to prevent nozzle clogging and to obtain ink with reproducible performance. The ink should be stable at least during the process of printing (8 hrs), and in the best case, for printed electronics applications, it is good to store the ink for several months because silver is expensive.

To evaluate the stability of nanofluids treated by HIFU with the presence of F127 copolymer, the viscosity of nanofluids, containing 5 wt% Ag nanoparticles, 0.6 wt% dispersant and treated by HIFU for 60 min, was measured against the time over 20 days (figure 5.7). It was found that there was almost no viscosity change up to 10 days and after this time, viscosity linearly but slowly increased with the time. The increase of viscosity from 2.1 mPa s in Day 1 to 2.3 mPa s in Day 20 was due to the agglomeration and the formation of larger particle clusters. However, no sedimentation was observed up to 20 days.

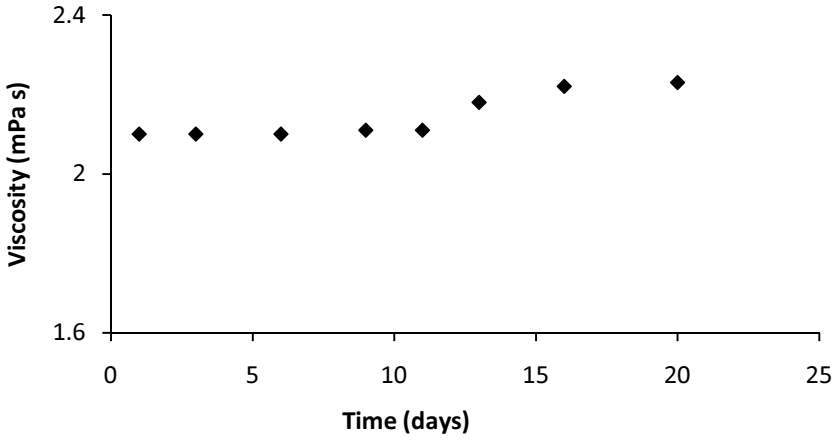

Figure 5.7 Viscosity change of nanofluid treated by HIFU in the presence of F127 against time

The formed large particle clusters due to the agglomeration could be broken and re-dispersed in the water if HIFU treatment is re-used and the rhoelogical properties of the dispersion can resume to the inital values, extending the shelf life of the ink up to 1 month.

5.3.2 Surface tension measurement

The surface tension plays an important role in any drop creation including inkjet printing. The ink suited for inkjet printing should have appropriate surface tension (25-50 mN/m) in order to facilitate drop formation.

The stalagmometric method has been explained in Section 3.3.2.2. In this project it was used for surface tension measurements of silver nanofluid. The first set of measurements was performed to check and calibrate our pendant dropset-up. Tests on Ag nanofluid were performed with different loading of (1, 3 and 5 wt %) Ag nanoparticles. The results of these tests are presented in table 5.3. For each test ten consecutive drops were measured.

Table 5.3 Surface tension results for water and Ag fluid using stalagmometric method

Fluid	Ag content (wt%)	Surface tension (mN/m)
water	0	71.8±0.2
Ag ink	1%	30.8±0.3
Ag ink	3%	30.5±0.3
Ag ink	5%	30±0.2

The measured values indicate that our stalagmometric method set-up and calculation is quite accurate and precise because the measured surface tension values for water were close enough to the literature values and the standard deviation is low. The presence of nanoparticles in the Ag fluid slightly changed the surface tension of the ink. The surface tension rises with decreasing silver content in a fluid. The surface tension value for 5 wt% of silver in ink is around 30 mPa s and it increases up to 30.8 mPa s when silver loading decreases to 1 wt%.This is attributed to the increase of water content in the ink formula.

5.3.3 Film characterisation

5.3.3.1 Conductivity measurement

The main requirement for printed materials, besides processability in liquid form and physicochemical properties, is their electronic functionality. The conductivity of the printed features, in the best case, should be as close as possible to the bulk value of a given metal.

In order to check the conductive properties of the Ag inks, printed films were prepared and tested using four points probes technique.

The prepared Ag ink has low viscosity (~2 mPa s) and desirable surface energy, 30 mN/m, that is lower than the surface energy of substrates (54 mN/m for Al_2O_3), hence it ensures

good wetting of the substrates by the ink; also this surface energy of the ink is lower than the inkjet printer requirement for surface energy (max. 60 mN/m) in order to jet droplets.

Figure 5.8 shows optical microscope pictures of inkjet printed ink on the alumina substrate. The printed line has a good geometry. However, in order to achieve conductive film, number of layers had to be printed due to the low content of Ag in the ink. After printing, the sample was sintered at 350 ºC. Direct physical contact between the particles occurred after the organic reagents were burnt off, and conductivity measurement was possible to undertake.

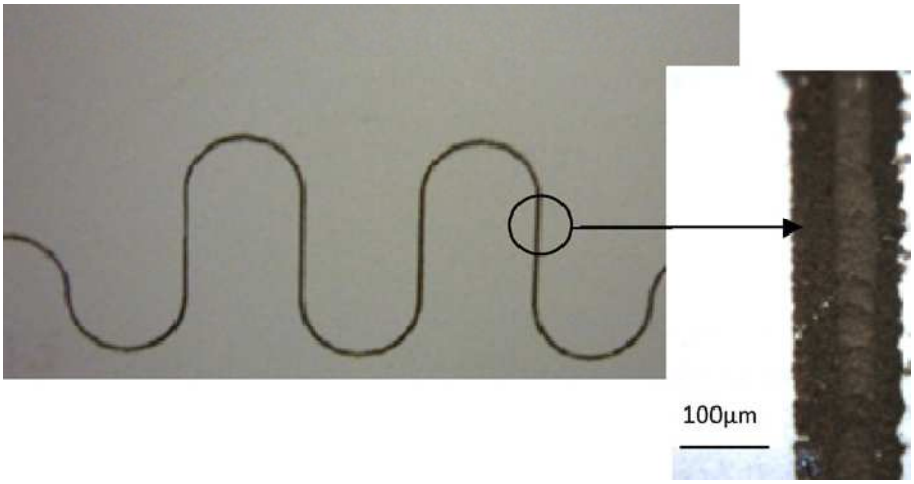

Figure 5.8 Printed Ag lines on alumina substrate

In this target single lines consisted of 60 layers with a length of 5 mm of the inks were inkjet printed onto alumina substrate and subsequently sintered at 350 °C for 60 min on a hot plate. The resistance was measured using four points probe technique. The electrical resistivity ρ of an inkjet printed line was calculated from resistance *R*, length l, and cross sectional area *A* of the line, using equation (5.3):

$$\rho = R \cdot A / l \tag{5.3}$$

The cross section area was determined by numerical integration of a measured profile (Dektak instrument, optical microscope, SEM). The obtained value was subsequently compared to the value of bulk silver (1.59×10^{-6} Ω cm) [159].

As Ag loading, 5 wt%, in the ink is low, the multilayer printing approach helps build up dense and conductive films. The film consisted of 60 layers showed a reasonably low resistivity.

Figure 5.9 shows the SEM pictures of printed Ag layers on Al_2O_3. The film in figure 10 (a) consisted of 60 layers and was sintered together at 350 °C for 60 min. The film in figure 10 (b) also consisted of 60 layers, but sintered at 350 ºC for 20 min after the deposition of each 20 layers. The resistivity of the film with layers sintered together showed a value of $(4 \pm 0.1) * 10^{-5}$ Ω cm, while the film sintered after the deposition of each 20 layers showed a $(2 \pm 0.1) * 10^{-5}$ Ω cm. As can be seen in figure 5.10, the sintering between printed layers improves final structure of the film in terms of its density which is directly linked to the better conductivity. The difference between grain structures might be due to easier evaporation of solvent that takes place while printing in steps. Printing high number of layers on top of each other results in a trapping of the water and surfactant molecules in a formed structure which eventually generates pores, hence reduces the density of the film, and thus lowers the conductivity of printed features.

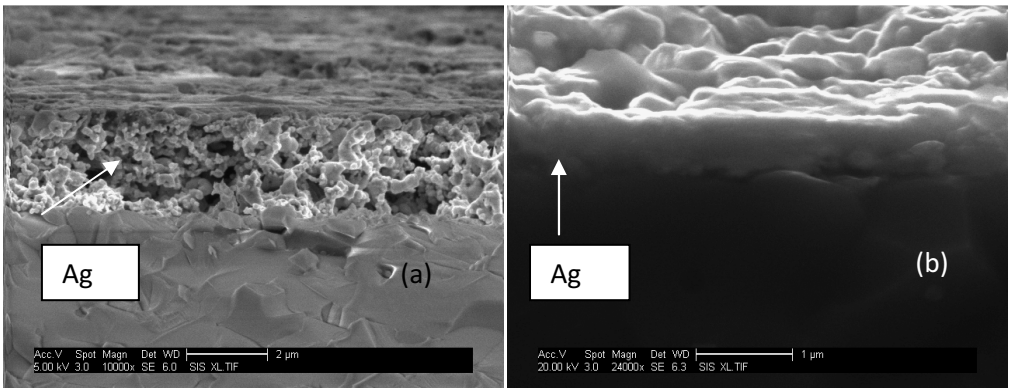

Figure 5.9 SEM micrographs showing (a) cross-section of printed silver on Al_2O_3.Ag film consisted of 60 layers fired at 350 °C for 60 min and (b) film consisted of 60 layers fired at 350 ºC for 20 min in 20 layers steps

5.4 Development of long- term stability of high loading silver ink - AG2 formula

To achieve a conductive track with 5 wt% Ag ink, 60 layers were required to be print. In order to reduce the number of layers in the silver nanoparticles film by increasing the thickness of a single layer with the goal of obtaining a dense and conductive film, high loading of Ag in an ink was used. Ag nanoparticles with acetone enabled us to formulate highly concentrated and stable dispersion of silver in aqueous media due to high surface charge density of the particles, which generates strong repulsive force and small size of the agglomerates. Through adjusting pH it was possible to obtain 25 wt% Ag loading dispersion. Further increasing the silver content weakens the stability of the fluid due to the decrease in the electrophoretic mobility of the particles [160]. To load more Ag NPs in an ink and form a stable dispersion, copolymer F127 was used. Figure 5.10 shows TEM pictures of silver particles dispersed in water with and without copolymer F127.

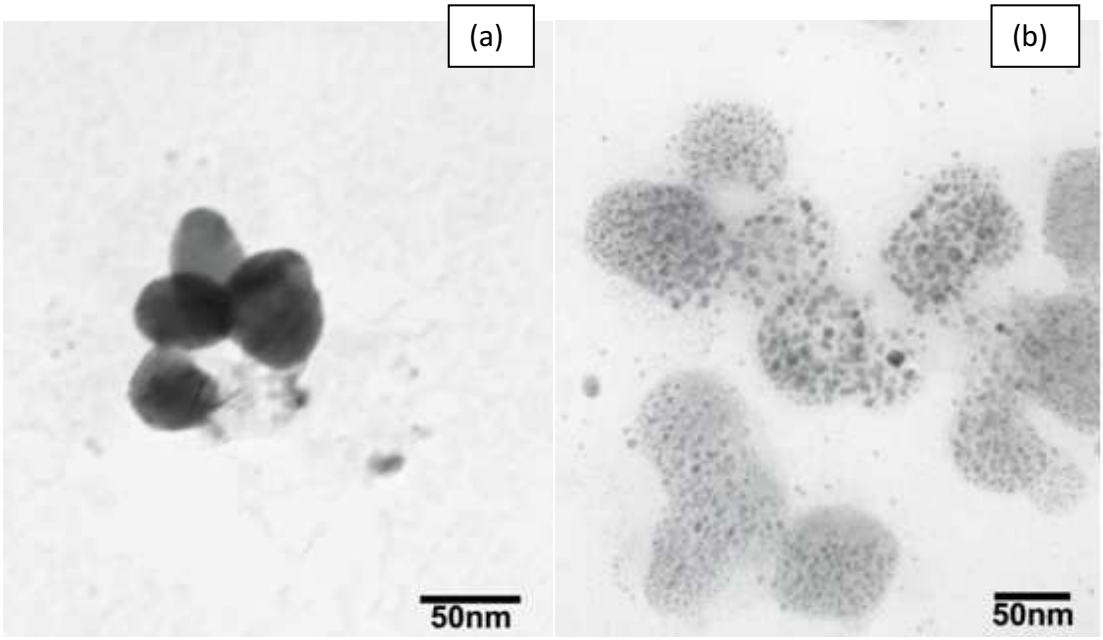

Figure 5.10 TEM micrographs of silver particles dispersed in water, (a) without and (b) with addition of F127

After the addition of the co-polymer F127 the particles reach the size of 10 nm. This shows that the dispersant acts not only as a stabilizer but also as a comminution aid, which promotes the breakage of the hard agglomerates [161].

The primary nanoparticles strongly attract each other through physical forces due to large surface area, immediately forming larger particles. Upon ultrasound treating, the agglomerates were separated and due to the presence of F127, the small particles were prevented from being agglomerated again. It was the surface modification that delayed the agglomeration or clustering. Resulted size of the dispersed particles was around 10 nm. As a result, a high Ag loading ink containing 45 wt % Ag could be produced.

5.4.1 Rheological behaviour and surface tension measurement

Rheology studies have been performed on silver ink (AG2). The influence of silver particles on viscosity was examined. Figure 5.11 presents the rheological behaviour of a silver ink and Table 5.4 shows the ink's properties in dependence on Ag solid loading.

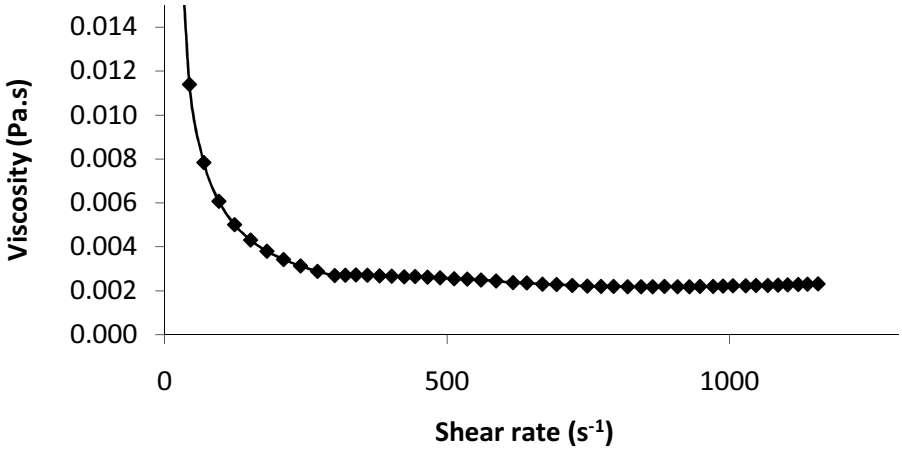

Figure 5.11 Rheological behaviour of silver ink (AG2)

As it can be shown, the ink exhibited Newtonian behaviour with a shear rate between 10^1- 10^3 s^{-1} which can be indication of well-dispersed suspension. In practice, if particle aggregation occurs, the inks shows shear-thinning behaviour, which is defined by a gradual

decrease in apparent viscosity with increasing shear rate [158]. As a result of increasing the shear rate the possible aggregates are broken down and consequently reduction in amount of solvent immobilized by the particles takes place, lowering the viscosity of the fluid in the same time [64].

Table 5.4 presents the change in viscosity and surface tension of the aqueous Ag suspensions with different solid contents (25, 35, 45 wt %). It can be seen, as expected, that the viscosity rises with increasing silver content in a fluid. The viscosity value for 25 wt% of silver in ink is 2.4 mPa s and it increases up to 3.3 mPa s when silver loading increases to 45 wt%. That is due to the increase of the interaction between silver particles when solid content increases. The surface tension slightly changed with the addition of Ag particles. At 25 wt% if silver content, surface tension for Ag fluid was 32.9 mN/m. Increasing the loading up to 35 wt% resulted in lower surface tension of 33.6 mN/m. Further increasing the content of silver in the ink lower the surface tension down to 33.6 mN/m. This is attributed to the decrease of solvent content, and especially water, with the increase of silver content.

Table 5.4 Properties of silver inks with different Ag loadings

Ag wt%	Viscosity (mPa s)	Surface tension (mN/m)
45	3.3±0.5	33.6±0.5
35	2.7±0.5	33.8±0.3
25	2.4±0.4	32.9±0.5

5.4.2 Stability studies

To evaluate the stability of Ag nanofluids, the viscosity measurement was taken against the time over 20 days (figure 5.12). It was found that there was almost no viscosity change up to 10 days and after this time, viscosity slowly increased with the time. The increase of

viscosity from 3.3 mPa s in Day 1 to 3.5 mPa s in Day 20 was due to the agglomeration and the formation of larger particle clusters. Once agglomerates are formed, a larger stress is necessary to break the polymer structure among particles when shearing takes place; therefore, a high relative viscosity would be observed in the fluids as shown in figure 5.12. However, no sedimentation was observed up to 20 days. The formed large particle clusters due to the agglomeration could be broken and re-dispersed in the water under the ultrasonic tratment and the rhoelogical properties of the dispersion can resume to the inital values.

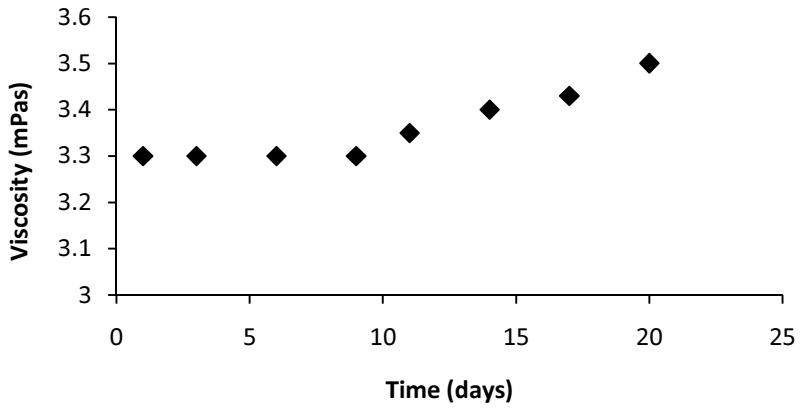

Figure 5.12 Viscosity change of Ag nanofluid against time

When we compare the stability of the AG1 and AG2 inks it can be noticed that in both cases the inks behave similar, there is no change in viscosity values in the same time range. Value of 2.1 mPa s and 3.3 mPa s for AG1 and AG2 respectively remains stable over first 10 days.

The silver particles in both inks can be easily re-dispersed using ultrasounds and the rhoelogical properties of the dispersionscan resume to the inital values and extend the shelf life of the ink up to 1 month.

5.4.3 Printability of silver ink

Once the stable and high concentrated dispersion of nanoparticles is obtained, the ink formulation must be adjusted to meet the given specification regarding the dimension of the patterns as well as the required resolution. Since the morphology of the printed lines depends on the interactions between the ink and the substrate, it is important to examine and optimise the printing parameters to achieve desired printed feature. Firstly, it is necessary to examine whether the prepared ink meets inkjet printing requirements. In a piezoelectric inkjet printing process, the generation of drops is based on pressure wave that is electrochemically induced. When a voltage is applied, the piezoelectric material changes shape, which generates a pressure wave in the fluid forcing a droplet of ink to be ejected from the nozzle. That happens only when the kinetic energy of the ink is sufficient to overcome the surface energy interactions.

There are three dimensional numbers, namely, the Reynolds (*Re*), the Weber (*We*) and the *Z* numbers (*Z*), which have been described in section 2.3.4. The ink properties have to be controlled within determined ranges. For example, with Dimatix DMP-283 a droplet can be ejected if Z is in the range 1-10. The viscosity values for the fluids possible to jet have to be in a range of 0.002-0.03 Pa s, and the surface tension can go up to 0.06 N m. The ink characteristics and the calculated dimensionless numbers are summed up in table 5.5. The optimized silver ink in the present work fulfils the conditions necessary to achieve a stable and right process with the inkjet printer used in this study (DImatix DMP 2831).

Table 5.5 Calculation of We, Re and Z dimensionless numbers for the silver ink from ink properties and printer

Ink	**Surface tension σ[N m^{-1}]**	**Viscosity η[Pa s]**	**Density ρ[kg/m^3]**	**Voltage V [V]**	**Nozzle diameter d [µm]**	**Velocity v[m s^{-1}]**	***We***	***Re***	***Z***
Ag ink 60%	33.6x10^{-3}	3.3 x 10^{-3}	995.8	32	21.5	14	89.2	76	8

5.4.4 Characterization of printed features

5.4.4.1 Conductivity measurement

This part of work focuses on the investigation of the minimum curing temperatures of silver ink. The minimum curing temperature is defined in this case as the temperature at which the sample becomes conductive, i.e. having a resistance lower than 40 MΩ which is the upper measuring limit of the used multi-meter.

Single lines consisted of various number of layers (1-5) with a length of 5 mm of the inks were inkjet printed onto alumina substrates and subsequently sintered to 450 °C on the hot plate. Differences in resistivity values between the various numbers of printed lines can be determined. Table 5.6 shows the thickness and resistivity value of the samples with different number of printed lines at different temperatures.

Table 5.6 Properties of printed film at different sintering temperature

		Resistivity (μΩ cm)			
No of layers	Thickness (μm)	Temperature (°C)			
		250	300	350	450
1	1	7.2±0.72	4.5±0.43	3.1±0.31	3.1±0.32
3	2.8	6.7±0.67	4.5±0.45	3.1±0.42	3.1±0.46
5	4.6	6.1±0.61	4.5±0.49	3.1±0.52	3.1±0.56

It is observed that the thickness increases with the number of layers. 1μm thick layer was obtained with 1 layer of Ag ink, while increasing the number of layers up to 5, resulted in 4.6 μm thick film. The resistance of the lines for silver ink decreases with the increase of temperature and for thicker layer starts with the lower values.

The minimum sintering temperature for the silver ink was 250 °C. It was expected that the smaller particles would sinter at the lower temperature because of their higher sintering activity [71, 72]. This suggests that the organic additives in the ink strongly affect the critical curing temperature and for that reason the TGA analysis was performed.

It might be seen from the figure 5.13 the lowest temperature at which printed features become conductive is mainly determined by the outlet of evaporation of organic additives in the ink. The decomposition temperature (at which the sample has the highest weight loss) was observed to be around 250 ºC. The weight loss is due to the removal of organic molecules through the decomposition process.

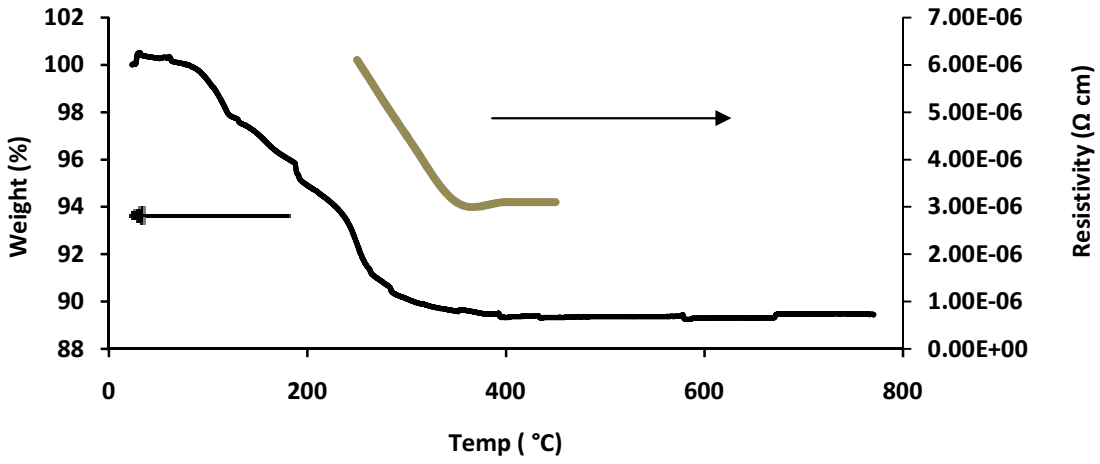

Figure 5.13 Resistance over a single inkjet printed line as function of temperature and thermogravimetric analysis (TGA) of silver nanoparticles.

The theoretical decomposition reaction for dioctyl sodium sulfosuccinate is as follows:

$$C_{20}H_{37}NaO_7S\ (s) \longrightarrow 74CO(s) + 34CO_2\ (g) + 2SO_3 + Na_2O_2 + 37H_2 \qquad (5.4)$$

The expected mass loss should be equivalent to 9.1% of the total mass, the analysis resulted in an actual mass loss of ~ 8.0 % overall mass loss which is very close to that of the theoretical calculated percentage loss.

The minimum temperature needed for the printed ink to become a conductive dense film was at 250 °C. The completion of the sintering process was at 350 °C at which the resistivity (3$\mu\Omega$ cm) was shown to be only twice higher than bulk Ag. The decrease in resistance depends on the temperature range in which the last part of the organics is burnt off.

The loss of mass does not immediately cause the lines conductive through particles connection. Combining the results of TGA analysis and resistivity measurement it can be observed that half of the organic part is required to be removed to ensure the film to be conductive. All organics have to be removed from the film before it reaches the lowest resistivity. Typical results were observed for 3 and 5 layers of the Ag ink.

Figure 5.14 presents the SEM cross-sectional and top views of dense silver track with well packed particles.

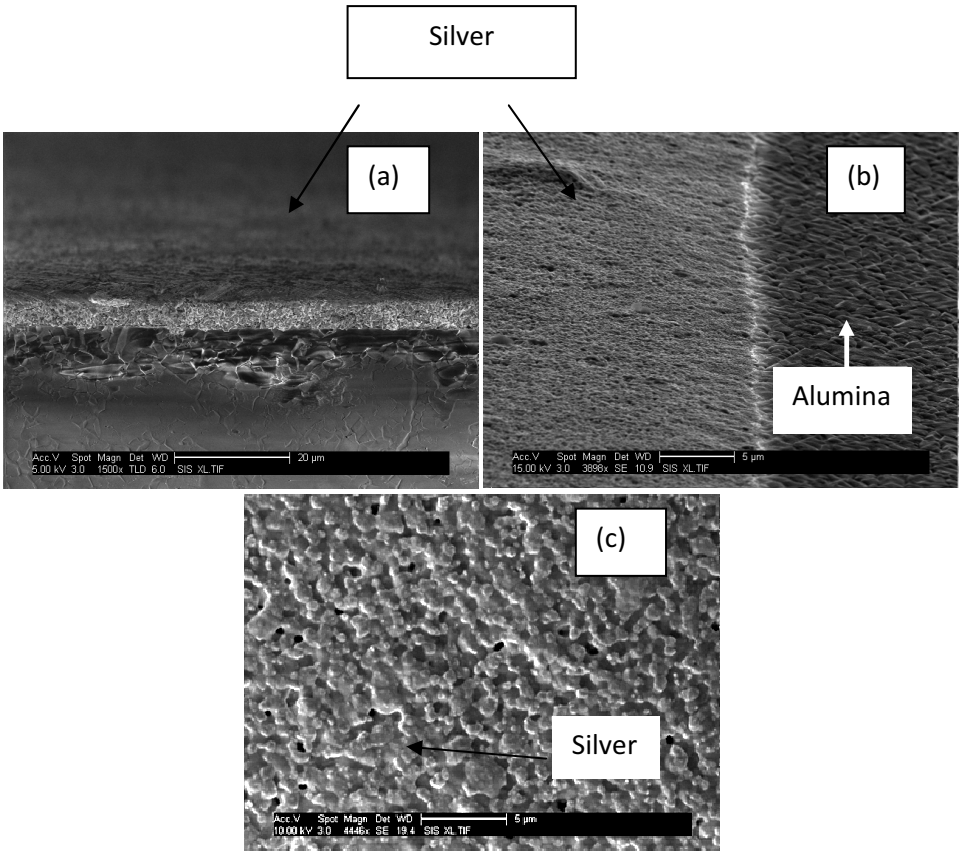

Figure 5.14 SEM micrographs of (a) cross-section; (b) and (c) top view of printed silver on Al_2O_3 and sintered at 350 °C

Low resistivity of printed tracks could also be obtained by dipping the printed tracks in acetone for 2 hours to dissolve surfactant (AOT) and then in water for 1 hour to dissolve copolymer (F127). Then the printed tracks were dried at room temperature for 60 min and the resistivity of the printed tracks reaches 230 $\mu\Omega$ cm or at a temperature up to 150 ºC for 1-10 min and the resistivity of the printed tracks can be as low as 3 $\mu\Omega$ cm (bulk silver metal 1.59 $\mu\Omega$ cm).

5.5 Increase of single layer thickness

The aim of this part of work was to formulate a high loading Ag ink in order to bring the advantage of reducing the number of printed layers (in the same time increase the resolution

of the printed features) required to obtain thick, dense and conductive film and also reduce the costs of the printing process.

The calculation (5.5-5.8) assumes that an ink droplet forms a spherical cap on the surface (a good assumption from our surface tension studies) with spherical radium *R*, cap radium *r* and contact angle (θ) (figure 5.15). It was then assumed that the dot remains at this diameter upon drying and sintering to give a uniform thickness i.e. no coffee stain effect.

Volume of the cap

$$V = \frac{\pi R^3(2-3\,sin(90-\theta)+sin^3(90-\theta))}{3} \tag{5.5}$$

Ignoring the added co-polymer and surfactant, and assuming that volumes are additive, the drop volume is also given by

$$V = M_{Ag}/\rho_{Ag} + M_{H2O}/\rho_{H2O} \tag{5.6}$$

where M and ρ are mass and density respectively. Also denoting mass loading as L

$$L = \frac{M_{Ag}}{M_{Ag}+ M_{H2O}} \tag{5.7}$$

Substituting in (5.5) and re-arranging

$$M_{Ag} = \frac{V}{1/\rho_{Ag}+ (1-L)/L\rho_{H2O}} = \pi r^2 t \tag{5.8}$$

where *t* is thickness of the film.

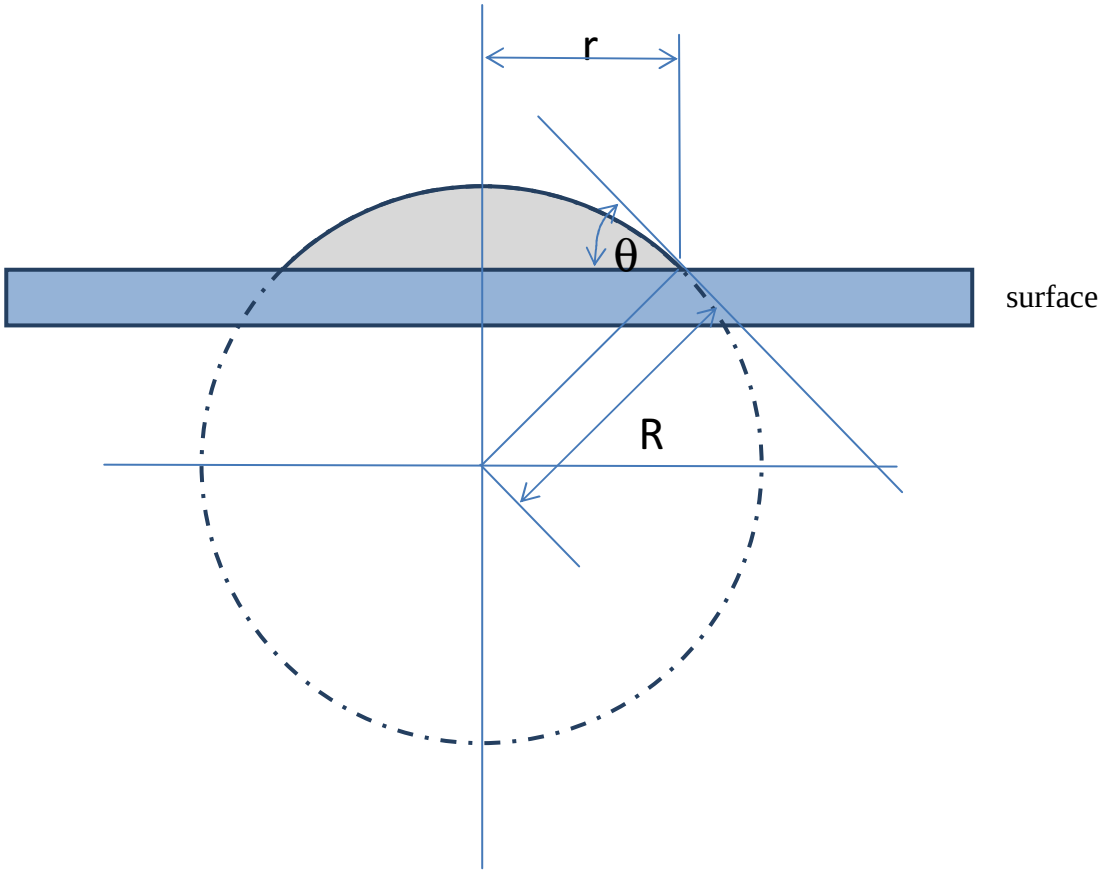

Figure 5.15 Schematic graph representing droplet on the surface

Based on the equation (5.10), thickness of a printed layer can be calculated if its mass is known, but this is only valid for the line printed with the dot spacing leading to the line consisted of dots just touching each other. In practice the dot spacing is reduced to increase the thickness of the printed lines. The results of experimental (for printed line with a given dot spacing, 20 µm) and calculated (for the line with the drops just touching each other) thicknesses are shown in figure 5.16. The calculated values give just the idea about thickness of the line thickness and prove that the thickness depends on the loading of the ink.

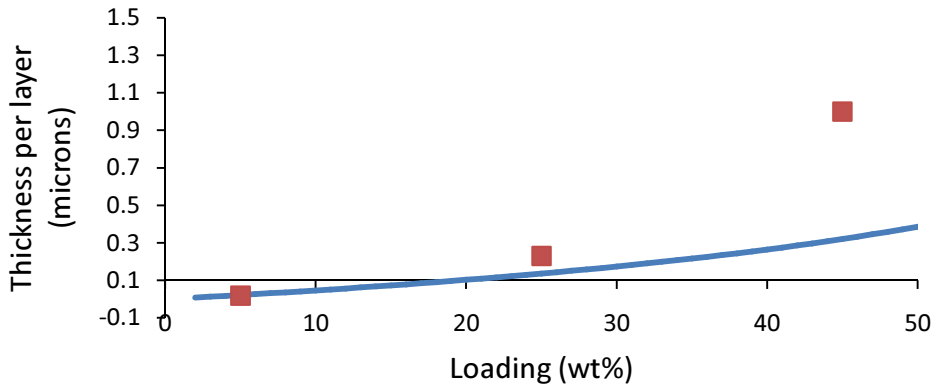

Figure 5.16 Thickness per layer for different loading of silver in an ink theoretical (blue line) and experimental (red squares) printed using 60 µm dot spacing

5.6 Conclusion

Ag inks with different solid loading were formulated. The treatment of synthesised Ag particles with solvent leads to the particle aggregation with various sizes and behaviour. The results showed how important the primary particles are in ink preparation. Treatment of Ag particles with IPA resulted in the formulation of 5 wt% ink when a combination of copolymer F127 and HIFU technique was employed. The investigation of HIFU treatment showed that the size of Ag agglomerates was reduced down to ~50 nm from ~ 200 nm untreated. The viscosity of the nanofluid was reduced after sonication indicating that the HIFU treatment could help separating the agglomerates and relatively stable inks indicated the high efficiency of the copolymer in stabilizing Ag nanoparticles in water.

Following encouraging results from our 5 wt% Ag ink, an Ag ink with higher Ag content (45 wt%) was formulated by treating the synthesised particles with acetone. The size of aggregates decreased down to 50 nm, and further use of copolymer resulted in 10 nm highly hydrophilic particles. This shows the properties of dispersant not only as a stabilizer but also as a comminution aid, which promotes the breakage of the hard agglomerates [161]. Copolymer F127 was found to be very effective as a stabilizer leading to the formation of high silver loading.

Both inks were printed on alumina substrates and the subsequent films show a very low resistivity and good shape definition. The resistivity of the printed Ag lines decreases as sintering temperature increases. The resistivity is $(2 \pm 0.1) * 10^{-5}$ Ω cm for AG1 ink and 3.1 ± 0.2 $\mu\Omega$ cm for AG2 after annealing at 350°C.

Additionally, the processing of thick films was investigated. It was found that the higher loading of metal content the thicker layer can be obtained. The use of high solid loading inks reduces the number of printed layers required for thick, dense and conductive film and thus increasing the resolution of the film, as well as leading to the reduction of the costs, and high efficiency of the printing process.

Chapter 6

Improvement of physical properties of the silver film

6.1 Introduction

A silver ink is a promising candidate for the electronics application as it is compatible with inkjet printing. To produce highly conductive silver tracks with a dense structure, sintering at high temperatures is required. Especially, in applications such as plasma display and solar cell [162], silver conducting films should be fired at high temperatures above 400 ºC. However after annealing at such high temperatures printed films present cracks and pores due to the large intrinsic volume reduction upon sintering nano sized silver powders resulting in a weak substrate adhesion [163].

In order to improve the strength and adhesion of the materials various additives have been used in particles dispersion [164-169]. However polymeric materials and resins present in most conductive inks lose their ability to bind particles together after high sintering temperature. On the other hand a presence of inorganic additives in a film, e.g. SiO_2 particles have been shown to enhance the interfacial properties of the dispersion [167]. Already, by 1980 the glass binder+metal+organic binder formulation was well established. The general theory was that the glass migrated to the metal-substrate interface to improve adhesion.

On the other hand when SiO_2 is presented in the sample, cracking and poor adhesion is expected to be prevented; owing to the hydrogen bonding formed at the interface SiO_2-Si/SiO_2-ceramic substrates. It has been found that the role of the hydrogen bonding in adhesion of particles to substrate surface plays very important role [169]. Peschel et al. [170] suggested that due to the low activation energy of hydrogen bond formation, many solid surfaces contain potential hydrogen bond donors and acceptors already at room temperature.

Among them, SiO_2-SiO_2 surface or Al_2O_3-SiO_2 surface have been found to have the hydrogen bonding.

In this part of work the effects of SiO_2 content on the microstructure and electrical properties of the deposited Ag films are investigated. Since the deposited films may be exposed to thermal or structural loads, the mechanical properties of the film play critical roles in stress induction. In this study, the hardness of a deposited silver track using the nanoindentation test was tested. The measurement of how good the film adheres to the substrate has been also performed.

6.1.1 Objectives

The objectives of this portion of the study were:

1. To investigate presence of SiO_2 in the Ag ink formula on physical properties of the printed film
2. To optimise the amount of SiO_2 with goal of obtaining dense and conductive film with improved adhesion than the sample without SiO_2

6.2 Effect of SiO_2 content on viscosity

Printed films usually present cracks and pores when sintered at high temperature. This is due to due to the large intrinsic volume reduction upon sintering nano sized silver powders resulting in a weak substrate adhesion. In order to improve the strength and adhesion of the Ag films SiO_2 was added to the ink formula and its effect on properties of the ink and later conductivity of the film were investigated.

First the rheological behaviour of silver inks was investigated as a function of SiO_2 to evaluate whether the SiO_2 dispersion is compatible with silver ink and to confirm the suitability of the inks for inkjet printing process. Silver inks were formulated using silver nanoparticles as a functional material, copolymer as a dispersant agent, and SiO_2

nanoparticles as a binder between the particles improving also adhesion of the inks to the substrate. Three different ink compositions were formulated. They all contain the same contents of silver powder and dispersant but different SiO_2 content (0 wt%, 0.05 wt% and 0.3 wt %). All the formulas were mixed based on their weight percentage and the suspensions were treated using ultrasounds.

Results shown in figure 6.1 indicated that the SiO_2 addition did not obviously influence the viscosity values. The ink remained viscosity values in an acceptable range for inkjet printing which is 1-30 mPa s, thus was inkjet printable and low in spreading on the substrate.

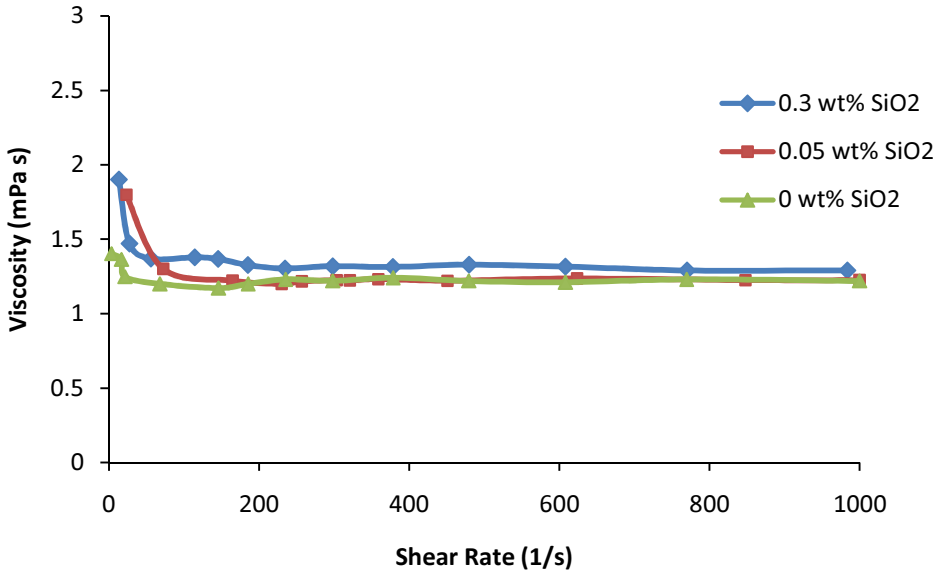

Figure 6.1 Rheological behaviour of silver ink with different SiO_2 content

The inks have a Newtonian behaviour as the viscosity remains constant over the shear range from 100/s to 1000/s. This suggests that the agglomerates of SiO_2 are weakly bonded together and thus easily fracture to form a dispersed suspension. The viscosity for ink with 0.05 wt% of SiO_2 is 1.24 mPa s, and for ink without SiO_2 is 1.27 mPa s. Increasing the amount of SiO_2 up to 0.3 wt% increased slightly the viscosity up to 1.38 mPa s. High loading of SiO_2 (0.3 wt %) increase the probability of agglomeration among the SiO_2 particles and

between the SiO_2 and the silver particles which resulted in slight increase of the viscosity value.

6.3 Dry film properties

To investigate the microstructure of the printed silver inks, films of 10 mm^2 dimensions were prepared by inkjet printing technique on an alumina substrate. The printed patterns were allowed to settle for 10 min, and then sintered at different temperature varied from 350 ºC to 700 ºC for 10 min.

As shown in Section 5.4.5, the removal of organic part took place at 350 ºC and then the sintering of the films started to occur. The microstructures of the sintered films with the addition of SiO_2 were observed under scanning electron microscope and the results are shown in figures. 6.2, 6.3, and 6.4. It is observed from the SEM results that the density of the Ag film improves with addition of the SiO_2 to the ink at all sintering temperatures 350, 500, and 700 °C.

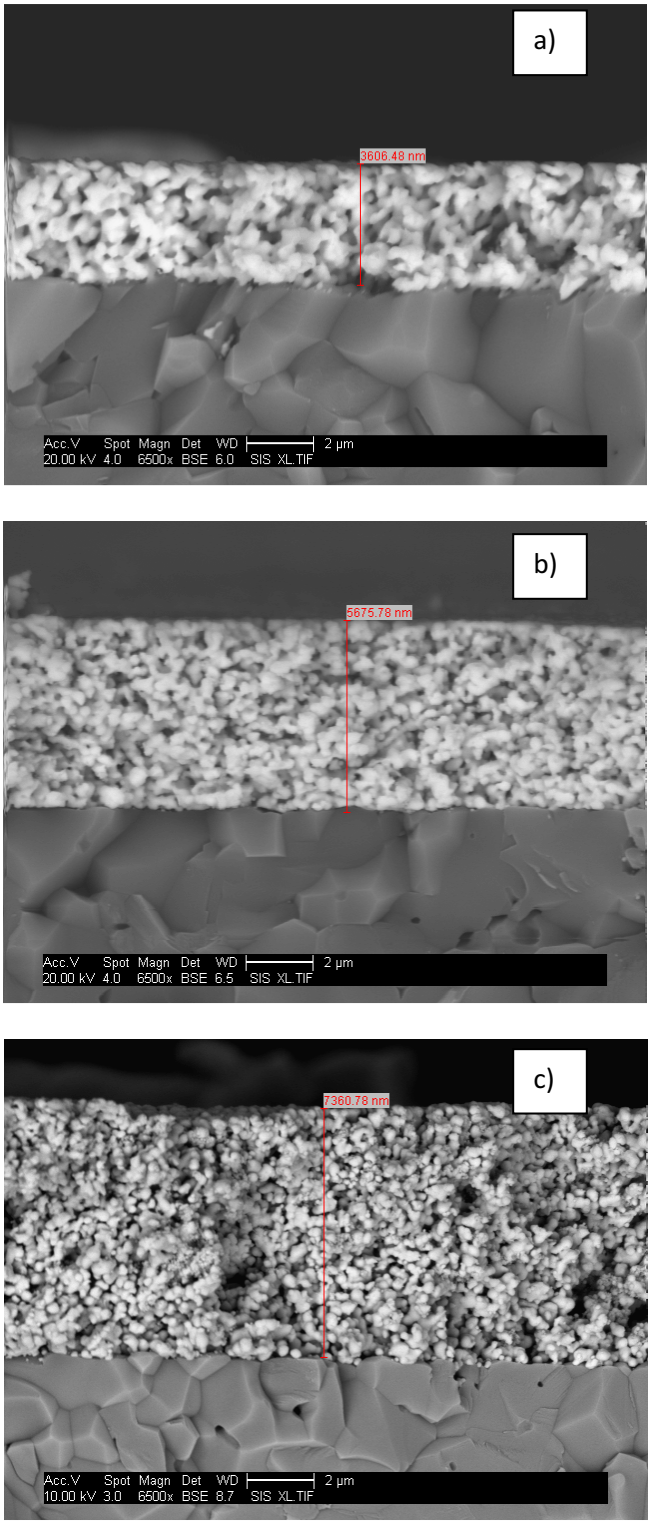

Figure 6.2 SEM micrographs of silver ink with (a) 0 wt%, (b) 0.05 wt%, and (c) 0.3 wt % of SiO_2 sintered at 350 °C

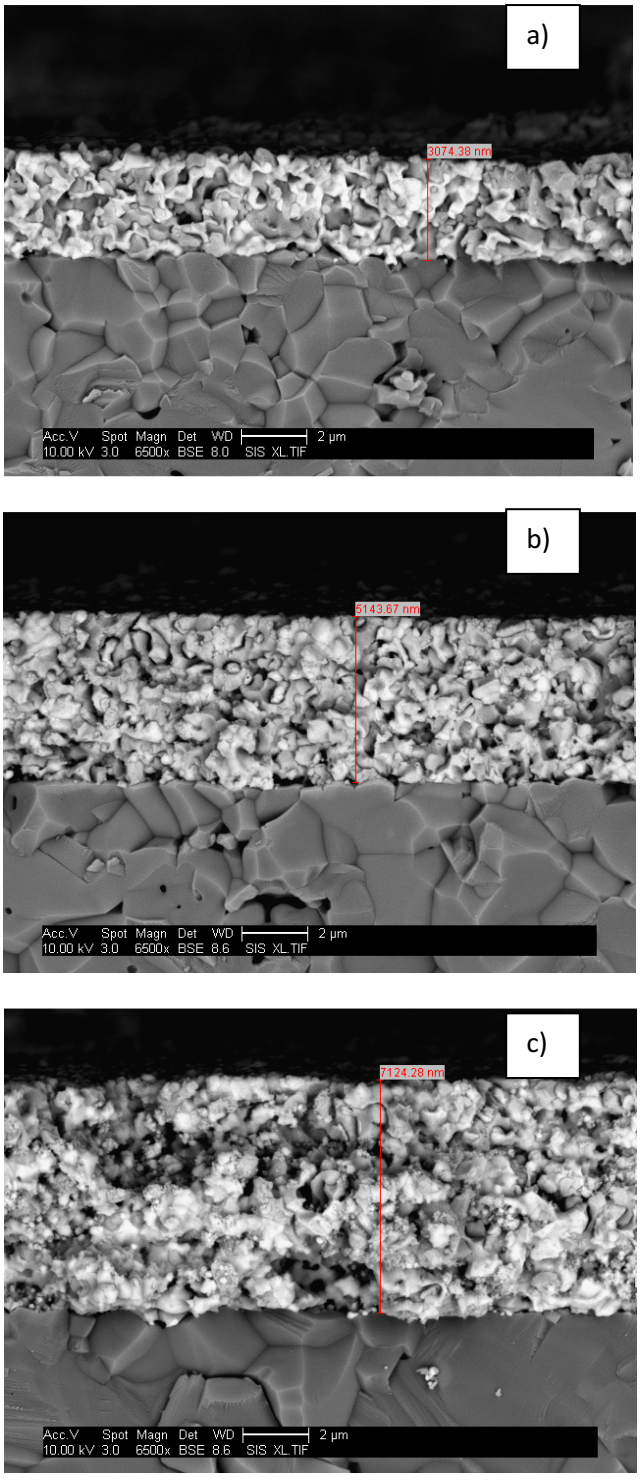

Figure 6.3 SEM micrographs of silver ink with (a) 0 wt%, (b) 0.05 wt%, and (c) 0.3 wt % of SiO_2 sintered at 500 °C

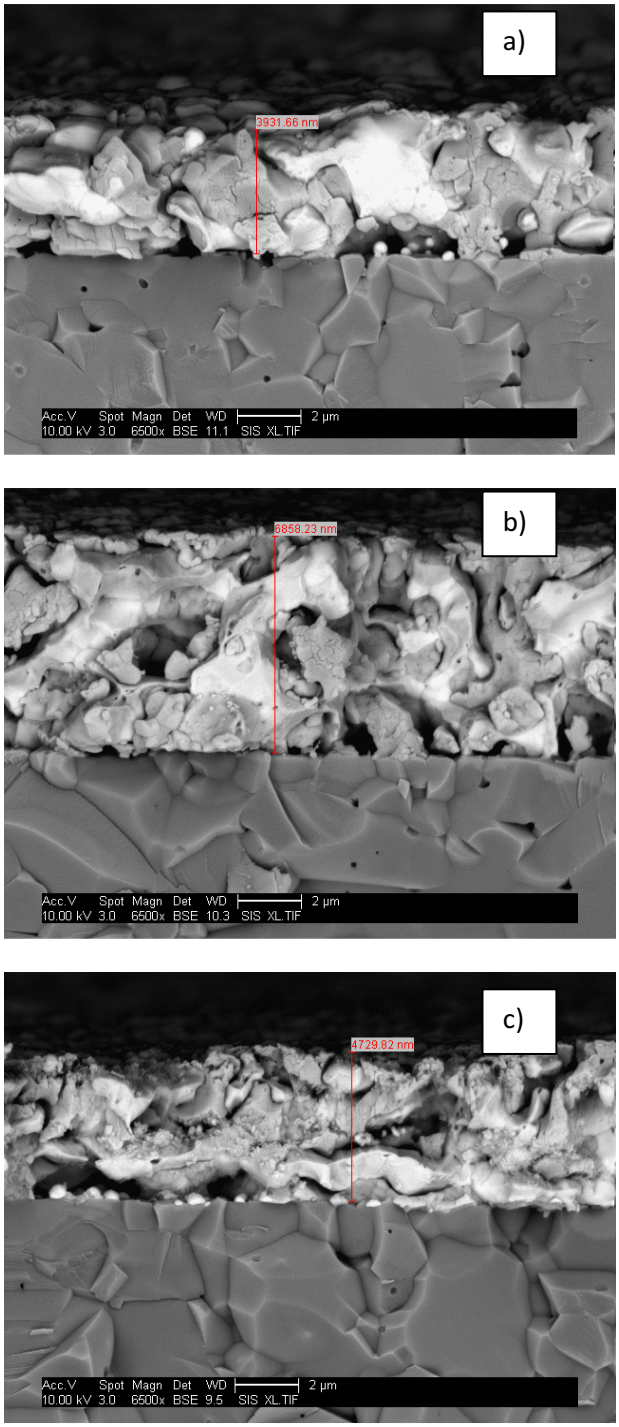

Figure 6.4 SEM micrographs of silver ink with (a) 0 wt%, (b) 0.05 wt%, and (c) 0.3 wt % of SiO_2 sintered at 700 °C

However there is no much visible difference between 0.05 wt % of SiO_2 and 0.3 wt% of SiO_2 in the density. Porous and non-uniform surface morphology for all samples is observed when sintering temperature was 350 ºC. All the films display denser surface

morphology when sintering temperature increased up to 500 ºC. A bigger size of the grain and their development with almost void free surface morphology is observed in all samples regardless the amount of SiO_2 at 700 ºC.

Based on the results it can be said that the microstructure of the silver films depends mainly on the sintering temperature and on SiO_2 binder in the ink formulation. 0.05 wt% of SiO_2 was enough to improve the density of the Ag film. However increasing this amount up to 0.3 wt % did not bring any significant changes.

6.4 Resistivity properties

The resistivity of the sintered metallic film was measured using Van der Pauw technique. The advantage of the van der Pauw (vdP) technique for resistivity measurements is that it allows to take a measurement without knowing exact sample geometry. Initially, the technique was developed in order to measure the resistivity and the sheet resistance of thin and flat samples of semiconductors, but it can also be applied to the case of superconductors.

Figure 6.5 shows resistivity of printed films as a function of SiO_2 content and sintering temperature. From the date it is seen that both the amount of SiO_2 added to the ink formula and sintering temperature affect the resistivity of the printed films.

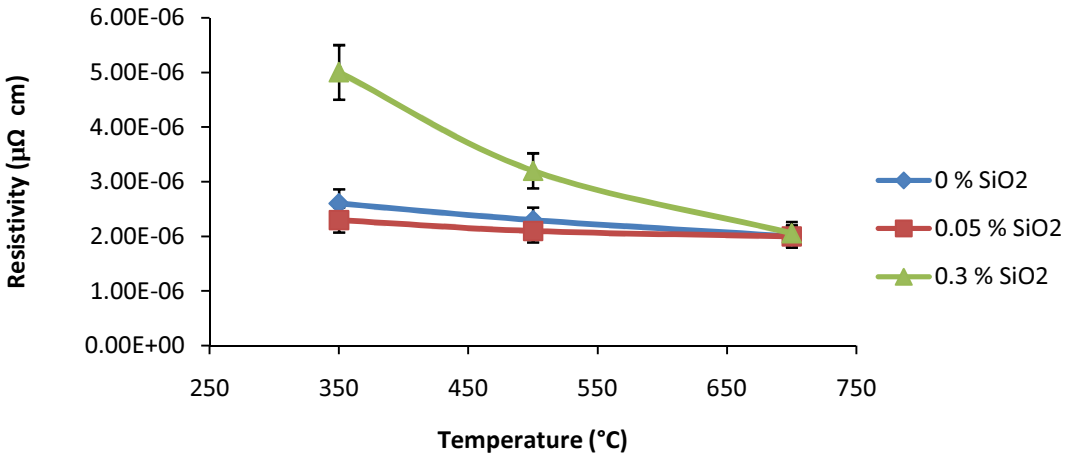

Figure 6.5 Resistance over a printed film with various SiO_2 loading as function of temperature

All the samples show an increase in resistivity as the temperature increases. Over the whole range of temperatures, the sample with 0.05 wt % of SiO_2 showed the lowest resistivity values (2.3, 2.15, and 2.1 µΩ cm for 350, 500 and 700 ºC respectively), and it can be inferred that SiO_2 acting as sintering aid, while the sample with 0.3 wt % of SiO_2 showed the highest (5, 3.2, and 2.1 µ Ωcm at 350, 500, and 700 ºC respectively). Based on the results, it can be said that the addition of small amount of SiO_2 acts as a binder between particles leading to low resistivity values. However, too much SiO_2 in the film can function as an electric insulator, leading to the increase of resistivity of the film. The sample without SiO_2 addition shows the middle resistivity value (2.6, 2.2, 2.1 µΩ cm at 350 ºC, 500 ºC, 700 ºC respectively). The Van der Paul technique is very accurate technique to estimate the resistivity, however slightly different values have been obtained for the sample without SiO_2 when compare to the previous measurement in chapter 5. The differences in values are due to the thickness variation of the film which is indicated by the error bars.

Obtained results demonstrate that the amount of binder plays important role in determining the electrical properties of the Ag films in addition to the other physical properties described in the chapter.

6.5 Adhesion tests

Adhesion is an important feature of the films in electronic environment. How good the film adheres to the substrate defines later properties of the final device.

Three methods were applied to check test the adhesion of the silver films with SiO_2 content to verify the most suitable for this kind of samples (a soft films on a hard substrate).

As the first method to carry out the adhesion test was chosen a nanoindenter in scratch test mode. In these tests a largest available load of 200 mN was used in a scan across a ~5μm thick, ~300 μm wide Ag track (printed onto alumina tape and sintered at 350 °C for 10 minutes). Figure 6.6 shows that the load of 200 mN was still not sufficient to scratch through the film, however it can be seen by the remained thickness after the test with applied load that the addition of SiO_2 enhances the hardness of the film.

As a second method for the adhesion test a conventional scratch tester was used. The minimum load that could be applied to the sample in this test was 1N. As a result the film without SiO_2 failed at the minimum load while the film with the addition of SiO_2 passed at 1N though failed at 2N (figure 6.7).

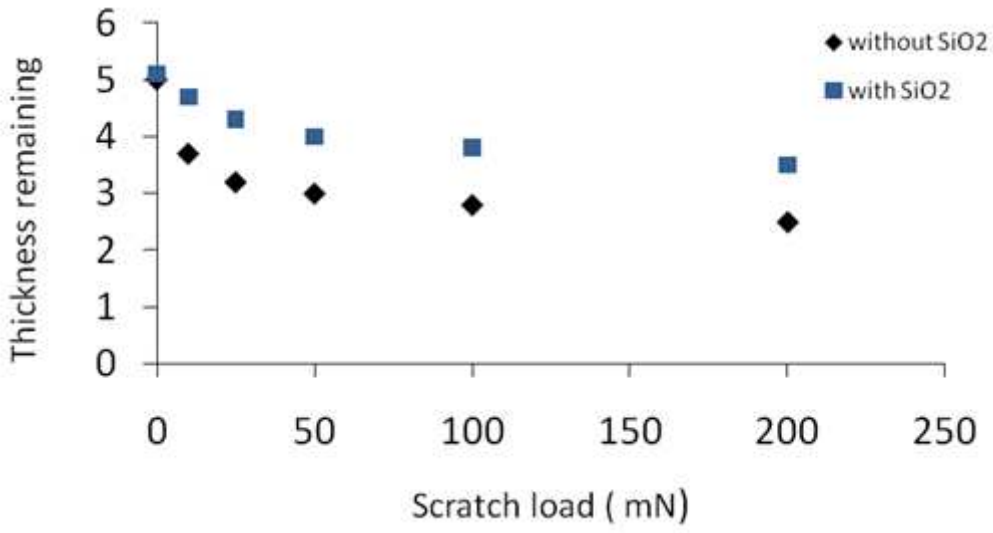

Figure 6.6 Ag track thickness measured after the removal of the load in scratch test

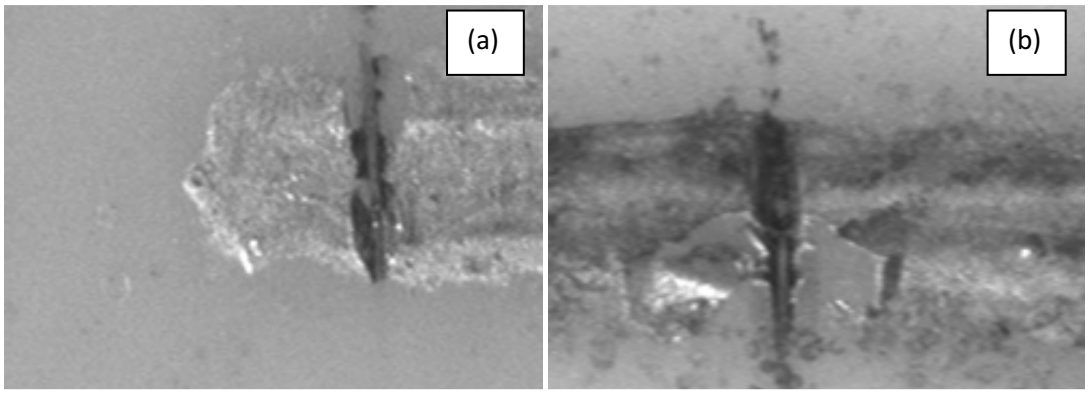

Figure 6.7 Optical images of printed silver tracks following scratch testing: without SiO_2, (a) 1N load , (b) with the addition of SiO_2, 2N load

This indicates that addition of SiO_2 improves adhesion of the film to the substrate possibly by as much as a factor of ~10 in terms of load to failure. However it was not possible to compare the influence of various content of SiO_2 in samples on the adhesion as all the samples failed at 2N.

Following this, trials to measure an adhesion of the films to the substrate have been carried out using a peel test. Since it was difficult to quantitatively determine the adhesion strength of thin metal films, instead of it, we applied an adhesion test which provides a qualitative evaluation of the film adhesion strength.

The metal films with an area of 10 mm x 10 mm were prepared by inkjet printing (figure 6.8). Three scotch 3M tapes varying with strength were used in the tests and they are:

- Blue, painter's tape for multi-surfaces, lowest adhesion (25 oz. / in)
- Green, masking tape for hard to stick surfaces, high adhesion (31 oz. / in)
- Yellow, masking tape for production painting, highest adhesion (35 oz. / in).

Results were recorded (figure 6.9) and listed in table 6.1. Figure 6.10 shows the optical microscope pictures of the tapes after the test for all samples. Visible marks of silver films on the tape can be observed depending on the SiO_2 content and sintering temperature.

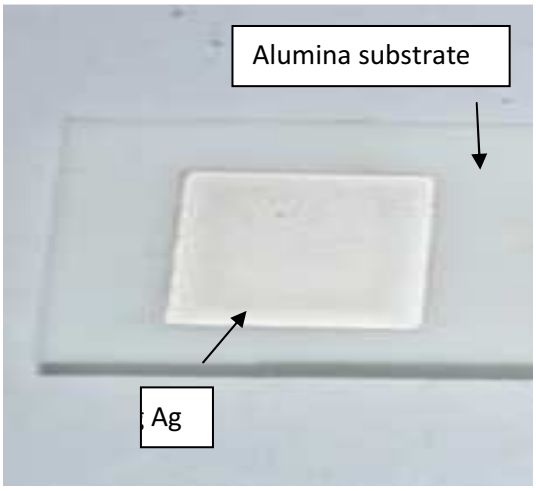

Figure 6.8 Optical microscope image of printed Ag

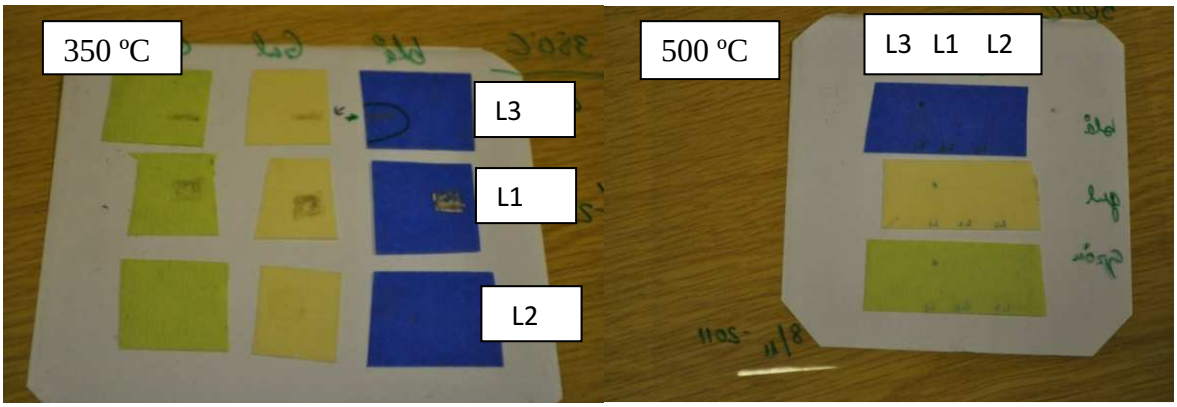

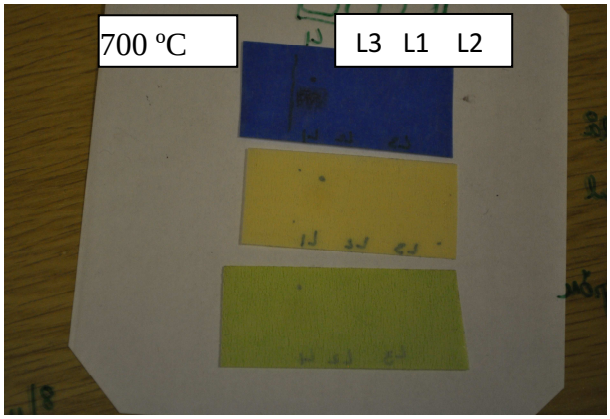

Figure 6.9 Optical microscope images of tapes after the test

Table 6.1 Results from peel test for silver film with 0 wt% (L1), 0.05 wt% (L2), 0.3 wt% (L3) of SiO_2 content sintered at various temperatures(350 ºC-700 ºC)

Tape used / Samples	Blue	Green,	Yellow
350°C L1	½ of the surface on the tape	½ of the surface on the tape	½ of the surface on the tape
350°C L2	Nothing on the tape	Nothing on the tape	Very small Ag marks on the tape
350°C L3	Small Ag marks on the tape	Small Ag marks on the tape	Small Ag marks on the tape
500°C L1	Nothing on the tape	Nothing on the tape	Nothing on the tape
500°C L2	Nothing on the tape	Nothing on the tape	Nothing on the tape
500°C L3	Nothing on the tape	Nothing on the tape	Nothing on the tape
700°C L1	Nothing on the tape	Nothing on the tape	Nothing on the tape
700°C L2	Nothing on the tape	Nothing on the tape	Nothing on the tape
700°C L3	Nothing on the tape	Nothing on the tape	Nothing on the tape

For the Ag film without SiO_2, and annealed at 350 ºC, 50 % of the film was detached with both tapes. For the Ag film with 0.3 wt% added SiO_2 annealed at 350 ºC, only 10% of the film was removed (removed area approx. 10%) with the yellow tape, indicating that adding SiO_2 helps improve the adhesion. The Ag film with 0.05 wt% SiO_2 was found to have the best adhesion at 350 ºC. Both 500 and 700 °C appear to be good sintering temperatures in terms of strong adhesion both with and without added SiO_2. Nevertheless, a high SiO_2 content is not beneficial to film conductivity, as shown as previously discussed (fugure 6.6) and for this reason, the optimal SiO_2 content for the Ag conductive ink is considered to be 0.05 wt%.

6.6 Mechanical properties

The ability to accurately measure the mechanical properties of thin metallic films is important in electronics, and particularly, in semiconductor industry as it needs to assess the device reliability. The technique for measuring thin film mechanical properties used in this work is nanoindentation. This technique has the advantage of being able to measure properties such as hardness and elastic modulus without removing a film from the substrate.

The discussion of experimental results will begin with an overview of the characteristics of the load displacement curves for the three samples, Ag film without and with addition of 0.05 wt% and 0.3 wt% SiO_2 nanoparticles. Figures 7-9 show experimental data for each of the materials at various sintering temperatures where an indentation was made to peak loads of 10 mN. The differences in hardness of the materials are noticeable from the differences in the depth. The softest sample is 0.3 wt % SiO_2-added Ag film, with a peak depth of almost 570 nm at 350 ºC, 580 nm at 500 ºC, and 600 nm at 700 ºC, while the hardest is pure silver film, which was penetrated to a depth of only about 470 nm at 350 ºC, 480 nm at 500 ºC, and 490 nm at 700 ºC. The displacement's values for sample with 0.05 wt% presence of SiO_2 were 520, 540, and 550 while sintered at 350, 500, and 700 ºC respectively.

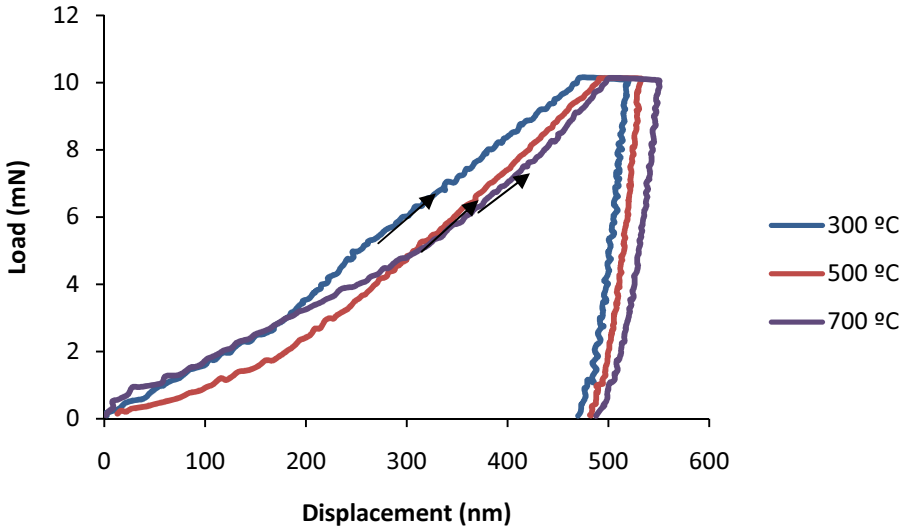

Figure 6.10 A view of the unloading/reloading portion of the load versus indenter displacement data for the sample of printed silver ink with 0wt % of SiO_2

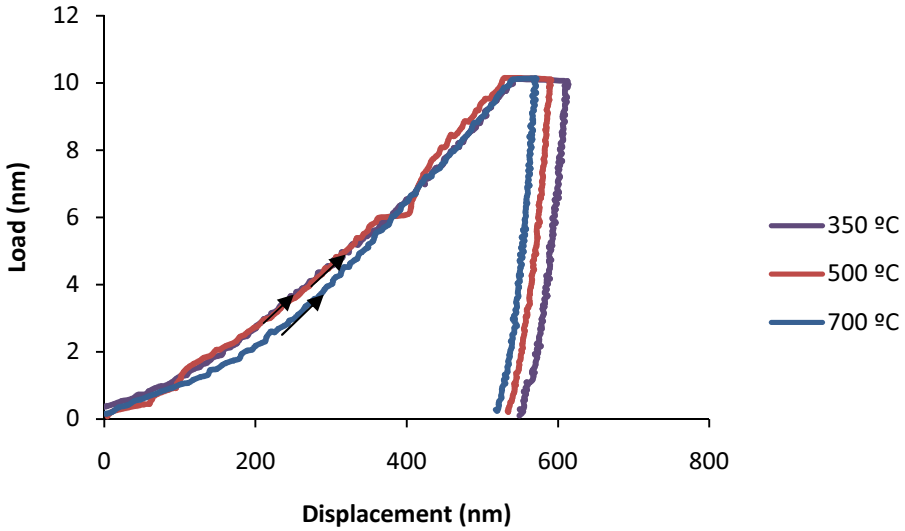

Figure 6.11 A view of the unloading/reloading portion of the load versus indenter displacement data for the sample of printed silver ink with 0.05 wt % of SiO_2

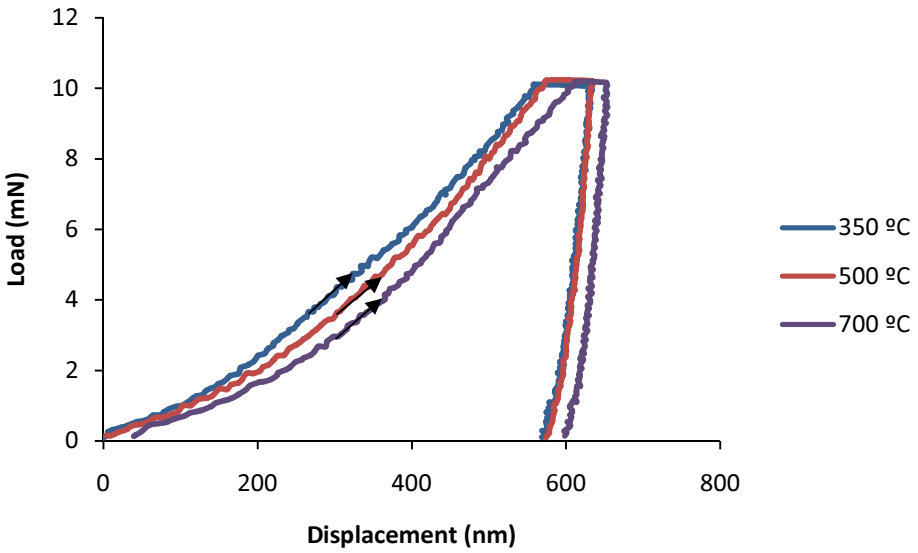

Figure 6.12 A view of the unloading/reloading portion of the load versus indenter displacement data for the sample of printed silver ink with 0.3 wt % of SiO_2

Under applied load, tested materials behaved in an elastic manner. When stress had been applied, strain was resulted. Once the stress was removed, the materials returned to their original state (i.e., the strain went back to zero). As can be seen, the sample materials show varying degrees of elastic recovery during unloading, the largest being that for 0.3 wt % SiO_2 film.

The elastic behaviour of all materials can be explained as a simple spring example. The bond force holding atoms in equilibrium positions in material linearly dependent on interatomic distance. During applying the load, the atoms will move respective to one another. The movement will stop when the bond force (resulting from change in interatomic distance) is in balance with the applied force. Once the loading is removed, the atoms will return to the original equilibrium positions. Therefore, the behaviour of the whole material is linear elastic.

Indentation hardness

To examine the change in hardness of the samples with various amounts of SiO_2 loading (0 wt%, 0.05 wt%, and 0.3 wt %), final hardness data from all three materials are plotted against SiO_2 content at different temperatures (350 ºC, 500 ºC, and 700 ºC) in figure 6.13. All samples show the behaviour typical of materials in which the hardness is relatively small compared to the behaviour observed in most models of metals.

According to the Oliver–Pharr method [79], the indentation hardness (H) is obtained from equation 6.2

$$H = P_m/A \tag{6.1}$$

Where P_m is the maximum applied load, and A is the contact area between the indenter and the silver film.

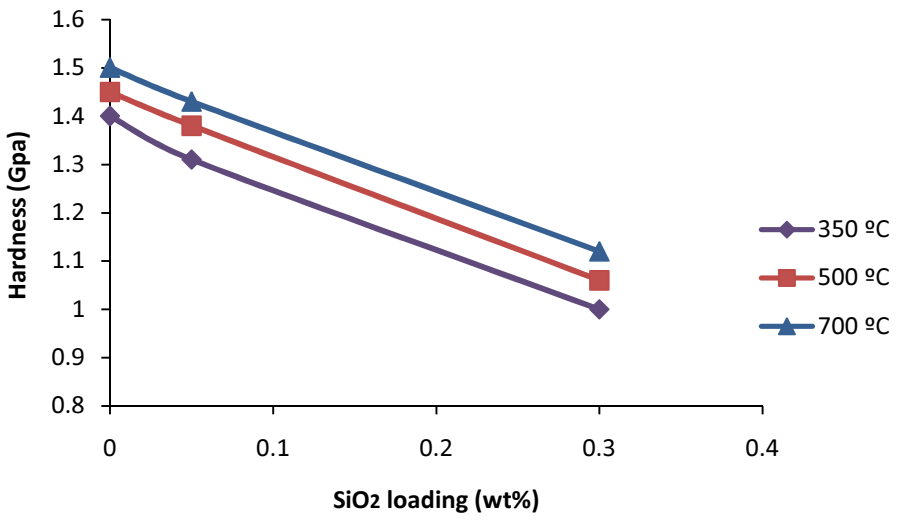

Figure 6.13 Hardness change against SiO_2 content in Ag ink formula at various temperatures

From the experiments, the hardness varies not only with the content of SiO_2 but also with temperature. Increasing the content of the SiO_2 soften the film. In the same time the higher sintering temperature the harder film is obtained for all samples. Examination of the curves shows that the hardness of the film without SiO_2 content is 1.4 GPa at 350 ºC and

increases up to 1.5 GPa while the sintering temperature rises up to 700 ºC. The small addition of SiO_2 (0.05wt%) does not change the hardness value much, however increasing the SiO_2 content up to 0.3 % softens the film significantly over the whole range of temperatures. The hardness of the films at 350 ºC was 1.31 and 1.1 for 0.05 wt% and 0.3 wt % respectively. These values increases up to 1.38 GPa and 1.06 GPa for 0.05 wt% and 0.3 wt% respectively, when temperature rises up to 500 ºC and then further arises to 1.43 GPa and 1.12 GPa for 0.05 wt% and 0.3 wt% respectively at 700 ºC. On the other hand pure Ag film is the hardest among the all samples.

6.7 Conclusion

An attempt has been made towards the development of silver ink with improved physical properties. As a result printable inks containing nanosized SiO_2 were prepared. The properties of the subsequently developed inks with different compositions were printed on the alumina tape. The effect of various amount of silica nanoparticles added to the ink formula on properties of Ag films, such as hardness, adhesion, morphology and resistivity have been studied using nanoindentation, peel test, and SEM. The results indicate that the presence of SiO_2 affects the properties of the Ag films. The percentage of the SiO_2 added in the ink was responsible for the development of microstructure for the sintered silver films. The addition of SiO_2 had also large effect on improving the conductivity of the films. The conductivity is, though, better when only a small amount of SiO_2 was added. Therefore, we can conclude that the presence of SiO_2 in the ink sample must be optimised. The results indicate that SiO_2 is also the major contributing factor in bonding the particles. The addition of a binder in the film materials is important not only for promoting the sintering and improving the densification but also for providing the adhesion to substrate. All the fired films showed very strong adhesion when sintered at 500 and 700 ºC. It is also revealed that the addition of SiO_2 to the ink softens the films irrespective of the SiO_2 content. Studies showed that SiO_2 can be

used for improving the physical properties of the film remaining their ability to bind the particles together after high sintering temperature and promoting the adhesion of the films to the substrates.

Chapter 7

Inkjet printing in recesses for improved dimensional control

7.1 Introduction

One of the challenges of printing conductive materials is to obtain desired morphology and geometry of the pattern.The morphology of the printed lines has an effect on the bulk electrical properties of the printed line. Smaller feature size enables the benefits of inkjet printing in functional applications, such as printed electronics.

Metal films directly deposited on a substrate typically show poor geometry due to spreading of the ink-a particularly serious issue for thicker films (composed of more than one printed layer) and films printed on rough substrates.

The ability of controlling the geometry of the printed features is very important in determining its electrical resistivity and mechanical adhesion. For conductive tracks, ideal printed lines should be straight and smooth. Additionally, in order to optimize the electrical performance of the printed features, defaults such as discontinuity of the deposit, spreading of the ink or edge irregularities have to be avoided.

The ceramics play an important role in electronics miniaturization and have potential to become a mass production technology for non-silicon microsystems. Using ceramic tapes it is possible to integrate small passive components on ceramic substrates in 3-D that give considerable possibilities for electronic miniaturization.

Since the behaviour of the ink depends on the interactions between an ink and the substrate, the effect of three different surface characters on the morphology of printed feature was measured. That was done by printing the lines of the Ag ink while varying the number of individual dots that were placed in a line within the span of 1 inch (= dot spacing), and varying substrate temperatures ranging from 23 to 60 ºC.

The other, an effective approach to control the geometry of printed features is to structure the topography of the substrate by embossing.

In this chapter, inkjet printing of a silver nano ink onto a predefined pattern in a substrate will be presented. The investigation of the possibility to control the track dimensions by printing the Ag track in an embossed recess is proposed. The ink jet printing of silver ink onto embossed alumina and Low Temperature Co-fired Ceramic (LTCC) substrates might be used as a means of providing the dimensional accuracy needed for the THz components. Once the channels have been formed by embossing, they can be filled with liquids or inks using capillary forces. At the sufficiently small contact angle the structured channels are filled with the liquid as a result of the capillary force. Printed features on flat and structured substrates silicon, alumina, LTCC were compared and results presented. As a result the ink well confined to the recess and the line would not be defined in such a way on a flat surface.

7.1.1 Objectives

The objectives of this portion of the study were:

1. To improve the geometry of printed pattern
2. To optimise the printing parameters such as dot spacing and substrate temperature with the goal of achieving well defined lines with reduced spread of the ink
3. To investigate inkjet printing of a silver nanoparticle ink onto a predefined topography pattern in a surface (embossed structures) of the ceramic substrates with the aim of improving the resolution of the printed features.

7.2 Inkjet printing of lines on unstructured substrates

7.2.1 Substrate characterisation

The properties of the substrate, such as surface energy and roughness influence the final printing results. The surface energy of the substrate has an important influence on the wetting properties, hence on the geometry of resulted feature. The information about how a solid is wetted by a liquid is taken from the measurement of the angle at which the liquid–vapor interface meets the solid–liquid interface. The surface tension of the ink should be lower than the surface energy of the substrate to perform printing. When the surface energy of the substrate is determined, it is easier to match the properties of the ink or assign if the surface pre-treatment of the solid is needed. Additionally it is also advisable to have low surface roughness to promote the ink transfer and obtain the appropriate resolution. A high degree of surface roughness can probably cause an uneven ink distribution and lower print density.

The measurements of surface tension of a solid substrate utilize the interaction of solid surfaces with a few test liquids. This procedure uses projection instruments and microscopes (OCA, Data physics) to measure the contact angle of a test liquid on a specified substrate and the OWRK method to determine surface energy of the surface.

The Owens–Wendt–Rabel–Kaelble (OWRK) [171] method is used to determine, both disperse and polar components of the surface energy of the substrates. According to their model, the surface tension is the sum of disperse and polar fractions:

$$\gamma = \gamma^{p} + \gamma^{d} \tag{7.1}$$

In this equation, γ (mJ.m^{-2}) is the surface energy, γ^{d} (mJ.m^{-2}) and γ^{p} (mJ.m^{-2}) are the disperse and the polar components respectively. After measuring the different contact angles obtained using different solvent, we can mark out a curve of the following form:

$$y = ax + b \tag{7.2}$$

In this equation, the x axis values and the y axis values can be calculated as following:

$$x = \sqrt{\frac{\gamma_L^p}{\gamma_L^d}} \tag{7.3}$$

$$y = \frac{(1+\cos\Theta)}{2} \times \frac{\gamma_L}{\sqrt{\gamma_L^d}} \tag{7.4}$$

$$a = \sqrt{\gamma^p} \tag{7.5}$$

$$b = \sqrt{\gamma^d} \tag{7.6}$$

γ^P_L (mN.m^{-1}) is the polar surface tension of the solvent, γ^d_L (mN.m^{-1}) is the disperse component. Θ is the contact angle in radian formed between the solvent drop and the substrate.

Four kinds of substrates, Si wafer, alumina, LTCC DP951, and LTCC CT700 have been analysed. Four kinds of solvent, with known polarity and surface tension values, have been used to determinate the surface energy of the substrates. Dynamic contact angles were calculated for each liquid independently. In table 7.1 the characteristics of the liquids are presented. Parameters x and y were calculated from equations (7.3) and (7.4) respectively.

Table 7.1 Surface energy values for used solvents

Solvent	**Surface energy (mN/m)**	**SE(disperse fraction) (mN/m)**	**SE (polar fraction) (mN/m)**	**X**	**Y**
Ethanol Amine	48.89	31.52	17.32	0.74	8.40
Diodomethane (CH_2J_2)	50.80	33.80	17.00	0.68	8.06
Ethylene Glycol	47.3	29.29	18.91	0.64	9.10
Glycerol	64	37.00	26.40	0.71	8.58

All tape surface energies values together with polar and dispersive contributions are given in Table 7.2. A value is considered as acceptable when the correlation index R^2 (calculated form equation 7.7) was higher than 0.8.

$$R = \frac{n\,(\sum(xy)) - (\sum(x))(\sum(y))}{\sqrt{[n\sum x^2 - (\sum x)^2]\,[n\sum y^2 - (\sum y)^2]}} \qquad (7.7)$$

where n is the number of pairs of data.

Table 7.2 Surface energy for Si, Alumina and LTCC

	Silicon wafer	**Alumina tape**	**LTCC DP951**	**LTCC CT700**
γ_p (mJ.m-2)	11.63 ± 1.32	25.17 ± 0.33	15.17 ± 0.09	18.20 ± 0.29
γ_d (mJ.m-2)	36.03 ± 0.63	28.8 1 ± 0.52	19.30 ± 0.04	19.30 ± 0.04
γ (mJ.m-2) Surface Energy	47.66 ± 0.82	53.98 ± 0.43	34.47 ± 0.13	37.5 ± 0.17
R^2	0.9972	0.9863	0.9962	0.9893

In the case of the Si wafer the contribution of the dispersive surface energy (36.03 mN/m) is higher than that of the polar (11.63 mN/m). Solvent based inks are preferable to print on this substrate. In order to formulate water based inks suitable to print on a Si wafer a wetting agent is required to promote ink adhesion to the substrate.

Results from alumina and LTCC tapes analysis show high surface energy with approximately equal disperse and polar fractions. These tapes are hydrophilic and can be printed by water based inks without adding adhesion promoters.

Energy surface for all substrates presented in this part of work is higher than the ink. So the silver ink can be printed on those tapes.

For the substrate roughness measurement of the tapes, the Altisurf 500 apparatus at Grenoble INP-Pagora was used and results are shown in figure 7.1.

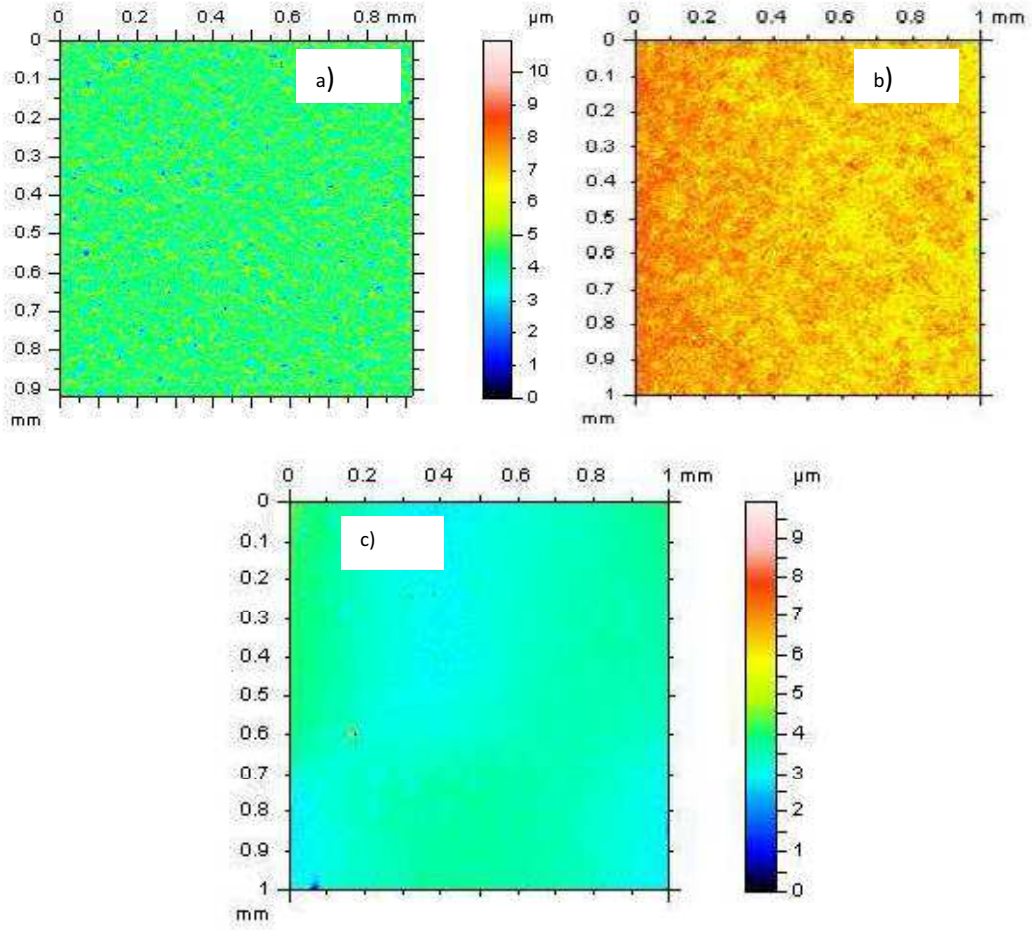

Figure 7.1 Roughness analysis results for (a) LTCC DP95, R_a 0.36 ± 0.01 µm, (b) LTCC CT700, R_a = 0.49 ± 0.07 µm, and (c) alumina, R_a 0.24 ± 0.03 µm

As it was said before, ceramic surface will need very low roughness in order to promote the ink transfer and achieve the appropriate resolution. A high degree of surface roughness can probably cause an uneven ink distribution and lower print density. Among all three substrates, LTCC CT700 shows the highest surface roughness (= 0.49 µm) (figure 7.1) and on this tape the ink spreads the most which will be presented later, in section 7.2.2.

The different widths of printed lines on different substrates are caused by different surface energies and roughness. A good example can be seen in figure 7.2 where printing under the same conditions, brought various width and geometry of the track. The adhesion of the ink on the silicon substrate was poor causing de-wetting of the ink and significant reduction in line width over most of the length of the track the printed track widens and

rounded at the edges loosing the geometry of a rectangle while using silicon substrate. The opposite effect was seen on alumina tape, where sharp geometry of the track was obtained. This is due to better adhesion of the ink to the rough substrate which results in limiting the spreading of the ink. The changes in the width of the track printed under the same conditions were also noticed while printing on LTCC DP951, alumina and LTCC CT700, which will be further discussed in section 7.2.2.

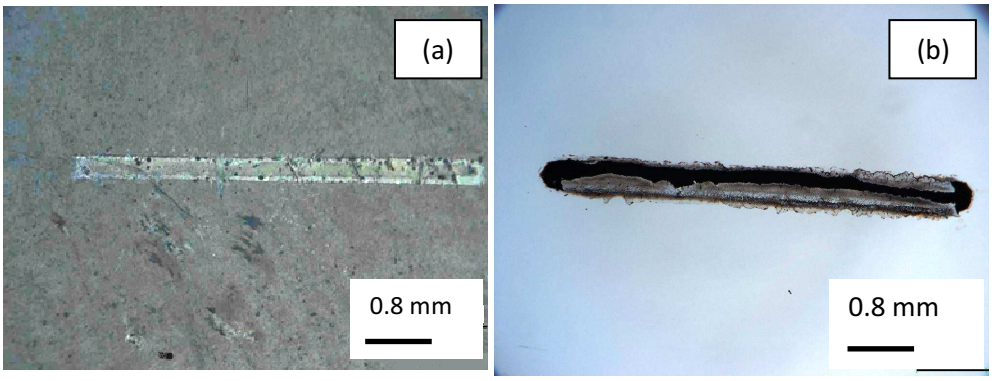

Figure 7.2 Silver lines printed on (a) alumina substrate, (b) silicon substrate

7.2.2 Investigation of process parameters on morphology of printed features.

The ability of controlling the geometry of the printed features is very important in determining its electrical resistivity as well as resolution. For conductive tracks, ideal printed lines should be straight and smooth. Additionally, in order to optimize the electrical performance of the printed features, defaults such as discontinuity of the deposit, spreading of the ink or edge irregularities have to be avoided.

Initial experiments were performed to verify the influence of the substrate temperature on the printed Ag ink behaviour and resulted lines geometry. Single Ag lines were printed onto ceramic substrate at different temperatures: room temperature, 40 °C, 50 °C, and 60 °C. For each thermal value, the lines were left to dry for about 5 minutes.

Figure 7.3 presents the final width of the printed lines on different substrates against substrate temperature, at given dot spacing. Increasing the dot spacing reduces the deposited

material and hence decreases the width of the printed line. As a result, it results in smaller printed features. When dot spacing was increased to larger than 60 µm, partially continuous lines were formed and further increase of the dot spacing led to individual droplets.

The width of the lines printed becomes narrower with the increase of the substrate temperature. However the decrease in the line width between 23 °C and 40 °C is greater than that between 40 °C and 60 °C, which may be due to the quicker evaporation of water at higher temperature, resulting in a lower degree of spreading.

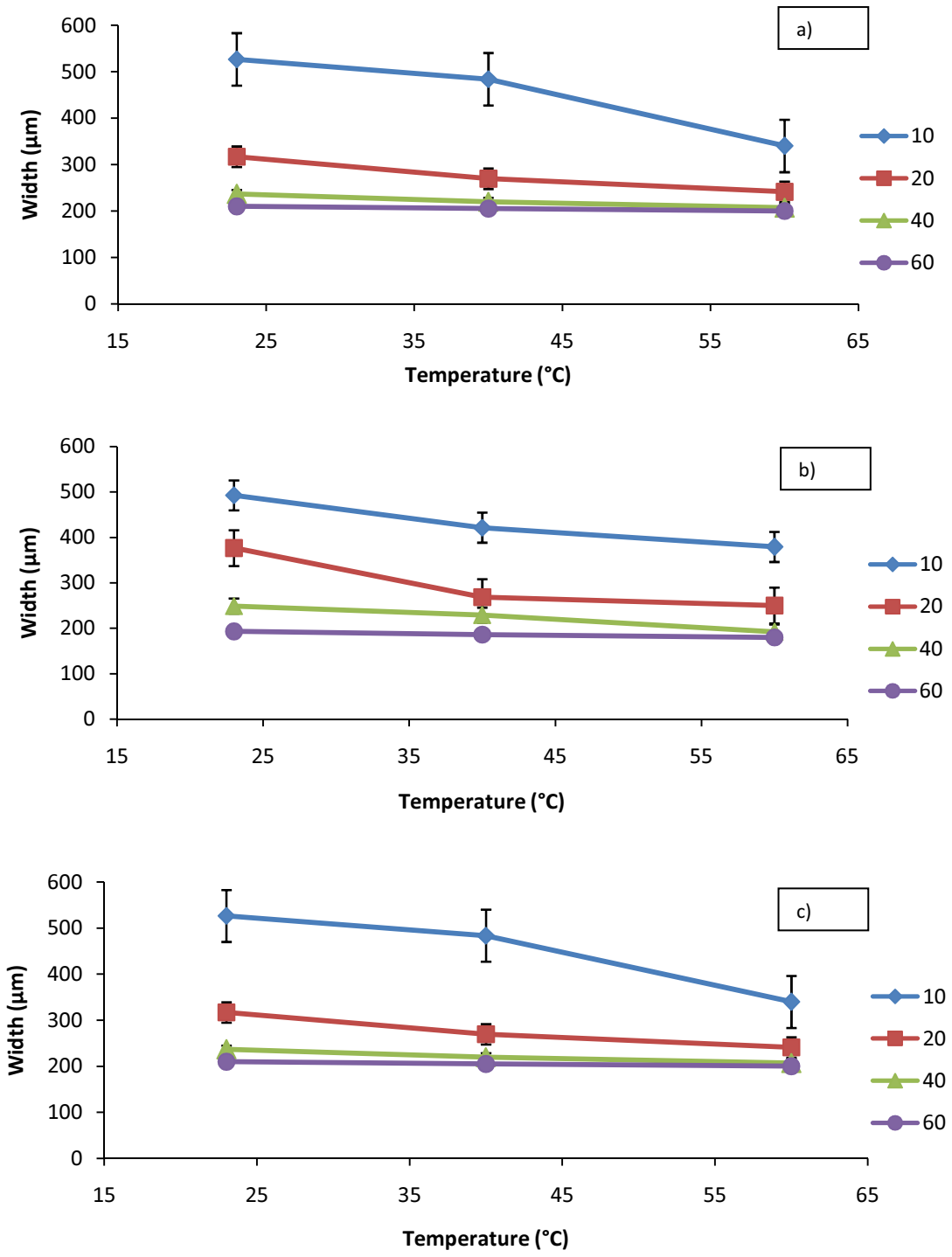

Figure 7.3 Width of the printed silver lines at different dot spacing (legend) on (a) CT700, (b) DP951, and (c) alumina substrates against substrate temperatures.

With increasing the substrate temperature, the width of the track is reduced. As the evaporation rate of water increases it results in the increase of solid concentration in the ink and subsequently the fast increase in viscosity. The increase of viscosity of the silver ink

decreases the mobility of the ink droplet and consequently prevents its spreading and ensures the desired print quality. However, for the cases of wider dot spacing, the temperature does not show such a significant influence. This is because the evaporation of droplets occurs fast enough as there is little influence of the interaction with neighbouring dots.

Figure.7.4 shows printed lines at 40 ºC on (a) CT700, (b) DP951and (c) alumina with 10 µm dot spacing, and on (d) CT700, (e) DP951 (f) alumina with 40 µm dot spacing. Increasing the dot spacing reduces the deposited material and hence decreases the width of the printed line. However this parameter should be optimised for each ink to be used.

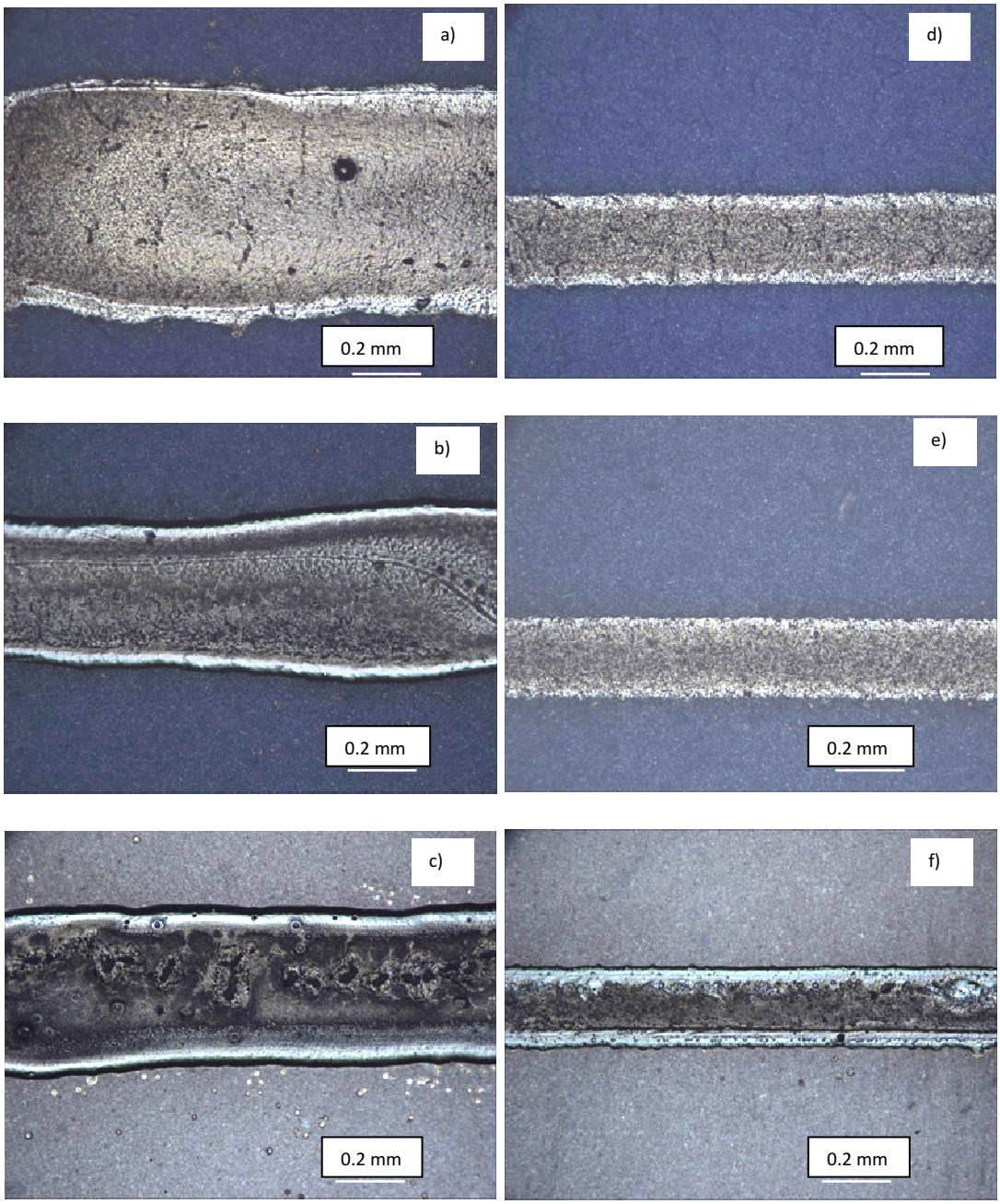

Figure 7.4 Optical microscope images of printed lines at 40 ºC on (a) CT700, (b) DP951 and (c) alumina with 10 µm dot spacing, and on (d) CT700, (e) DP951, and (f) alumina with 40 µm dot spacing.

Although the optimized temperature and dot spacing enabled to obtain narrow and straight lines, in case of building up a thickness, the width of the lines changed. Increasing the number of printed layers causes the spreading of the ink, hence increase in the width and poorer the geometry of the lines (table 7.3).

Table 7.3 Width of the printed lines on various substrates

Substrate	Width (µm)		
	1 layer	3 layers	5 layers
LTCC sintered	280	284	285
Alumin green	208	270	300
Alumina sintered	248	256	286

7.3 Investigation of conductive silver tracks in patterned channels

Direct deposition of the thick film (composed of more than one layer) on the substrate, especially on through substrate shows poor geometry of the metal films and reduces its resolution which is due to spreading of the ink. Although the combination of optimised substrate temperature and dot spacing brought good results in a printed film in terms of its geometry and the width of the track, there was still a problem when more than one layer of ink was printed. To enable printing more layers and simultaneously remaining the geometry of the track, a new method for controlling the morphology of inkjet printed lines was proposed. The new technique is based on printing the ink into the structured channels with predefined topography. The structures are formed by embossing and laser. The silver ink was inkjet printed over the embossed channels filling a single channel, as a consequence of capillary forces. After the ink was deposited, the width of the formed track was taken, as good as a recess was defined if no spill over was observed.

The fabricated structures, obtained with embossing tool and laser machine can be seen as micro-channels in a ceramic surface. Three different surfaces were analysed. Commercial LTCC sintered tape, CT700, provided by project partners Micro System Engineering, (Germany) and two alumina tapes, sintered and green developed by Swerea IVF (Sweden).

LTCC sintered tape

The channels in LTCC tape were formed by embossing. The typical printing results are shown in figure 7.5. It might be noted that the directing of the ink into the channels has taken place successfully. One of the most notable features of this track is that it shows little variation in its width over its total length, and the width of the formed track was taken, as good as a recess was defined if no spill over was observed.

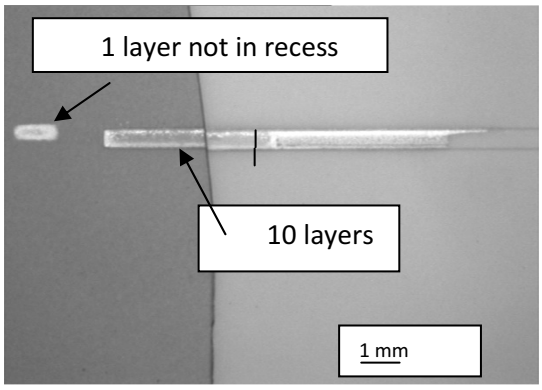

Figure 7.5 Optical microscope image of 10 layer and single layer tracks

These tracks were also examined using SEM. Figure 7.6 shows a typical view of the track on sintered LTCC. The obtained track composed of 10 layers of the ink is straight with good conformance to the edges. At either side of the track in figure 7.6 the thin deposit of the film that is coated on both sides can be seen. Although the ink wets the sidewalls, it does not go over the top as well as the formed film is very thin and should not contribute significantly to the track's conductivity.

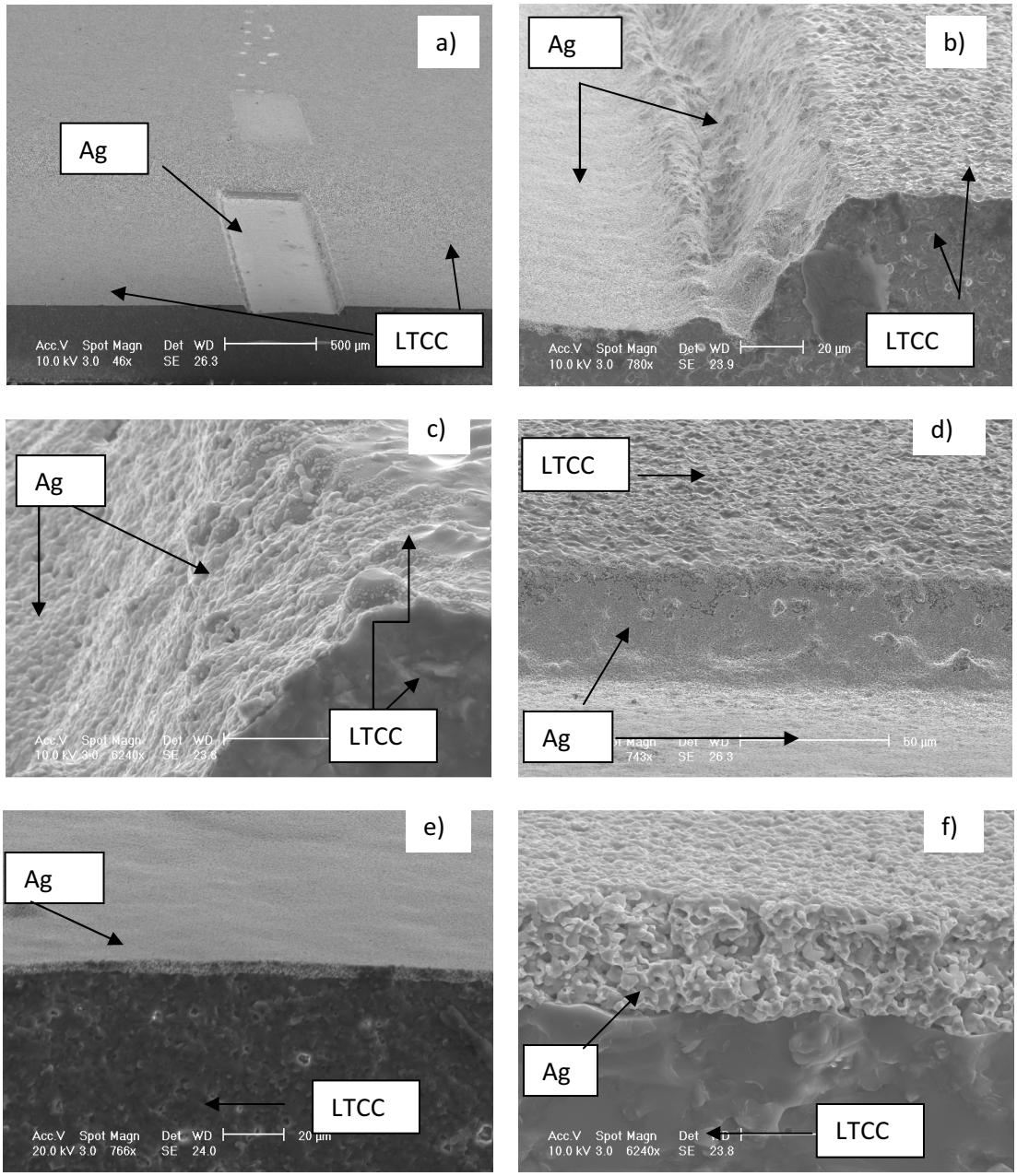

Figure 7.6 Ten layer Ag track 5 mm long printed on sintered LTCC starting in the corner of the recess, (a) close-up of corner, (b,c) higher magnification close, (d) the end face of the recess, (e) cross section, (f) close-up of the cross section

In figure 7.6 (a) we can see the top view of the embossed channel filled with the ink and no spillage is observed. A higher magnification close-up (figure 7.6 (b)) shows ink runs up to the top but not over the top of the recess. Ink flowing up to the end face of the recess shows coverage rather patchy at top (figure 7.6 (c)). The cross section of the dried Ag ink

track (figure 7.6 (e)) formed at the bottom of the recess, and a good uniform coverage on the floor of recess can be observed. Close-up shows a good dense ink film with quite uniform thickness (figure 7.6 (f)).

The volume of the formed track was found to be in good agreement with the solids content of the silver nanoparticle ink (45 %). The initial thickness of the film is 20 times larger than the final thickness which indicates that most of the solvent is still present when the ink finishes filling the channel. The thickness of the film was ~ 5µm and the total width of the feature is about 500 µm.

Figure.7.7 shows SEM image of Ag track printed on LTCC substrate away from recess. It can be seen that in the edge it is not straight along the way and is much more irregular when compared to the track printed in a recess (figure 7.6). The average of the irregularities is around 20 µm.

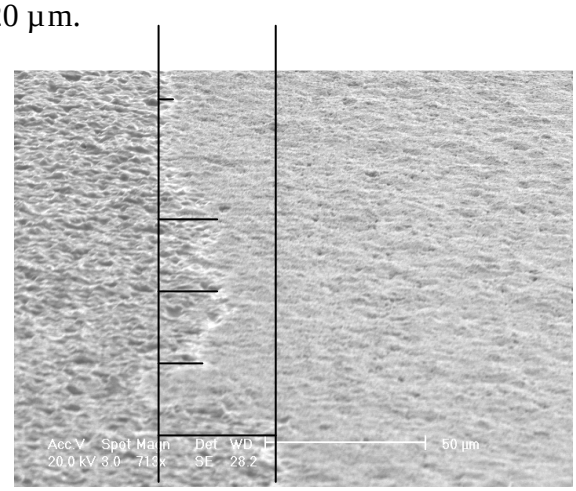

Figure 7.7 Edge of rectangular line printed away from recess (on the blank substrate)

Alumina sintered tape

Figure 7.8 shows a track that was formed in the alumina substrate by laser structuring. Six laser machined arrays with a range of depths. 350, 400 and 450µm wide recesses from top right array were selected for first trials. Dektak measured depth was 53-58 µm for these

recesses. After printing the sample was cleaved along black line and the piece A was carbon-coated and examined using SEM.

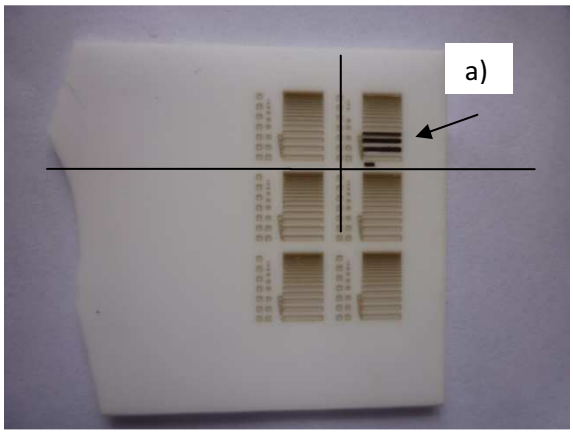

Figure 7.8 Microscope image of six laser machined arrays on alumina substrate

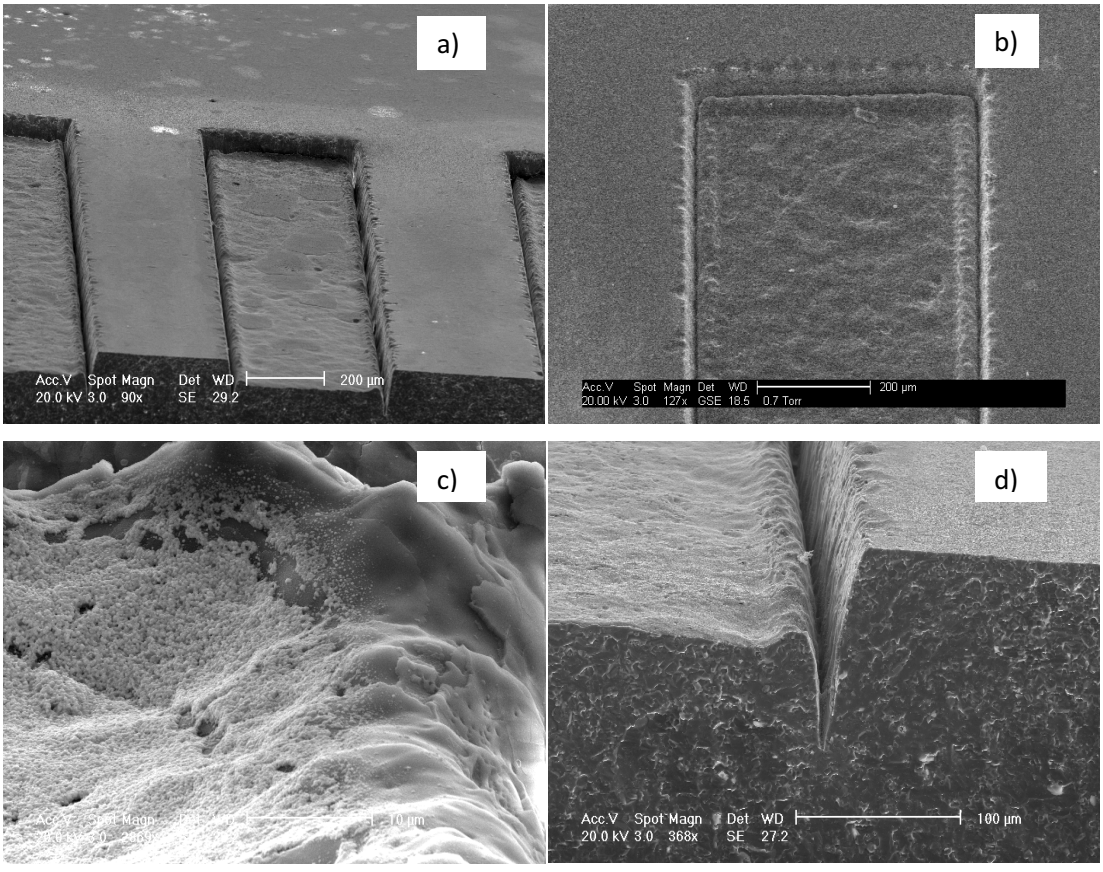

Figure 7.9 SEM micrographs of a Ag track prepared by laser structuring. Alumina substrate structure (sintered), (a) top view, (b) the end of the track, (c) close – up of the edge, and (d) the bottom, cross section

No overspill was observed when 10 layers of ink were deposited in 450 µm recess (figure 7.9). Close-up of the recess shows that the ink stops at edge of the deep groove (figure 7.9 (b)). A deep groove at edge as visible in figure 7.9 (d) is due to the laser machine process.

Figure 7.10 (b) shows the optical microscope image of an Ag track printed on an alumina substrate away from the recess. As can be seen in figure 7.10 (a) the track shows good conformance to the recess edges, however a small area with slight spill over is noticeable. Still this has a better geometry than the track printed next to the recess where irregularities in the form of ~ 100 µm waves are present (figure 7.10 (b)).

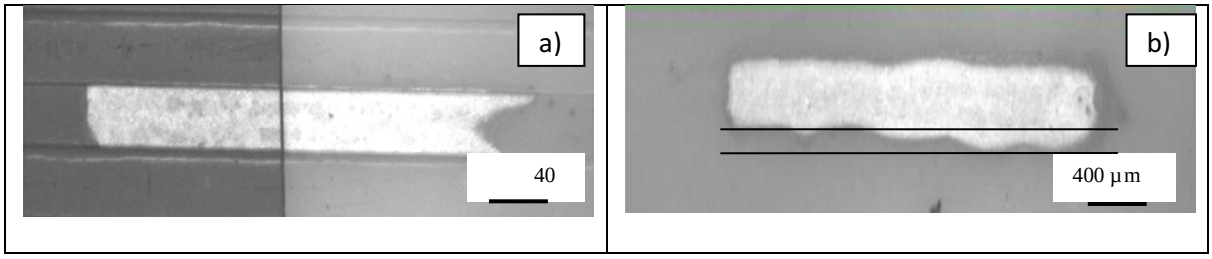

Figure 7.10 Optical images of Ag track with (a) sample pieced together after cleaving and (b) Ag track printed away from recess for comparison

Alumina green tape

Figure 7.11 shows a Ag track that was formed in the alumina green substrate by embossing.

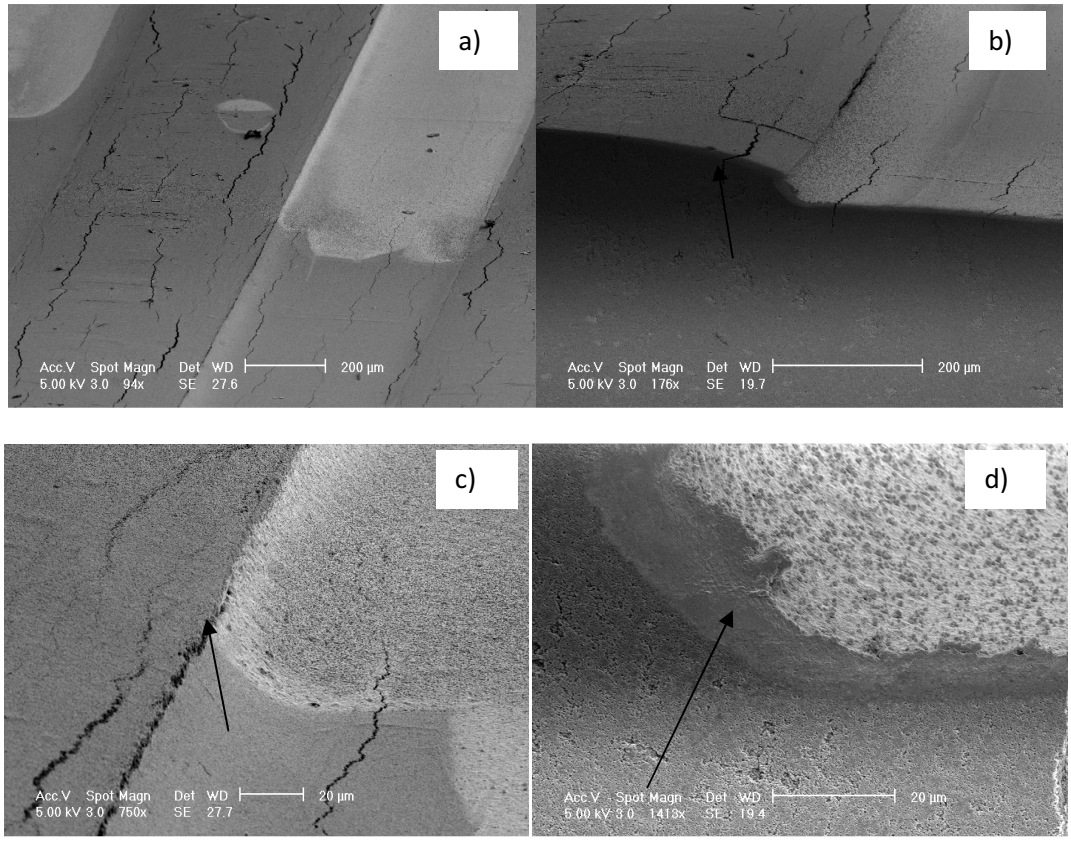

Figure 7.11 SEM micrographs of a Ag track prepared by embossing in green alumina tape. a) and b) Top view, c) and d) close-up of the edge

As can be observed in figure 7.11 (c), the silver track at higher magnification shows ink only just visibly rising up at edge (thin line arrowed) and hence well confined. An ink layer in recess at cut edge (figure 7.11 (d)) shows smooth cut achieved and also appears to show ink has seeped into alumina (apparently infiltrated area arrowed). Low magnification of the track in figure 7.11 (b) shows infiltrated area and good conformance of ink to side of recess, although this may be due to confinement by the crack that appears to be running along the edge. An ink layer track away from cut edge showing good edge conformance. (figure7.11 (a)).

7.4 Conclusion

The problem addressed in this chapter was the poor geometry of the metal films when are directly deposited on a substrate, due to spreading of the ink. This is particularly serious issue for thicker films (composed of more than one printed layer) and films printed on rough substrates.

In order to control the geometry of inkjet printed features on a flat substrate aqueous Ag ink was printed on heated substrates. The width of the track printed under the same conditions varied with the substrates, e.g. at room temperature the width of the track was ~ 490, 520 and 680 µm for LTCC DP951, alumina and LTCC CT700 respectively when printing with 10 µm dot spacing. The different width of the printed lines on different substrates is caused by different surface energies and roughness.

Straight and smooth lines with improved morphological control and resolution were achieved using the optimal temperature of 40 ºC.

Finally, increasing the dot spacing and the substrates temperature resulted in narrow printed line and improved geometry of printed patterns because of the limited ink spreading. This combination made it possible to print lines with a diameter of 200 µm.

To enable consecutive printing of Ag ink layers and at the same time to retain the geometry of the track, a new method has been presented. This consists of printing the ink into the structured channels with predefined geometry in ceramic substrates. These grooves were formed into the ceramic substrates by means of either embossing or laser machining.

Advantages of having a structured substrate include a very good and controllable geometry of the track and elimination of non-uniform spreading which consequently leads to the better performance of the final device. The width of the track remains the same while printing more than one layer ensuring improved resolution of the printed features.

Chapter 8

Silver nanowires synthesis and dispersion preparation

8.1 Introduction

There is currently great interest in nanowires for increasing the functionality of thin film electronic devices and also - since they can be incorporated in inks and directly deposited onto substrates - driving down processing costs. Such metal nanowires films may have high conductivity while remaining a metal volume content as low as 1 wt% and thus may be highly transparent.

The work presented here focuses on synthesis, formulation and printing of Ag nanowires. The work was prompted by the electronics industry wide quest for materials with increased flexibility, lower cost and higher transmittance to replace indium tin oxide (ITO) the most extensively used material for transparent electrodes. Various new materials have been investigated for this application among which are carbon nanotubes (CNT) [172], graphene [173], and Ag nanowires [174].

In the present work silver nanowires were synthesised and the effect of parameters such as polymer concentration and reaction temperature on the morphology of the final material was investigated. The resulted nanowires were dispersed in methanol with the help of copolymer F127 and subsequently printed by Mayer rod onto plastic and glass substrates so forming conductive and transparent films. The dispersing properties of four different dispersants (AOT, CTAB, PVA, and F127) in two solvents (water and methanol) for Ag NWs have been checked. F127 dispersed in methanol turned to be the best surfactant-solvent combination yielding the highest dispersion of AgNWs.

8.1.1 Objectives

The objectives of this portion of the study were:

1. To synthesise and identify the influential factors in the synthesis of Ag NWs
2. To optimize the best conditions of the synthesis and achieve the ultimate goal of a thin (< 100 nm) and long (> 5 µm) Ag NWs
3. To formulate Ag NWs ink. Optimising the amount of the dispersant with the goal of obtaining high loading dispersion of AgNW
4. To deposit prepared AgNWs ink onto plastic and glass substrate and investigate the functionality of the film

8.2 Synthesis and characterisation of silver nanowires

As a synthesis method for AgNWs , the polyol process was investigated due to its simplicity, time efficiency and high yield of the obtaining particles advantages. Effect of various parameters on the morphology of the final material was analysed.

The formation of the 1D Ag nanostructures by reducing $AgNO_3$ with ethylene glycol in the presence of Pt seeds and poly (vinyl pyrrolidone) experiences two steps [175]. In the first step, 5 nm Pt nanoparticles are formed by reducing $PtCl_2$ with EG.

$$2HOCH_2 - CH_2OH \longrightarrow 2CH_3CHO + 2H_2O \quad (8.1)$$

$$CH_3CHO + PtCl_2 \longrightarrow CH_3CO - COCH_3 + Pt + 2HCl \quad (8.2)$$

The second step involves nucleation and growth of Ag nanowires by adding $AgNO_3$ and PVP solutions into the reaction medium.

$$HO\text{-}CH_2\text{-}CH_2\text{-}OH \longrightarrow 2\ CH_3CHO + 2\ H_2O \quad (8.3)$$

$$2\ CH_3CHO + 2\ Ag^+ \longrightarrow CH_3CO\text{-}OCCH_3 + 2\ Ag + 2H^+ \quad (8.4)$$

The formed Ag atoms from reduction reaction of $AgNO_3$ with EG nucleate through homogenous and heterogeneous nucleation [176]. The heterogeneous nucleation results in

formation of Pt nanoparticles which serve as nuclei for the epitaxial growth of Ag NW from the silver nanoparticles with a diameter of 20-30 nm formed in the solution. The homogenous nucleation yields silver nanoparticles with a diameter of 1-5 nm. They are very well-dispersed because of the presence of PVP which could chemically adsorb onto the surfaces of silver solid through O-Ag bonding [175]. Increasing the temperature of the reaction causes the small nanoparticles progressively disappearing to the benefit of larger ones via a process known as Ostwald ripening [135] and so the nanowires are produced. The Ostwald ripening is a spontaneous process which is based on dissolving small crystals or sol particles, and their redeposit onto larger crystals or sol particles. Larger crystals are more energetically favoured than smaller crystals. Although the formation of many small crystals is kinetically favoured (i.e. they nucleate more easily), they are energetically less stable than the ones already well ordered and packed in the interior. This is due to larger surface area to volume ratio molecules on the surface of small crystals. Thus, many small crystals will attain a lower energy state if transformed into large crystals.

Nanowires have the properties different from the bulk materials as the electrons in nanowires are quantum confined laterally and thus occupy energy levels that are different from the traditional continuum of energy levels found in the bulk materials. The need for longer and thinner nanowires is due to their ability to significantly decrease the percolation threshold in surface conductance [135].

8.2.1 PVP concentration effect on geometry of silver nanowires

The morphology of the Ag NW strongly depends on the concentration of PVP. Figure 8.1 shows SEM pictures of samples synthesised using a procedure described in section 3.1.3, except that the concentration of PVP increased from 2.5 µmole to 50 µmole.

As it can be seen in figure 8.1, concentration of PVP played a crucial role. Using 2.5 µmol of PVP (figure 8.1 (a)) resulted in 3 µm long and 120µm wide Ag nanowires. By increasing the PVP concentration up to 3.8 µmol, a longer (10 µm) and thinner in diameter (100 nm) Ag nanowires were obtained compared to the sample in figure 8.1 (a). The difference in morphology between samples in figure 8.1 (a) and (b) might be due to the low concentration of PVP in (a) which leads to incomplete coverage of PVP on side surfaces so the nanowires became thicker during their length growth [135].

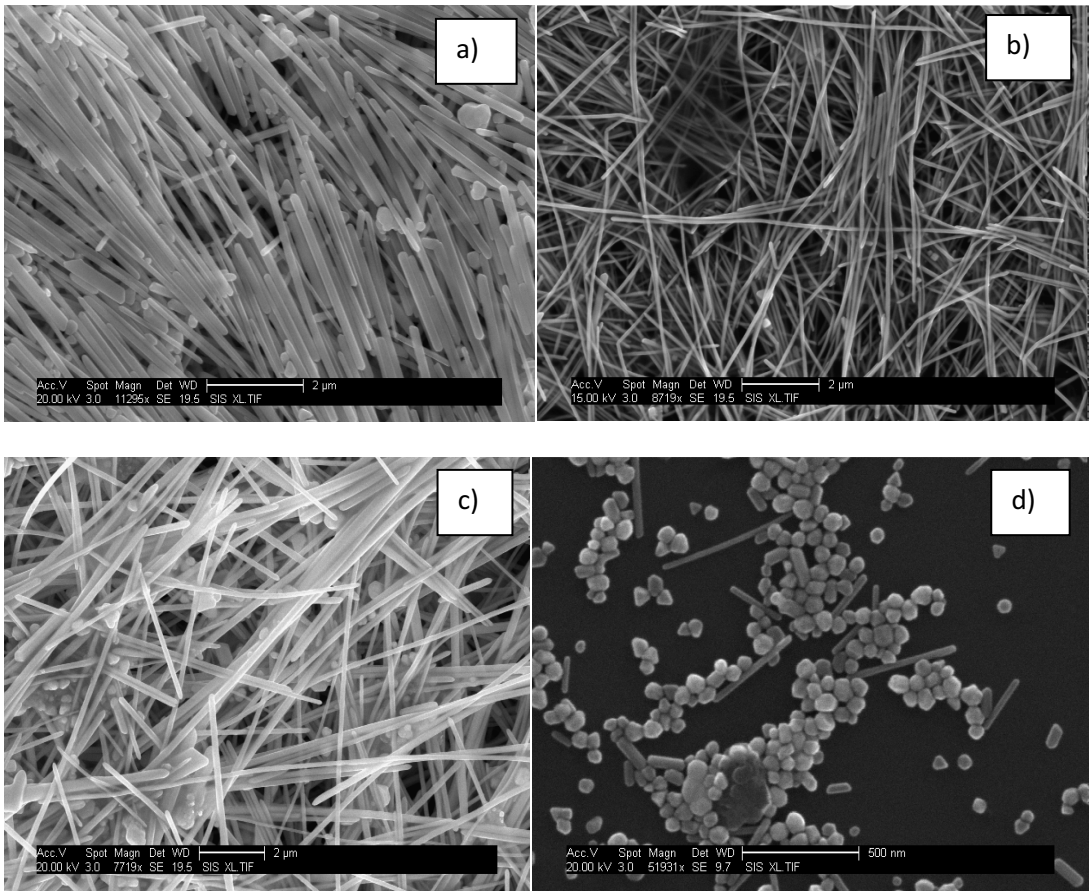

Figure 8.1 SEM micrographs of Ag NW synthesised at different PVP concentration, (a) 2.5 µmol, (b) 3.8 µmol, (c) 5 µmol, and (d) 50µmol

In figure 8.1 (c) it can be noticed that further increase in the PVP concentration results in the presence of nanoparticles at the expense of nanowires. Increasing the PVP concentration further up to 5 µmol produces primarily silver nanoparticles with an average

size of ~50 nm. It is worth to note that no wires (using this concentration of PVP) were obtained even after the solution had been heated at 170ºC for the next 3 hrs.

The exact role of PVP is not clear at the moment. One possible function is a kinetic control of the growth rates of different crystallised faces through absorption and desorption process when PVP interacts with these faces [41]. The high concentration of PVP might increase the coverage layer of PVP on faces of the seeds, leading to an isotropic growth.

8.2.2 Temperature effect on the morphology of silver nanowires

Temperature was also found to be an influential factor in the formation of Ag NW. Figure 8.2 shows SEM of final products obtained at different reaction temperatures.

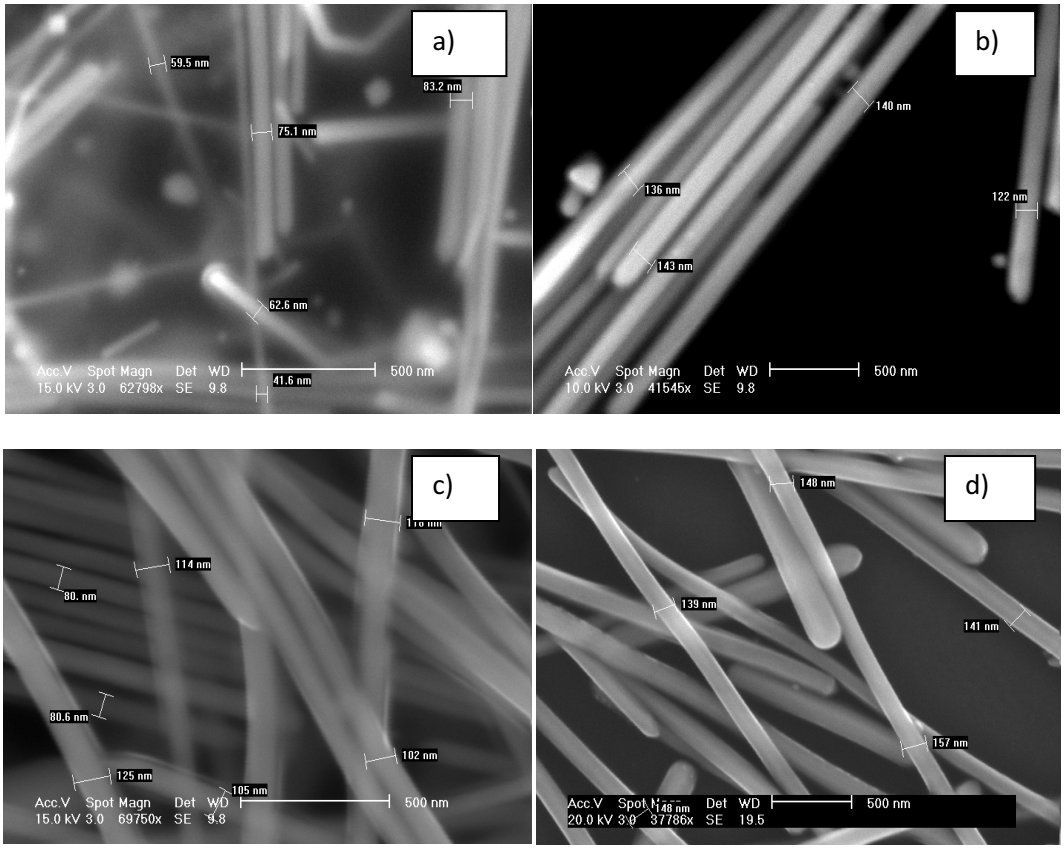

Figure 8.2 SEM micrographs of Ag NWs synthesised at various temperatures, (a) 140, (b) 160, (c) 170, and (d) 180 ºC

When the reaction mixture was heated at 160 ºC the diameter of formed Ag NW was observed to be ~150 nm (figure. 8.2 (b)). Increasing temperature to 170 ºC resulted in a decrease of the diameter ~100 nm (figure. 8.2 (c)). However, further increasing temperature to 180 ºC the diameter of the obtained AgNWs increased again to about 150 nm. When the reaction temperature was set at 140 ºC a very low percentage of NWs were obtained. Although the lowest diameter (~70 nm) could be obtained at 140 ºC however many spherical particles rather than nanowires were found in the final product. This is because at lower temperatures the activation of the specific faces for the anisotropic growth of NWs cannot take place due to lack of energy that could activate that growth [135].

Again it was seen that the temperature is a very important factor to control because itinfluences the morphology of produced Ag MWs.

8.3 Dispersion of nanowires

Chemical methods for making dispersion use dispersants to change the surface energy of the nanowires, which helps improve their wetting characteristics and reduce their tendency to agglomerate in the solvents.

To determine the best dispersant-solvent combination for Ag NWs, two solvents, water and methanol and different dispersants, AOT, CTAB, F127, and PVA were investigated.

8.3.1 Calibration curve

The dispersions of Ag NWs in dispersant solutions were characterized using UV–vis spectrophotometer operating between the ranges of 200–900 nm wavelength to record the absorbance. According to the Beer-Lambert Law, absorbance of the sample material is proportional to its concentration.

Concentration of Ag NWs dispersed into the solution was determined by plotting first the calibration curve. For this purpose a number of solutions of the Ag NW each of accurately known concentration were prepared. Then for each solution ($V_1 = 1.5*10^{-3}$ mol/L, $V_2 = 4.6*10^{-3}$ mol/L, $V_3 = 7.7*10^{-3}$ mol/L, $V_4 = 1.3*10^{-2}$ mol/L), measure the absorbance at the wavelength of strongest absorption was measured. Subsequently a graph of that absorbance against concentration was plotted to obtain a calibration curve (figure 8.3).The corresponding concentrations for AgNWs samples were read from the graph.

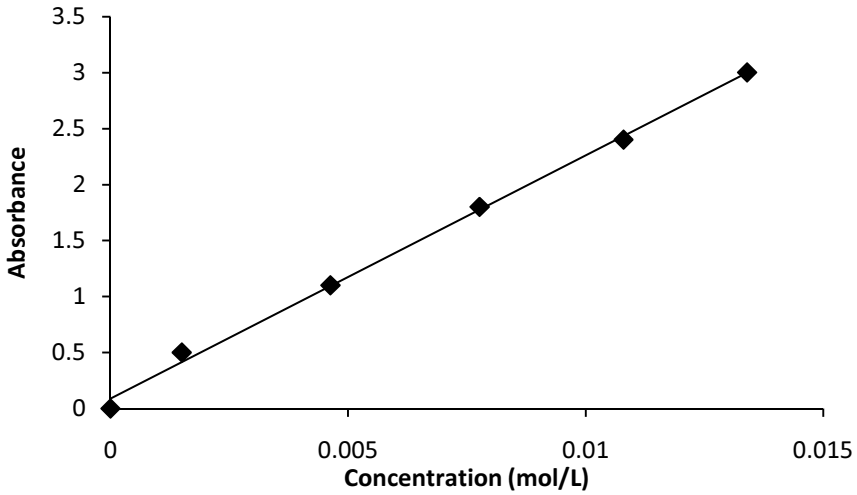

Figure 8.3 Calibration curve (Absorbance as a function of Ag NWs concentration)

8.3.2 Comparison of dispersing properties of the dispersants.

In order to compare the dispersing properties of the four dispersants, Ag NWs in two kinds of solvents were prepared at concentrations ranking from 16 $*10^{-3}$ mol/L to 7 $*10^{-3}$ mol/L, keeping the concentration of surfactant (0.25 wt %) constant. These samples were ultrasonicated for 10 min.

Dispersions were analyzed with UV–vis spectroscopy and the maximum extractable concentration of Ag NWs (at 0.25 wt% surfactant concentration) was determined for each of the surfactants. The baseline correction was carried out using pure 0.25 wt% solutions of the four surfactants so that their absorbance values got subtracted from that of Ag NWs dispersions.

Figure 8.4 shows the UV–vis spectra of Ag NWs with varying concentrations of nanowires in surfactant solutions in water and methanol.

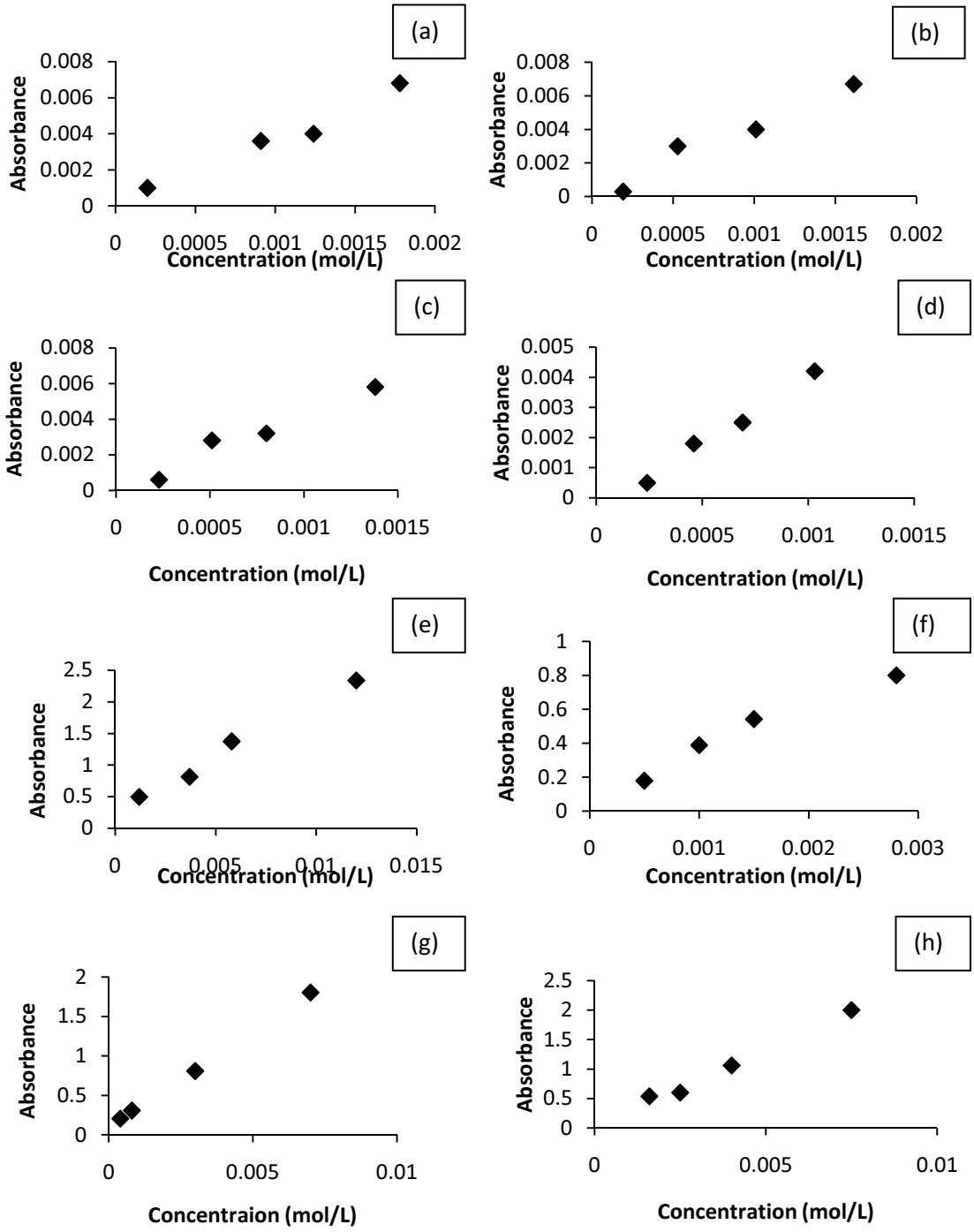

Figure 8.4 UV–vis spectra of various concentrations of silver nanowires in (a) F127, (b) CTAB, (c) AOT, and (d) PVA in water and (e) F127, (f) CTAB, (g) AOT, and (h) PVA in methanol

In all samples, the absorbance increases with the concentration of Ag NWs. However, different values at the same initial AgNWs concentration were obtained for different dispersant which is related to their dispersing properties.

With the knowledge about absorption values for the given solution, we could compare the dispersing properties of the surfactants by calculating a parameter which is called extractability (a percentage recovery into the solution), using the equation 8.5 [177], and it represents the measure of dispersion of silver nanowires in solution.

$$\% \text{ extractability} = C_1/C * 100 \quad (8.5)$$

where $C_1$is the concentration of Ag NW recovered in solution and C is the concentration of Ag NWs originally taken into dispersant solution.

In order to compare the dispersing power of surfactants, first, four dispersants were dispersed in water and percentage extractability was calculated at different concentrations of nanowires (figure 8.5).

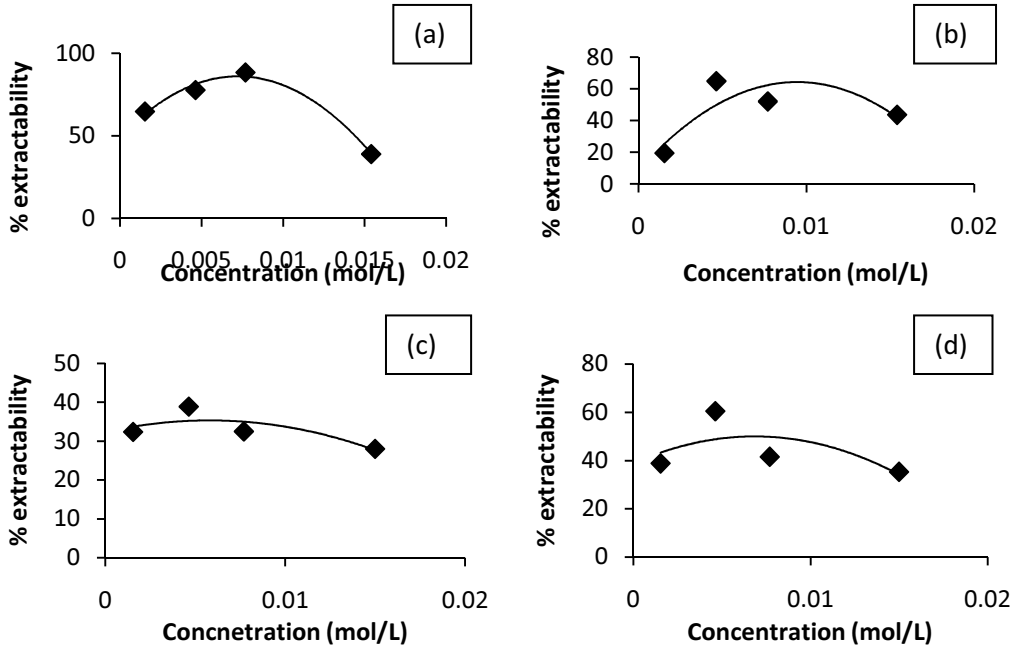

Figure 8.5 shows changes in percentage extractability with variation of concentration of Ag NW in water for a) F127, b) CTAB, c) AOT, and d) PVA

In all samples, percentage extractability versus concentration shows linear increase with the increase in concentration of Ag NWs until the maximum extractability limit was obtained. This might be due to low Ag NWs concentrations, so the amount of dispersant is sufficient to coat the silver nanowires surface homogeneously [176]. The maximum extractability limit was achieved at Ag NWs concentration of $7*10^{-3}$ mol/L for F127 and 4.6 $*10^{-3}$ mol/L for three other dispersants, CTAB, AOT, and PVA, indicating that the dispersant amount is just sufficient to disperse the Ag NWs. For further increases in the concentration of nanowires, the dispersant concentration turns insufficient to fully disperse the agglomerates of Ag NWs, as the percentage extractability decreases at high concentrations. The maximum amount of Ag NWs was extracted in the case of F127, where percentage extractability reached 88%. Others dispersant showed lower extractability, namely 65, 40, and 60% for CTAB, AOT, and PVA respectively. It is noteworthy that 40 % of extractability is achieved for three dispersants F127, AOT and PVA when 0.015 mol/L of Ag was used for dispersion. Results showed that the same amount of F127 could disperse large amounts of AgNWs as compared to other dispersants.

Based on the experimental results, the dispersing power of the four dispersants follows the trend: F127>PVA>AOT >CTAB

However, different behaviour of the dispersants was observed when methanol was used as a solvent. Figure 8.6 shows changes in percentage extractability with variation of concentration of Ag NW for F127 (a), CTAB (b), AOT (c), and PVA (d) dispersant.

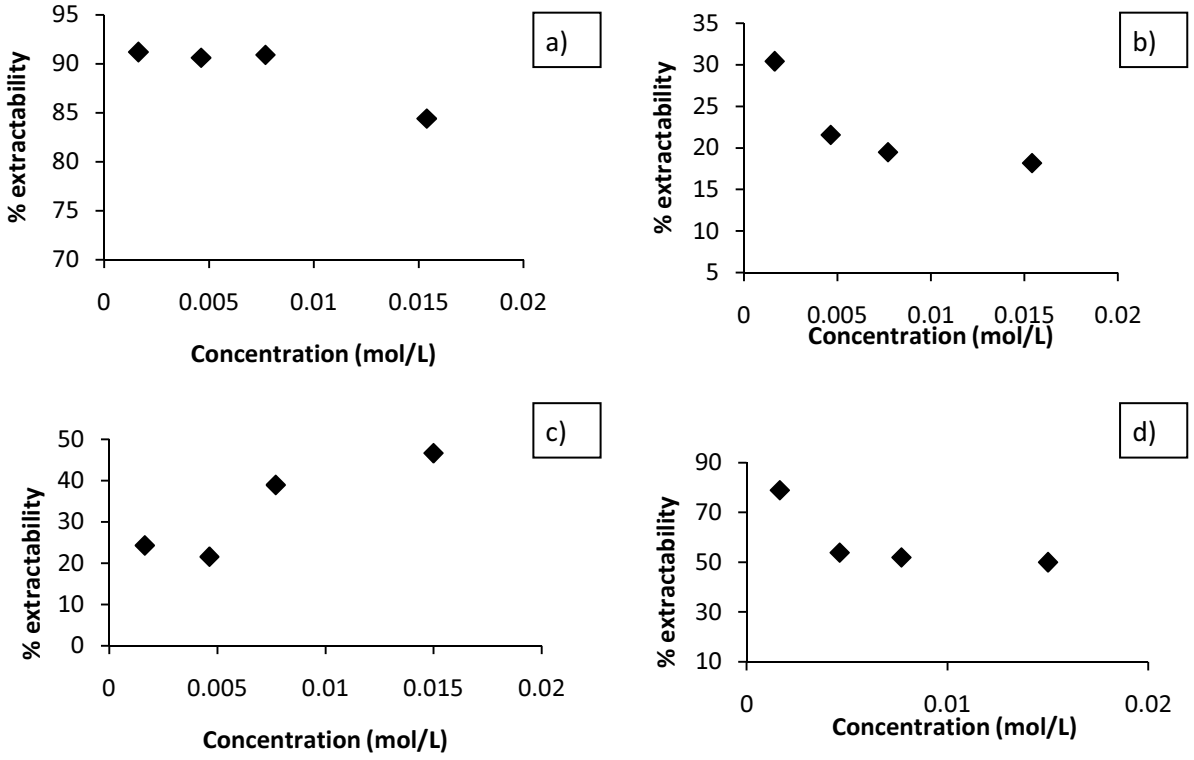

Figure 8.6 Changes in percentage extractability with variation of concentration of Ag NW in methanol for a) F127, b) CTAB, c) AOT, and d) PVA

The best dispersant in methanol solutions turns to be F127 extracting 90 % of Ag NWs for the concentration of silver powder from $1.6*10^{-3}$ mol/L to $4.6*10^{-3}$ mol/L. Increasing the concentration of Ag NWs resulted in lower percentage of extractability (80 %) of the F127. For CTAB and PVA the extractability decreases with increasing the AgNWs concentration. The highest value achieved was 80% for PVA and 30 % for CTAB. AOT turns to have the high dispersing properties when the highest concentration of Ag NWs was used, reaching 45 % of extractability properties.

8.3.3 Determination of optimum Ag NWs to copolymer F127 ratio

Based on the results from 8.3.2 the copolymer F127 dispersed in methanol was selected as the best surfactant-solvent combination yielding the highest dispersion of Ag NWs. In order to find the optimum Ag NW-to-F127 ratio, a second set of experiments were performed. In

these experiments, concentration of F127 was varied from 0.05 to 0.25 wt%, keeping the amount of Ag NWs constant, using methanol as a solvent. Constant Ag NWs concentrations used in these experiments were the maximum extractable concentrations of Ag NWs chosen from the first turn of experiments for 0.25 wt% surfactant concentration. Constant Ag NWs concentrations were selected to be 7 mmol and again, the samples were analyzed using UV–vis spectroscope. Results are shown in figure 8.7. The best optimum amount of F127 to assure good dispersion was found to be 1.3 wt%.

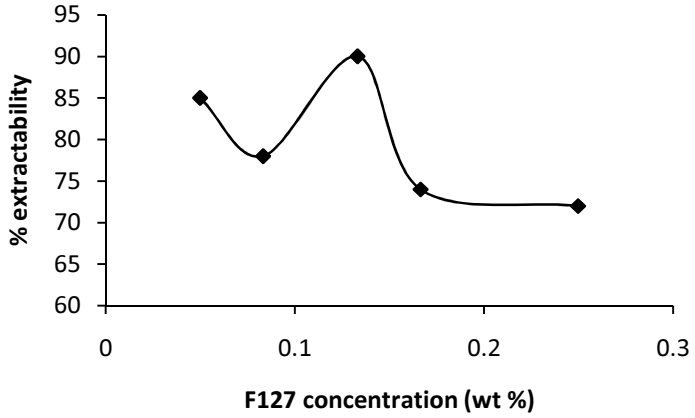

Figure 8.7 Changes in percentage extractability with variation of concentration of F127 in methanol

8.3.3 Ag NW film characterisation

Resistivity and transparency of the films

The resistance and transparency of the deposited Ag NW films were analysed to verify the properties of the Ag material. The aim of this part of work was to obtain transparent conducting material that can be further used in various electronic devices. Most of the industrial applications require sheet resistance lower than 500 Ω sq^{-1} for transparent electrodes, for OLED displays and solar cells should be less than ~ 50 Ω sq^{-1}, and for touch screens a range of 200–500 Ω sq^{-1} values is acceptable. The transparency of the film should

higher than 50 %. It is also desirable that such devices can be fabricated using a low-cost strategy, such as Mayer rods or the roll-to-roll fabrication.

Silver inks were formulated using Ag NWs as a functional material, copolymer F127 as a dispersant agent, and methanol as a solvent. To deposit a film, Ag NW ink was dropped on a glass substrate (figure 8.8 (a)) and on a plastic (figure 8.8 (b)), and then, a Meyer rod was pulled over the solution, leaving a uniform, thin layer of Ag NW. After that the wet coating of Ag NW on a substrate was dried on a hot plate at temperature of 120 ºC for 10 min.

Figure 8.8 (c) shows Ag NW ink in methanol solution. To achieve uniform, agglomeration free films, Ag inks were sonicated for 10 minutes just before use.

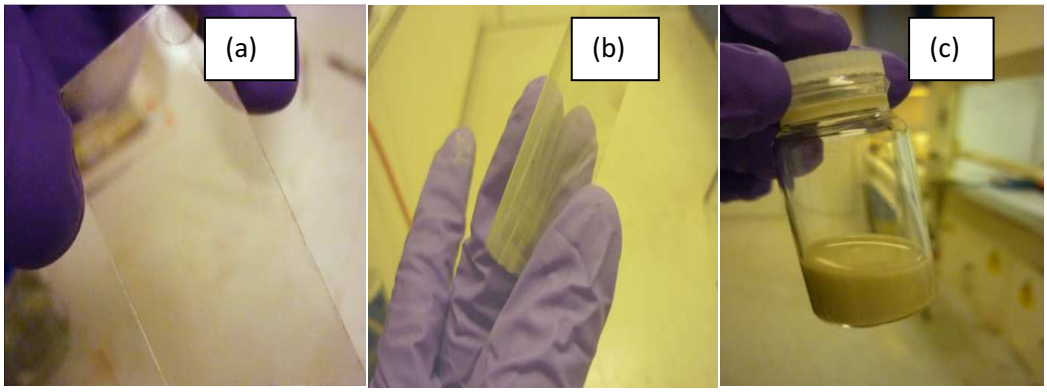

Figure 8.8 AgNW ink deposited on (a) glass, b) plastic, and (c) dispersed AgNWs in methanol

Figure 8.9 shows the transmittance values for Ag NW films of various densities deposited on glass substrates. The denser the film was the lower transmittance was obtained. Increasing the density of the film decreases the resistivity of the films. This is due to the reducing the number of holes in the film which results in more uniform electrical field distribution [176].

Moreover, in the near-infrared regions, the transmittance of the Ag NW films is constant which is important for solar cell application.

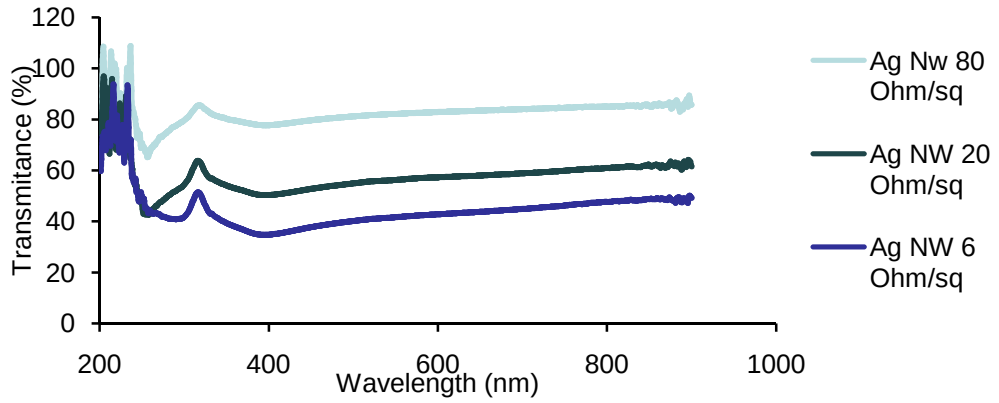

Figure 8.9 Optical transmittance of transparent Ag NWs films with various resistivity values measured with a UV-vis spectrometer

Figure 8.10 shows the sheet resistance versus transmittance curve for Ag NWs films with varying density. Sheet resistances as low as 6, 20 and 80 Ω/sq for corresponding transmittances of 40, 58 and 80 % were obtained after the heating the films at 120 ºC. The ITO films have higher resistivity at any transmittance compare to AgNWs films. Sheet resistances of 60, 196, and 780 Ω/sq for corresponding transmittances of 77, 82, and 80 % respectively were reported in the literature [179].

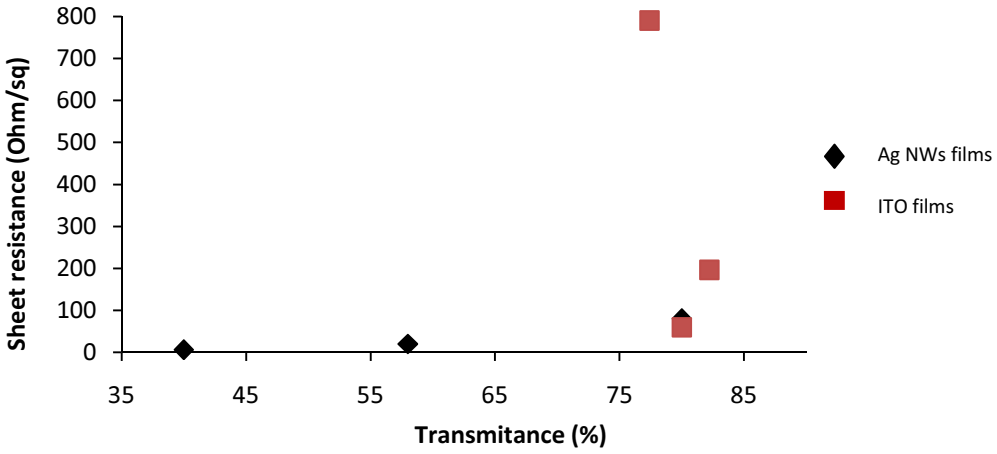

Figure 8.10 Sheet resistance vs transmittance for Ag NW and ITO films

By adjusting the density of the films it was possible to reach a resistivity of 6 Ω/sq. This resistivity value meets requirements of utility for solar cell and organic light emitting diode-OLED application.

8.4 Conclusions

Silver Ag NWs were synthesised using seed-assisted, polyol process. Resulted wires were 10 µm long and 100 µm wide. Two important factors were responsible for Ag NWs synthesis: the pre-formation of Pt seeds in the solution that could serve as nuclei for the subsequent growth of silver nanowires and the use of PVP that could kinetically control the growth rates of silver through chemical surface modification. Control over the morphology of these AgNWs could be achieved by varying the reaction conditions, including reaction temperature and PVP concentration. Increasing the reaction temperature from 140 to 180 °C led to the formation of short nanowires. 170 ºC gave the longest and thinnest nanowires and was set as an optimum. An increase in the concentration of PVP slightly reduced the diameter of resultant nanowires (3.8 µmol), too high concentration led to nanoparticles in the final product.

In order to choose the best dispersant-solvent combination for AgNWs four dispersants (F127, CTAB, AOT, and PVA) and two solvents (water, methanol) have been analysed. The best combination turned to be F127-methanol. The high molecular weight of copolymer F127 might be as an advantage in dispersion of Ag NWs. Although Ag NWs were also well dispersed in water with addition of F127, the fluid as prepared gave less uniform film that the one in methanol.

For the film deposition, Mayer rods were successively employed. Resulted films were conductive and transparent. Resistivity value of 80 Ω/sq and 80% transmittance in the visible

spectral range were achieved, which is comparable to some of ITO films. Additionally, the transmittance range is much flatter than that for ITO in the visible and near-infrared range.

Chapter 9

Conclusion and future work

9.1 Conclusion

The work presented in this thesis focuses on the synthesis of nanomaterials, formulation and printing of Ag nanoparticle and nanowire inks for two distinct applications. Inkjet printing of Ag nanoparticle films on ceramic substrates has been undertaken with the aim of providing a smaller size of printed feature at lower cost than can be obtained with the conventionally used screen printing.

Monodispersed Ag nanoparticles with a size down to 50 nm were successfully synthesized and dispersed in aqueous medium up to 5%. For the first time a copolymer F127 was used for Ag ink formulation. Following encouraging results from the 5 wt% ink, a Ag ink containing a higher Ag solid content (45 wt%) has been formulated by treating the synthesised particles with different solvent (acetone).The effect of the surface characters of substrates, printing temperature and dot spacing on the size and morphology of printed silver features was investigated.

An attempt has been done to improve the physical properties of the printed features. For these reason SiO_2 have been used as an adhesion promoter and bonding agent between the particles. The effect of nanoSiO_2 content as an inorganic binder on the morphological and electrical properties of the silver conducting films formed by inkjet printing method was investigated. Adhesion and hardness property of the silver films after adding SiO_2 to the silver ink and sintering at various temperatures were also examined.

The investigation of the possibility to control the track dimensions by printing the Ag track in an embossed recess was proposed. The silver ink was jet printed onto embossed

alumina/LTCC substrates to provide the dimensional accuracy. Once the channels have been formed by embossing, they could be filled with inks using capillary forces.

Work on Ag nanowires films was prompted by the wide quest of electronics industry for materials with increased flexibility, lower cost and higher transmittance to replace indium tin oxide (ITO, the most extensively used material for transparent electrodes). Towards these objectives silver nanowires were synthesised and dispersed in methanol with the help of copolymer F127. They were subsequently deposited on plastic and glass substrates forming a conductive and transparent film. The effect of temperature, polymer concentration and solvent treatment on the size and morphology of silver nanowires was investigated. Various dispersants were tested to obtain the best silver nanowire ink formula. The properties of deposited film, such as transparency and resistivity were tested.

Synthesis of Ag nanoparticles

The experimental work focused on developing the new method for synthesising silver particles. An objective was to develop a process that would allow the creation of large numbers of particles easily separating from the solution and being capable of making a contribution to the formation of stable ink.

Two methods of synthesis have been tested in order to achieve the target, wet chemistry and scCO_2technique.For silver particles wet chemistry turned out to be a most suitable method in terms of the yield and further processing.

The 20 nm diameter, spherical particles were obtained through the control of reaction parameters, such as capping agent, concentration of $AgNO_3$, AOT and NaOH.

The best initial concentration of $AgNO_3$ had to be lower than ~0.3 M to obtain small size and regular shape of the particles. Using AOT instead of PVP as a stabilizer simplified the separation of the Ag particles from the solution. The molar ratio between AOT and $AgNO_3$

have been found to be important and was set as 2:1 to assure the smallest size of particles (20 nm). The concentration of NaOH was crucial in controlling the shape of the particles, 0.005 mol was set as an optimum to obtain the spherical and small particles.

Formulation and examination of silver ink

The aim of this part of work was to reduce the number of layers in the film processing by increasing the thickness of a single layer. That was done by using high loading metal ink. A lot of work was put to develop and understand the formulation of stable silver dispersion. The advantages of having high content of metal in a fluid include reducing the costs of the process and getting a better resolution of the printed features.

During the study, the loading of the particles in ink produced by the original process was improved mainly by using a different solvent treatment of the particles. An increase in the loading, from 5 wt % till 45 wt % of silver particles favoured the achievement of denser and thicker film with one layer printing. As a result, the better resolution and lower resistivity of the printed track were possible to be obtained while keeping the same process parameters. Surface treatment of synthesised Ag particles by solvent showed how important this step is in formulating a high loading ink. It has been found that the sizes of aggregates and properties are dependent on this treatment. Treatment of Ag particles with IPA resulted in the formulation of 5 wt% Ag ink (AG1) with the presence of copolymer F127under HIFU agitation. A HIFU technique successively reduced the size of Ag agglomerates down to ~50 nm from ~ 200 nm untreated.

A higher 45 wt%Ag ink (AG2) was formulated by treating the synthesised particles with an acetone. As a result the size of aggregates decreased down to 50 nm, and further use of copolymer resulted in highly hydrophilic particles with the size of 10 nm. Copolymer F127 was found to be very effective as a stabilizer leading to the formation of high silver loading.

Rheology studies have been performed on so prepared silver inks to understand the behaviour of the inks and in the same time showing well-dispersed suspension and suitability for use in inkjet printing process. The influence of silver loading on the viscosity of the subsequent inks has been checked. The viscosity increased with higher content of particles due to the increase of the interaction between silver particles when solid content increases. The viscosity of 2.1 mPa s and 3.3 mPa were obtained for 5 wt% ink and 45 wt% ink respectively. The small changes in viscosity value were observed over a period of 20 days indicating a good stability of the fluids.

Both inks were printed on LTCC substrates and the printed lines showed a very low resistivity and good shape definition. The resistivity of the printed Ag lines decreaseed as a function of annealing temperature, and it was measured to be $20 \pm 0.1 \mu\Omega$ cm for AG1 ink and $3\pm 0.2\ \mu\Omega$ cm for AG2 after annealing at 350°C. However to obtain low resistivity,the film thickness of 1 µm was necessary,and thus the number of printed layers (70) was required in case of AG1 ink due to the low loading of Ag particles. It was found that the higher loading of metal content the thicker layer can be obtained. UsingAG2 ink needs only one layer to obtain thick, dense and conductive film.

Influence of SiO_2 on the properties of a silver film

Addition of 0.05 wt % of SiO_2 to the Ag ink was effective in improving the microstructure of the fired films and together with increasing sintering temperature, a uniform grain was produced. The final film density and hence electrical resistivity were thus improved with the optimised SiO_2 content. The addition of a binder in the film materials was important not only for promoting the sintering and improving the densification as well as resistivity but also for providing the adhesion to substrate. The adhesion of the silver film to the substrate was improved by increasing a sintering temperature and addition of 0.05 wt% of SiO_2 into the ink formula.

Improving the geometry of printed patterns

Direct deposition of the thick film (composed of more than one printed layer) on the substrate, especially a rough substrate shows a poor geometry of the metal films which is due to spreading of the ink. To avoid or at least minimize this effect we proposed two approaches.

Printing straight and smooth lines with improved morphological control and resolution were possible to achieve by using the optimal temperature of substrate at 40 ºC. Increasing the dot spacing further limited ink spreading, hence resulting in narrow printed lines and improved geometry of printed patterns. As a result of this combination (temp. and dot spacing) it was possible to print lines with a diameter of 200 µm. However with increasing the number of printed lines the track become wider and gradually lost its geometry.

To enable printing more layers and simultaneously remaining the geometry of the track, a new method for improving the morphology of inkjet printed tracks has been described by printing the ink into the structured channels with predefined topography. These grooves have been fabricated into the ceramic substrates by means of either embossing or laser machine. After pre-patterning the substrate, silver ink was printed over the as-formed patterns. 10 layers were possible to print one on the top of another without causing any difference in width or geometry of the track since the ink stayed in the recess with no spill over observed.

Synthesis of Ag nanowires (NW) and ink formulation

Silver NWs were synthesised using solvothermal method. The optimised amount of PVP (3.8 µM), and optimised reaction temperature (170 ºC) in the synthesis lead to produce 10 µm long and 120 µm wide Ag NW. The effect of five different surfactants in various solvents on stability and film uniformity of the AgNW dispersion was investigated. Water, and methanol were tested as a dispersion medium and the AOT, CTAB, PVA, and F127 were chosen as a

dispersing agents. F127 dispersed in methanol turned to be the best surfactant-solvent combination yielding the highest loading dispersion of AgNW. Meyer road coating method was successfully applied to produce Ag NW films on glass and plastic substrates. Sheet resistance as low as 6, 20 and 80 Ω/sq for corresponding transmittances of 40%, 58% and 80 were obtained after the heating the films at 120 ºC.

9.2 Future work

- The wet chemistry method developed in this work is a very promising technique for the synthesis of Ag nanoaprticles. The one limit of this process is the high temperature required to obtain conductive film on the substrate. To improve the synthesis method for Ag nanoparticles in order to obtain the same conductivity properties at lower sintered temperature (150 ºC) of the film is very desirable as it would widen the applications of the inks, such as printing Ag inks on plastics. This might be done by replacing the surfactant (capping agent) by the one with lower melting point.
- Further increasing ink loading would improve the resolution of thick films. The smaller feature size can be also achieved by chemically treating substrate surface to adjust the energy of the substrate and simultaneously using the inks with optimal rheological properties.
- Printing on top of predefined topography structures has to be further tested. Structuring narrower tunnels might be helpful in improving the resolution of the features. The surface character of the substrate plays an important role in filling the channel by the ink. Surface treatment of the substrates by evaporating a monolayer of the hydrophobic/hydrophilic polymer would allow filling the channel with the ink in a very precise way.
- The most extensively material used for transparent electrodes is indium tin oxide (ITO). Further work on Ag nanowire films has to be done to increase flexibility, lower cost and higher transmittance so the replace of indium tin oxide (ITO). Towards this objective, synthesis of Ag NW has to be improved to lead to formation of longer and thinner Ag

nanowires. This might be done by changing some of the parameter in the synthesis, e.g. catalyst or polymer.

To obtain more uniform film more tests have to be done with the Mayer rods. Further investigation of factors such as the groove size in wire wound rod, viscosity and surface tension of fluids might be helpful in obtaining a uniform film.

Future work might also involvethe adjustment of AgNW fluids properties to make it suitable for inkjet printing.

References

[1] E. L. Eisenstein, The printing revolution in early modern Europe (2nd ed.), *Cambridge University Press*, (2005)

[2] H. Sirringhaus, M. Ando, Materials challenges and applications of solution processed organic field-effect transistors. *MRS Bulletin*, 33, (2008), 676

[3] C. Mack, Fundamental principles of optical lithography: the science of microfabrication, *Wiley*, (2007)

[4] D. Wallace, D. Hayes, C. Ting, V. Shah, D. Radulescu, P. Cooley, K. Wachtler, and A. Nallani, Ink-jet as a MEMS manufacturing tool. *In International Conference on Integration and Commercialization of Micro and Nanosystems B*, (2007), 1161-1168

[5] Y. Zhang, C. Liu, and D. Whalley. Direct-write techniques for mask less production of microelectronics: A review of current state-of-the-art technologies. *In International Conference on Electronic Packaging Technology and High Density Packaging, (ICEPT-HDP '09)*, (2009), 497–503

[6] S. Magdassi (Editor), The chemistry of Inkjet inks, *Worlsd Scientific Publishing* Co. Pte. Ltd

[7] B.-J. de Gans, P.C. Duineveld, U.S. Schubert, Inkjet printing of polymers: state of the art and future developments, *Adv Mater*, 16, (2004), 203–213

[8] M. T. Bernius, M. Inbasekarn, J. O'Brien, W.Wu, Progress with light- emitting polymers. *Adv. Mater*, 12 (23), (2002), 1737-1750

[9] S.-C. Chang, J. Liu, J. Bharathan, Y. Yang, J. Onohara, J. Kido Multi color organic light-emitting diodes processed by hybrid inkjet printing. *Adv Mater*, 11 (9), (1999), 734-737

[10] B. Comiskey, J.D. Albert JD, H. Yoshizawa H, J. Jacobson, An elec-trophoretic ink for all-printed reflective electronic displays, *Nature*, 394, (1998), 253

[11] K.Finkenzeler, RFID Handbook: Fundamentals and applications in contactless smart cards radio frequency, indentification, and near-field communication, *Wiley*, (2003)

[12] Z. Bao, Y. Feng A. Dodabalapur, V.R. Raju, A.J. Lovinger, High-Performance Plastic Transistors Fabricated by Printing Techniques, *Chem. Mater.*, *9* (6), (1997), 1299-1301

[13] B. S. Ong, Y. Wu, P. Liu, and S. Gardner, High-Performance Semiconducting Polythiophenes for Organic Thin-Film Transistors, *J. Am. Chem. Soc.*, 126 (11), (2004), 3378-3379

[14] M. Mengel, J.Nikitin, Inkjet printed dielectrics for electronic packaging of chip embedding modules, *Journal Microelectronic Engineering*, 87, (2010), 593-596

[15] J. A. Lewis, J. E. Smay, J. Stuecker, and J. Cesarano, Direct ink writing of three dimensional ceramic structures. *Journal of the American Ceramic Society,* 89 (12), (2006), 3599-3609

[16] J. A. Lewis. Direct-write assembly of ceramics from colloidal inks. *Current Opinion in Solid State and Materials Science,* 6(3), (2002), 245-250

[17] X. Zhao, J. R. G. Evans, M. J. Edirisinghe, and J. H. Song. Formulation of a ceramic ink for a wide-array drop-on-demand ink-jet printer, *Ceramics International,* 29 (8), (2003), 887-892

[18] B.-J. Gans, P.C. Duineveld, U.S. Schubert, Inkjet printing of polymers: State of the art and future development, *AdV. Mater.*, 16, (2004), 203-213

[19] T. Xu, J. Jin, C. Gregory, J.J Hickman, T. Boland, Inkjet printing of viable mammalian cells, *Biomaterials*, 26, (2005), 93-99

[20] E. Tekin, P.J. Smith, S. Hoeppener, A.M. J. Berg, A.S. Susha, A. Rogach, J. Feldmann, U.S. Shubert, Inkjet printing of luminescent CdTe nanocrystal-polymers composities, *Adv. Funct. Mater*., 17, (2007), 23-28

[21] R. Dorey and R. Whatmore, Electroceramic Thick Film Fabrication for MEMS, *Journal of Electroceramics*, 12, (2004) 19-32

[22] H. P. Le, Progress and trends in ink-jet printing technology, *Imag. Sci Technol.*, 42, (1998), 49

[23] G. D. Martin, S. D. Hoath and I. M. Hutchings, Inkjet printing - the physics of manipulating liquid jets and drops, *Journal of Physics: Conference Series*, 105(1), (2008)

[24] P. F. Blazdell and J. R. G. Evans, Application of a continuous ink jet printer to solid free forming of ceramics, *Journal of Materials Processing Technology*, 99(1), (2000), 94-102

[25] D. H. Lee and B. Derby, Preparation of PZT suspensions for direct ink jet printing, *Journal of the European Ceramic Society*, 24(6),(2004), 1069-1072

[26] T. Wang and B. Derby, Ink-Jet Printing and Sintering of PZT, *Journal of the American Ceramic Society*, 88(8), (2005), 2053-2058

[27] (a) D. B. Bogy, F. E. Talke, Experimental and Theoretical Study of Wave Propagation Phenomena in Drop-on-Demand Ink Jet Devices, *IBM J. Res. Develop. 28,* (1984), 314
(b) C. Ainsley, N. Reis, B. Derby, Freeform fabrication by controlled droplet deposition of powder filled melts, *J. Mater. Sci.*, 27, (2002), 3155

[28] (a) J. F. Dijksman, Hydrodynamics of small tubular pumps, *J. Fluid Mech.,* 139, *(*1984), 173.
(b) K. A. M. Seerden, N. Reis, J. R. G. Evans, P. S. Grant, J. W. Halloran, B. Derby, Ink-Jet Printing of Wax-Based Alumina Suspensions, *J. Am.Ceram. Soc., 84* (2001), 2514

[29] Y. Shin, P. J. Smith, Theoretical investigation of the influence of nozzle diameter variation on the fabrication of thin film transistor liquid crystal display color filters , *J. Appl. Phys.*, 103, (2008), 114905

[30] A. D. Bermel and D. E. Bugner, Particle size effects in pigmented ink jet inks *J. Imaging Sci. Technol*. 43, (1999), 320,

[31] H. Kipphan (editor), Handbook of print media: Technologies and production methods, Springer, New York, (2001)

[32] A.Ciba Speciality Chemicals. Polymer specialities selection guide

[33] Fedele L., Colla L., Bobbo S., Barison S., Agresti F., Experimental stability analysis of different water-based nanofluids, *Nanoscale Res. Lett.*, 6, (2011)

[34] Zhu, H., Zhang, C., Liu, S., and Tang, Y., Effects of Nanoparticle Clustering and Alignment on Thermal Conductivities of Fe_3O_4 Aqueous Nano- fluids, *Appl. Phys. Lett.*, 89, (2006), 023123H.T.

[35] Zhu, Y.S. Lin, Y.S. Yin YS, A novel one-step chemical method for preparation of copper nanofluids. *J. Colloid Interface Sci*. 277, (2004), 100

[36] Chopkar M., Das P. K., Manna I., Synthesis and Characterization of Nanofluid for Advanced Heat Transfer Applications, *Scr. Mater.*, 55, (2006), 549–552

[37] Akoh, H., Tsukasaki, Y., S.Yatsuya, A. Tasaki, Magnetic properties of ferromagnetic ultrafine particles prepared by vacuum evaporation on running oil substrate. *Journal of Crystal Growth*, 45, (1978), 495-500

[38] Wagener, M., Murty, B. S., and Gunther, B. Preparation of metal nanosuspensions by highpressure DC-sputtering on running liquids. In Komarnenl, S., Parker, J. C., and Wollenberger, H. J. (Editors), Nanocrystalline and Nanocomposite Materials II, volume 457, 149– 154. *Materials Research Society*, Pittsburgh PA (1997)

[39] Zhu, H., Lin, Y., and Yin, Y. A novel one-step chemical method for preparation of copper nanofluids. *Journal of Colloid and Interface Science*, 227, (2004), 100-103

[40] F.E. Kruis, H. Fissan, A. Peled, Synthesis of nanoparticles in the gas phase for electronic, optical and magnetic applications—a review, *Journal of Aerosol Science*, (1998), 511- 535

[41] C. Frances and C Laguerie, Fine wet grinding of an alumina hydrate in ball milling, *Powder technology*, 99, (1998), 147-153

[42] J.E. Funk and D.R. Dinger, Predictive process control of crowded particulate suspension, Kluwer Academic Publisher, (1994)

[43] F.N. Shi and T.J. Napier-Munn, Effect of slurry rheology on industrial grinding performance, *International Journal of Mineral Processing*, 65, (2002), 125-14

[44] Y. Xuan, and Q. Li, Heat transfer enhancement of nanofluids. *International Journal of Heat and Fluid Transfer*, 21, (2000), 58-64

[45] S. M. S. Murshed, K. C. Leong, Enhanced thermal conductivity of TiO_2 – Water based nanofluids, *International Journal of Thermal Sciences*, 44, (2005), 367-373

[46] Y. J. Hwang, Y. C Ahn, H. S. Shin, C. G. Lee, G. T Kim, H. S. Park, and J. K Lee, Investigation on characteristics of thermal conductivity enhancement of nanofluids, *Current Applied Physics*, 6, (2005), 1068–1071

[47] a) E. Tamjid and B. H. Guenther, Rheological and sedimentation behaviour of nanosilver colloids for inkjet printing. *Int. J. Nanomanufacturing* 5, (2010), 383
b) A. B. R. Mayer, Colloidal metal nanoparticles dispersed in amphiphilic polymers. *Polym. Adv. Technol*. 12, (2001), 96

[48] H. Tan, J. M. Xue, B. Shuter, X. Li and J. Wang, Synthesis of PEOlated Fe_3O_4@SiO_2 Nanoparticles via Bioinspired Silification for Magnetic Resonance Imaging. *Adv. Funct. Mater*. 20, (2010), 722

[49] G.D. Angelescu, M. Vasilescu, M. NASTASESCU; r: Baratoiu; D. Donescu, V.S: Teodorescu, Synthesis and association of Ag(0) nanoparticles in aqueous Pluronic F127 triblock copolymer solutions, *Colloids and Surfaces A: Physicochemical and Engineering Aspects*, 394, (2012), 57-56

[50] P.j. Smith, D.Shin, J.E. Stringer, B.Derby and N. Reis, Direct ink-jet printing and low temperature conversion of conductive silver patterns. *J.Mater.Sci*. 41, (2006), 4153

[51] C. Hayashi, Ultrafine particles, *J.Vacuum Sci. Technol. A*., 5, (1987), 1375-1384

[52] J. Perelaer, Berend-Jan de Gans, and U. S. Schubert, Ink-jet printing and microwave sintering of conductive silver tracks. *Adv. Mater*. 18, (2006), 2101

[53] S. Jeong, H.C. Song, W.W. Lee , S.S Lee, Y. Choi, W. Son, E.D. Kim, C.H. Paik, S.H Oh, B.H. Ryu, Stable Aqueous Based Cu Nanoparticle Ink for Printing Well-Defined Highly Conductive Features on a Plastic Substrate, *Langmuir*, 27, (2011), 3144-3149

[54] S. Jeong, H. C. Song, W. W. Lee, Y. Choi, and B. H. Ryu, Preparation of aqueous Ag Ink with long-term dispersion stability and its inkjet printing for fabricating conductive tracks on a polyimide film. *J. Appl. Phys*. 108, (2010), 102805

[55] J. S. Taurozzi, V. A. Hackley, M. R. Wiesner, Preparation of nanoparticles dispersion from powdered material using ultrasonic distribution, National Institute of Standards and Technology, Materials Science and Engineering Laboratory, Gaithersburg, MD 20899, USA, (2010)

[56] W. Wang, Q. Zhang, Z. Liu, Z. Libor, Highly efficient size reduction of nanoparticles by the shock wave method. *Functional Materials Letters*, 3, (2010), 299

[57] Y A. Buyevich and S. K. Kapbsov, Segregation of a fine suspension in channel flow., *Journal of Non-Newtonian Fluid Mechanics* 86, (1999), 157-184

[58] P.F. Blazdell, J.R.G. Evans, Application of a continuous ink jet printer to solid free forming of ceramics, *Journal of Material Processing Technology*, 99 (1), 2000), 94-1021

[59] Barnes, H.A., Hutton, J.F., Walters, K., Rheology Series 3, *An Introduction of Rheology*, Elsevier, Amsterdam, (1993)
[60] A. W. Adamson, Physical Chemistry of surfaces, *Wiley*, New York, (1967)

[61] W. Russel, D. Saville, W. Schowalter, Colloidal dispersion, *Cambridge University Press*, Cambridge, (1989)

[62] R.J. Hunter, Zeta potential in colloid science: principles and applications, *Academic Press, London*, UK, (1988)

[63] A.V. Delgado, F. Gonzalez-Caballero, R.J. Hunter, L.K. Koopal, and J. Lyklema, Measurement and Interpretation of Electrokinetic Phenomena (IUPAC Technical Report) *Pure Appl. Chem.* 77(10), (2005), 1753–1805

[64] D.J. Shaw, Introduction to colloid and surface chemistry, *Butterworth Heinemann*, London, UK, (1992)

[65] R.J. Hunter, Introduction to modern colloid science, *Oxford Science Publications*, (1993),

[66] D.H. Everett, Basic principles of colloid science, *The Royal Society of Chemistry*, London, UK, (1994)

[67] Q. Kong, X. Chen, J. Yao and D. Xue, Preparation of poly(N-vinyl-2-pyrrolidone)-stabilized transition metal (Fe, Co, Ni and Cu) hexacyanoferrate nanoparticles, *Nanotechnol*., 16, (2005), 164

[68] H. Rensmo , A. Ongaro , D. Ryan and D. Fitzmaurice , Self-assembly of alkane capped silver and silica nanoparticles, *J. Mater. Chem*., 12, (2002), 2762

[69] E. Egorova , A. Revina, Optical Properties and Sizes of Silver Nanoparticles in Micellar Solutions, *Colloid J*., 64 (2002) 301

[70] R.M. Meixner, D. Cibis, K. Krueger, H. Goebel, Characterization of polymer inks for drop-on-demand printing systems, *Micro-Syst. Technol.* 14 (8), (2008) 1137

[71] Fakhouri, G. Mermoud, J.Y. Kim, A. Martinoli, J. Brugger, Drop-on-demand inkjet printing of su-8 polymer, *Micro Nanosyst.*, 1, (2009)

[72] K.A. M. Seerden, N. Reis, J. R. G. Evans, P. S. Grant, J. W. Halloran, B. Derby, Ink-Jet Printing of Wax-Based Alumina Suspensions, *J. Am. Ceram. Soc.*, 84, (2001), 2514

[73] R. Noguera, M. Lejeune, and T. Chartier. 3D fine scale ceramic components formed by ink-jet prototyping process. *Journal of the European Ceramic Society*, 25, (2005), 2055-2059

[74] K.L. Mittal, Adhesion Measurement of Thin Films, *Electrocomp.Sci. Technol*., 3, (1976), 21

[75] R.A. Mc. Kyton, J.J. Wallis, Thin film materials and deposition techniques for infra-red coatings, *FA Tech. Rep*., (1974), 74028

[76] D.M. Mattox, Interface formation and the adhesion of deposited thin films, *SC Monogr*., Sandia Corp (1905)

[77] H.K. Pulker , A.J. Perry, R. Berger, Adhesion, *Surface Technology*, 14, (1981), 25-39

[78] M.D.Coghill, Scratch adhesion testing of soft metallic coatings on glass, *Surface and Coatings Technology*, 41, (1990), 135-146

[79] W.C. Oliver and G.M. Pharr. Measurement of hardness and elastic modulus by instrumented indentation: Advances in understanding and refinements to methodology, *J. Mater. Res.* 19, (2004), 3

[80] L.J. van der Pauw, A method for measuring the resistivity and hall coefficient on lamellae of arbitrary shape, *Philips Res. Rep*. 13, (1958)

[81] H.H. Lee, K.S. Chou, K.C. Huang Inkjet printing of nanosized silver colloids, *Nanotechnology*, 16, (2005), 2436-2441

[82] S.B Fuller, E.J. Wilhelm, J.M Jacobson, Inkjet printed nanoparticle microelectromechanical systems, *J. Microelectromech Sys*t., 11, (2002), 54-60

[83] G. Haacke, Transparent conducting coatings. *Ann. Rev.* Mater. Sci. 7, (1977), 73–93

[84] Granqvist, C. G. Transparent conductors as solar energy materials: A panoramic review. *Sol. Energy Mater. Sol. Cells 91*, (2007), 1529-1598

[85] G. Thomas, Materials science: Invisible circuits, *Nature* 389, (1997), 907–908

[86] L. Hu, D.S. Hecht, G. Gruner, Percolation in transparent and conducting carbon nanotube networks. *Nano Lett., 4*, (2004), 2513-2517

[87] Y. Zhou, L. Hu, G. Grüner, A method of printing carbon nanotube thin films. *Appl. Phys. Lett. 88, (*2006), 123109

[88] G. Eda, G. Fanchini, M. Chhowalla, Large-area ultrathin films of reduced graphene oxide as a transparent and flexible electronic material. *Nat. Nanotechnol. 3, (*2008), 270-274

[89] V.C. Tung, M.J. Allen, Y. Yang, R.B. Kaner,. Highthroughput solution processing of large-scale graphene. *Nat. Nanotechnol*. 4, *(*2009) 25-29

[90] J. Wu, M. Agarwal, H.A. Becerril, Z. Bao, Z. Liu, Y. Chen, P: Peumans, Organic light-emitting diodes on solutionprocessed graphene transparent electrodes, *ACS Nano, 4*, (2010) 43-48

[91] J. Wu, H.A. Becerril, Z. Bao, Z. Liu, Y. Chen, P. Peumans, Organic solar cells with solution-processed grapheme transparent electrodes. *Appl. Phys. Lett. 92, (*2008), 263302

[92] J. -Y Lee, S. T. Connor, Y Cui, P Peumans, Solutionprocessed metal nanowire mesh transparent electrodes. *Nano Lett.*, *8*, (2008), 689-692

[93] S. De, T. M. Higgins, P. E Lyons, E. M. Doherty, P. N Nirmalraj, W.J. Blau, J.J. Boland, J. N Coleman, Silver nanowire networks as flexible, transparent, conducting films: Extremely high DC to optical conductivity ratios. *ACS Nano, 3*, (2009), 1767-1774

[94] N. Reis, C. Ainsley, B. Derby, Ink-jet delivery of particle suspensions by piezoelectric droplet ejectors , *J. Appl. Phys.* 97, (2005), 094903

[95] P. J. Smith, B. Derby, N. Reis, A. Wallwork, C. Ainsley, Measured Anisotropy of Alumina Components Produced by Direct Ink-Jet Printing, *Key Eng. Mater.*, 693, (2004), 264

[96] J. Peraler, A. M.J van den Berg, A. W.M. de Laat, P. J. Smith, U. S. Schubert, Geometric control of inkjet printed features using a gelating polymer, *J. Mater. Chem*., 2007, 17, 677–683 |

[97] P. C. Duineveld, The stability of ink-jet printed lines of liquid with zero receding contact angle on a homogeneous substrate, *J. Fluid Mech*., 477, (2003), 175

[98] H. Sirringhaus, T. Kawase, R. H. Friend, T. Shimoda, M. Inbasekaran, W. Wu, E. P. Woo, High-Resolution Inkjet Printing of All-Polymer Transistor Circuits, *Science*, 290, (2000), 2123

[99] Chou, P. R. Krauss, P. J. Renstrom, Imprint of sub-25 nm vias and trenches in polymers, *Appl. Phys. Lett*, 67, (1995), 67, 3114

[100] L. S. Roman, O. Ingana, T. Granlund, T. Nyberg, M. Svensson,M. R. Andersson, J. C. Hummelen, Trapping Light in Polymer Photodiodes with Soft Embossed Gratings, *Adv. Mater*. 12, (2000), 189

[101] J. R. Lawrence, P. Andrew, W. L. Barnes, M. Buck, G. A. Turnbull, I. D. W. Samuel, Optical properties of a light-emitting polymer directly patterned by soft lithography, *Appl. Phys. Lett*. 81, (2002), 1955

[102] J. Z. Wang, Z. H. Zheng, H. W. Li, W. T. S. Huck, H. Sirringhaus, Dewetting of conducting polymer inkjet droplets on patterned surfaces, *Nature Mater. 3,* (2004), 171

[103] (a) S.M. Moghimi, A.C. Hunter and J.C. Murray, Long-circulating and target-specific nanoparticles: theory to practice. *Pharmacol Rev*, 53, (2001), 283–318
(b) J. Panyam and V. Labhasetwar, Biodegradable nanoparticles for drug and gene delivery to cells and tissue. *Adv Drug Delivery Rev*, 55, (2003), 329-347

[104] F.E. Kruis, H. Fissan, A. Peled, Synthesis of nanoparticles in the gas phase for electronic, optical and magnetic applications—a review, *Journal of Aerosol Science*, (1998), 511- 535

[105] J.J Ramsden, The nucleation and growth of small CdS aggregates by chemical reaction, *Surf. Sci*., 156 (1985) 1027

[106] J. Turkevich, P. Cooper, S. and J. Hillier, A study of the nucleation and growth processes in the synthesis of colloidal gold, *Discuss. Faraday Soc.* 11 (1951) 55

[107 D. D Evanoff Jr and G. Chumanov, Synthesis and Optical Properties of Silver Nanoparticles and Arrays, *Chem Phys Chem* 6, (2005), 1221

[108] A.Y. Olenin, Y.A. Krutyakov, A.A. Kudrinskii, G. V. Lisichkin, Formation of surface layers on silver nanoparticles in aqueous and water-organic media, Colloid Journal, 70, (2011), 71-76

[109] Y. Yin et al., Synthesis and characterization of stable aqueous dispersions of silver nanoparticles through the Tollens process , *J. Mater. Chem.* 12, (2002), 522

[110] A. Taleb, C. Petit, and M. P. Pileni, Synthesis of Highly Monodisperse Silver Nanoparticles from AOT Reverse Micelles: A Way to 2D and 3D Self-Organization, *Chem. Mater.*, 9, (1997), 950-959

[111] A. Pyatenko, K. Shimokawa, M. Yamaguchi, O. Nishimura and M. Suzuki, Synthesis of silver nanoparticles by laser ablation in pure water, *Appl. Phys. A*, 79, (2004), 80

[112] J.J. Ramsden, The Photolysis of Small Silver Halide Particles , *Proc. R. Soc. Lond. A* 392, (1984), 4427- 444

[113] D. Dickson, Nanostructured magnetism in living systems, *J. Magn. Mater*., 203, (1999), 46

[114] J. Wan , W. Cai, X. Meng, E. Liu, Monodisperse water-soluble magnetite nanoparticles prepared by polyol process for high-performance magnetic resonance imaging, *Chem Commun*, 47, (2007), 5004-5006

[115] C. Becker, M. Hodenius, G. Blendinger A. Sechi, T. Hieronymus Uptake of magnetic nanoparticles into cells for cell tracking, *J Magn Magn Mater*., 311,(2007), 234-237

[116] Y.P. Sun, R.Guduru, F. Lin, T. Whiteside, Preparation of Nanoscale Semiconductors through the Rapid Expansion of Supercritical Solution (RESS) into Liquid Solution, *Ind. Eng. Chem. Res.*, (2000) 4663–4669

[117] R. Thakur, R. B. Gupta, Formation of phenytoin nanoparticles using rapid expansion of supercritical solution with solid cosolvent (RESS-SC) process, *International Journal of Pharmaceutics*, 308, (2006) 190-199

[118] M.J. Meziani, P. P. F. Beacham, F. Lawrence, Y.-P. Sun, Nanoparticle formation in rapid expansion of water-in-supercritical carbon dioxide microemulsion into liquid solution *J. Supercrit. Fluids*, 34, (2005), 91

[119] M Ji, XY Chen, CM Wai, JL Fulton, Synthesizing and Dispersing Silver Nanoparticles in a Water-in-Supercritical Carbon Dioxide Microemulsion, *J. Am. Chem. Soc*. 121, (1999), 2631

[120] H. Ohde, M. Ohde, F. Bailey, H. Kim, C.M. Wai, Water-in-CO_2 Microemulsions as Nanoreactors for Synthesizing CdS and ZnS Nanoparticles in Supercritical CO_2, *Chem. Mater, Nano Lett.,* 721, (2002)

[121] G. Muhrer, M. Mazzotti, Precipitation of lysozyme nanoparticles from dimethyl sulfoxide using carbon dioxide as antisolvent, Biotechnol. Prog. 19 (2003) 549,

[122] P. Chattopadhyay , R.B. Gupta, Supercritical CO_2-Based Production of Fullerene NanoparticlesInd. *Eng. Chem. Res*. 39, (2000), 2281

[123] T. Adschiri, K. Kanazawa, K. Arai, Rapid and continuous hydrothermal crystallization of metal oxide particles in supercritical water, *J. Am. Ceram. Soc.*, 75, (1992), 1019

[124] T. Adschiri, Y. Hakuta, K. Arai, Hydrothermal synthesis of metal oxide fine particles at supercritical conditions, *Ind. Eng. Chem. Res.*, 39, (2000), 4901

[125] L. Fan, K. Yokota, K. Fujimoto, Supercritical phase fischer-tropsch synthesis: Catalyst pore-size effect, *Aiche Journal*, 38, (1992), 1639-1648

[126] W. V. Prescott, A. I. Schwartz (Editors), Nanorods, nanotubes, and nanomaterials research progress, *Nova Science Publisher*, (2008)

[127] A. Kamyshny and S. Magdassi, Colloid Stability: The Role of Surface Forces, (2007)

[128] D. Goia and E. Matijevic, Preparation of monodispersed metal particles, *New J. Chem*, 22, (1998), 1203-1215

[129] G. Cao, Nanostructures and Nanomaterials, *Imperials College Press*., (2004)

[130] Y.G Sun, B.T. Mayers, Y.N. Xia, Template-engagedreplacement reaction: A one-step approach to the large-scale synthesis of metal nanostructures with hollow interiors, *Nano Letters*, 2, (2002), 5, 481-485

[131] F. Fievet, J.P. Lagier, B. Blin, B. Beaudoin, M. Figlarz, Omogeneous and heterrogenous nucleations in the polyol process for the preparation of micron and sub-micron size metal particles, *Solid State Ionics*, 32, (1989), 198-205

[132] Y. Xia, Y. Xiong, B.Limb, S.E. Skrabalak, Shape-controlled synthesis of metal nanocrystals: Simple chemistry meets complex physics?, *Angewandte Chemie- International Edition,* 48, (2009), 60-103

[133] K.E Korte, S.E. Skrabalak, Y.Xia Rapid synthesis of silver nanowires through a CuCl- or $CuCl_2$- mediated polyol pocess, *Journal of Materials Chemistry*, 18, (2008), 437-441

[134] B. Wiley, Y.G. Sun, Y.N Xia, Polyol synthesis of silvewr nanostructures : Control of product morphology with Fe (II) or Fe(II) species, *Langmuir*, 21, (2005), 8077-8080

[135] Y.G. Sun, Y.D. Yin, B.T. Mayers, T. Herricks, Y.N Xia, Uniform silver nanowires synthessiby reducing $AgNO_3$ with ethylene glycol in the presence of seeds and poly (vinyl pyrrolidone), *Chemistry of Materials*, 14, (2002), 4736-4745

[136] E Matijevic, Preparation and properties of uniform size colloids, *Chemistry of Materials*, 5, (1993), 412-426

[137] B. Wiley, Y. Sun, Y. Xia, Synthesis of Silver Nanostructures with Controlled Shapes and Properties, *Acc Chem Res.*, 40 (2007) 1067.

[138] E.H.C. Parker (ed.), The *Technology and Physics of Molecular Beam Epitaxy*, Plenum, New York, (1985)

[139] K.-S. Chou, Y.-C Lu, and H.-H Lee, Effect of alkaline ion on the mechanism and kinetics of chemical reduction of silver, *Materials Chemistry and Physics*, 94 (2005), 429-433

[140] Z. Zhang, B. Zhao, L. Hu, PVP Protective Mechanism of Ultrafine Silver Powder Synthesized by Chemical Reduction Processes, *J.Solid State Chem.*, 121, (1996) ,105

[141] X. Feng, H. Ma, S. Huang, W. Pan, X. Zhang, F. Tian, C. Gao, Y. Cheng, and J. Luo, Aqueous−Organic Phase-Transfer of Highly Stable Gold, Silver, and Platinum Nanoparticles and New Route for Fabrication of Gold Nanofilms at the Oil/Water Interface and on Solid Supports, *J. Phys. Chem., B.*, 110, (2006), 12311

[142] R.A. Salkar, P. Jeevanandam, S.T. Aruna, Y. Koltypin, and A. Gedanken, The sonochemical preparation of amorphous silver nanoparticles, *J. Mater. Chem.*, 9, (1999), 1333

[143] Y. Yin, Z. Li, Z. Zhong, B. Gates, Y. Xia, and S. Venkateswaran, Synthesis and characterization of stable aqueous dispersions of silver nanoparticles through the Tollens process, *J. Mater. Chem.*, 12, (2002), 522

[144] A.J.P van Zyl, D. de Wet-Roos, R. D. Sanderson, B. Klumperman, The role of surfactant in controlling particle size and stability in the miniemulsion polymerization of polymeric nanocapsules, *Europan Polymer Journal*, 40, (2004), 2717-2725

[145] M. Ji, X. Chen, C.M. Wai and J.L. Fulton, Synthesizing and Dispersing Silver Nanoparticles in a Water-in-Supercritical Carbon Dioxide Microemulsion, J. Am. Chem. Soc., 121, (1999), 2631

[146] Y.P. Sun, Supercritical Fluid Technology in Materials Science and Engineering, *Marcel Dekker Inc*, New York (2002)

[147] Y.-W. Chih, W.-T. Cheng , Supercritical carbon dioxide-assisted synthesis of silver nano-particles in polyol process, *Materials Science and Engineering: B*, 145, (2007), 67-75

[148] H. Ohde, F. Hunt, C.M. Wai, Synthesis of Silver and Copper Nanoparticles in a Water-in-Supercritical-Carbon Dioxide Microemulsion, *Chem. Mater*., 13, (2001), 4130

[149] K.S. Morley, P.C. Partricia, P.B. Webb, A.R. Berry, F.J. Allison, G. Moldovan, P.D. Brown, S.M. Mowdle, Clean preparation of nanoparticulate metals in porous supports: a supercritical route, *J. Mater. Chem.,* 12, (2002), 1898

[150] J. Liu, P. Raveendran, Z. Shervani, Y. Ikushima, Y. Hakuta, Synthesis of Ag and AgI Quantum Dots in AOT-Stabilized Water-in-CO_2 Microemulsions, *Chem.-Eur. J.* , 11, (2005), 1854

[151] E. Reverchon, R. Adami, Nanomaterials and supercritical fluids, *J. Supercrit. Fluids*, 37, (2006), 1

[152] K.H. Lieser, Steps in Precipitation Reactions and this is more sensitive to temperature during the process, *Angew. Chem. Int. Ed. Engl.*, 8, (1969), 188

[153] S. Auer, D. Frenkel, Suppression of crystal nucleation in polydisperse colloids due to increase of the surface free energy, *Nature* 413, (2001), 711

[154] S.C. Liao, W.E. Mayo, K.D. Pae, Theory of high pressure/low temperature sintering of bulk nanocrystalline TiO_2, *Acta Mater*., 45, (1997), 4027

[155] P.S. Shah, J.D. Holmes, K.P. Johnston and B.A. Korgel. *J. Phys. Chem. B,* **106** (2002), p. 2545. Size-Selective Dispersion of Dodecanethiol-Coated Nanocrystals in Liquid and Supercritical Ethane by Density Tuning

[156] Y.-W. Chih, W.-T. Cheng , Supercritical carbon dioxide-assisted synthesis of silver nano-particles in polyol process, *Materials Science and Engineering: B,* 145, (2007), 67-75

[157] M. Saharay and S. Balasubramanian.,Enhanced Molecular Multipole Moments and Solvent Structure in Supercritical Carbon Dioxide, *Chem. Phys. Chem*., 5, (2004), 1442

[158] H. G Yang, C.-Z. Li, H.-C. Gu, T.-N Fang, Rheological behavior of titanium dioxide suspensions *J. Colloid Interface Sci. 236,* 2001, 96

[159] B. Sawyer, E.J. Fuller, J.M Jacobson, Ink-Jet Printed Nanoparticle Microelectromechanical Systems, *J. Microelectromech. Syst.,* 11, (2002), 54

[160] M. Kaszuba, J. Corbett, F. M. Watson, High-concentration zeta potential measurements using light-scattering techniques, *Phil. Trans. R. Soc. A,* 368 (2010), 4439

[161] P.C Kapur, T.W. Healy, P.J. Scales, D.Boger, D. Wilson, Role of the dispersant in kinetics and energetic of stirred ball mill. *International Journal of Mineral Processing*, 47, (1996), 141-152

[162] D.H. Jang, D.J. Kim, B.Y. Lee, S.S. Kim, M.S. Kang, D.K. Min, J.H. Moon, Nanosized glass frit as an adhesion promoter for ink-jet printed conductive patterns on glass substrates annealed at high temperatures, *Adv. Funct. Mater*., 18, (2008), 2862-2868

[163] S. Rane, T. Seth, G. Phatak, D. Amalnerkar, M. Ghatpande, Effect of inorganic binders on the properties of silver thick films, *J. Mater. Sci., Mater. Electron*. 15, (2004), 103

[164] M.R. Locatelli, B.J. Dalgleish, K. Nakashima, A.P. Tomsia, A.M. Glaeser, New approaches to joining ceramics for high-temperature applications, , *Ceramics International*, 23, (1997), 313-322

[165] Yu Yang, Chun-Xiang Lu, Xiao-Lei SU, Gang-Ping Wu, Xin-Kui Wang, Effect of nano-SiO_2 modified emulsion sizing on the interfacial adhesion of carbon fibres reinforced composities, , *Materials Letters*, 61 (2007) 3601-3604

[166] L.T. Tianya1, S. Jing, W. Wei1, G. Yongxin, S. Jianda, F. Zhengxiu, Employing SiO_2 Buffer Layer to Improve Adhesion of the Frequency-doubled Antireflection Coating, . *Journal of Wuhan University of Technolotgy-Mater. Sci*., (2009)

[167] a) Effect of nanoparticles SiO_2 on the perfortmance of nanocompositties, Y. Zheng, R. Ning, Materials letters 57 (2003) 2940-2944
b) X.Wu, E. Sacher, M. Meunier 1999 The effect of hydrogen bonds on the adhesion of inorganicn oxide particles on hydrophilic silicon surfaces J.Appl.Phys.86 1744

[168] K. Gaw, M. Jikei, M. Kakimoto, Y. Imai, Adhesion behaviour of polyamic acid cured epoxy, *Polymer*, 38, (1997), 4413-4415

[169] B. Taylor, J. Felten, J. Larry, Progress in and technology of low-cost silver containing thick-films conductors, *IEEE Transacions on Components, Hybrids, and Manufacturing Technology*, 3, (1980), 504-517

[170] G. PPeschel, K. H. Aldifinger, Viscosity anomalies in liquid surface zones IV. The apparent viscosity of water in thin layers adjacent to hydroxylated fused silica surfaces, *J.Colloid.Interface Sci*., 34, (1970), 505

[171] D. K. Owens and R. C. Wendt, Estimation of the surface energy of polymers, *Journal of applied polymer science*, 18, (1969), 1741-1747

[172] Y. Zhou, L. Hu, G. Grüner, A method of printing carbon nanotube thin films. *Appl. Phys. Lett.*, *88*, (2006), 123109

[173] V. C. Tung, M.J. Allen, MY. Yang, R.B. Kaner, High throughput solution processing of large-scale graphene. *Nat. Nanotechnol*, *4*, (2009), 25-29

[174] S. Higgins, P.E. Lyons, E.M Doherty, P.N. Nirmalraj, W.J Blau, J.J Boland, J.N Coleman, Silver nanowire networks as flexible, transparent, conducting films: Extremely high DC to optical conductivity ratios. *ACS Nano*, *3*, (2009), 1767-1774

[175] H.H. Huang, X.P. Ni, G.L. Loy, C.H. Chew, K.L. Tan, F.C. Loh, J.F Deng, G.Q. Xu, Photochemical Formation of Silver Nanoparticles in Poly(*N*-vinylpyrrolidone), *Langmuir*,12, (1996), 909

[176] L.Hu, H.S Kim, J.-Y. Lee, P. Peumans,‡ and Yi Cui†, Scalable Coating and Properties of Transparent, Flexible, Silver Nanowire Electrodes, *ACS Nano*, 4, (2010), 2955-2963

[178] R. Rastogi, R. Kaushal, S.K. Tripathi, A.L. Sharma, I. Kaur, L. M. Bharadwaj, Comparative study of carbon nanotube dispersion using surfactants Journal of *Colloid and Interface Science*, 328, (2008), 421-428

[179] D.S. Ginley, C.Brigth, Transparent conducting oxides.*MRS Bull.,* (2000), 15-18